



**Alasmariya Islamic University
Faculty of Science
Department of Chemistry**

Biosynthesis of Gold Nanoparticles from (*Annona muricata*) Seeds Extract as a Cytotoxic Agent for Cells Death in Breast Cancer

Submitted by: Amina Muftah Ali Alfalos

**Supervised by: Prof. Adel Mohamed Mlitan
Professor of Biochemistry at Misurata University
Co-Supervised by: Dr. Moktar Almabruk Aburzeza
Associate Professor of Organic Chemistry at Alasmariya University**

**Thesis Was Submitted in Partial Fulfillment of The Requirements
for The Degree of Master in Chemistry.**

Academic year (2025)



قرار لجنة مناقشة رسالة الإجازة العالية (الماجستير)

علا بقرار السيد/ رئيس الجامعة رقم (406) لسنة 2025م، الصادر في 11/5/2025م، القاضي بتشكيل لجنة

لمناقشة رسالة علمية للحصول على درجة الإجازة العالية (الماجستير) في تخصص: الليسانس.

المقدمة من الطالبة: أمنية مصباح الفلوس، كلية: العلوم.

وعنوانها: لتحليل الجغرافيا الجيولوجية لبيئات الذهب النادوية بمنطقة بدرية بحرة العسقل

كامل محقق لعل الخلاب في سلطان التمدد

وتتكون اللجنة من الاساتذة:

1. د. عادل محمد سليمان الجامعة: الجامعة الإسلامية مشرفا ومقررا.

2. د. مختار المبروك أبو زيد الجامعة: الجامعة الإسلامية مشرفا ثانيا.

3. د. سليم علي المبروك الجامعة: الجامعة الإسلامية عضوا داخليا.

4. د. سالم محمد ادريس الجامعة: الجامعة الإسلامية عضوا خارجيا.

عقدت اللجنة جلسة علنية على تمام الساعة: 9:00 من صباح يوم الثلاثاء الموافق: 7/5/2025م، بقيادة

الاجتماعات بالكلية لمناقشة الرسالة وتقويم مستواها العلمي والمنهج الذي اتبعه الباحث والمصادر التي استخدمها في دراسته.

وقررت ما يلي:

بعد اتمام الطالب أمنية مصباح الفلوس لمتطلبات الدراسات العليا واجتياز امتحاناتها ومناقشة رسالتها

وتقويمها تقرر:

1. إجازتها بدون ملاحظات () .

2. إجازتها بملاحظات () ويمنح الطالب فرصة للتعديل و الأخذ بالملاحظات خلال: من تاريخ المناقشة

3. عدم إجازتها () .

توقيع أعضاء لجنة المناقشة:

1. د. عادل محمد سليمان الجامعة: الجامعة الإسلامية التوقيع: عادل سليمان

2. د. مختار المبروك أبو زيد الجامعة: الجامعة الإسلامية التوقيع: مختار المبروك أبو زيد

3. د. سالم محمد ادريس الجامعة: الجامعة الإسلامية التوقيع: سالم محمد ادريس

4. د. سليم علي المبروك الجامعة: الجامعة الإسلامية التوقيع: سليم علي المبروك

يعتمد:

رئيس الجامعة



عميد الكلية

الإقرار

أنا الموقعة أدناه مقدمة الرسالة التي تحمل العنوان:

Biosynthesis of Gold Nanoparticles from (*Annona Muricata*) Seeds Extract as a Cytotoxic Agent for Cells death in Breast Cancer

التخليق الحيوي لجسيمات الذهب النانوية لمستخلص بذور ثمرة القشطة

(*Annona Muricata*) كعامل محفز لموت الخلايا في سرطان الثدي

أقر بأن ما اشتملت عليه الرسالة انما هو نتاج جهدي الخاص، باستثناء ما تمت الإشارة إليه حيثما ورد، وأن هذه الرسالة جزء منها لم يقدم من قبل لنيل أية درجة علمية أو بحث لدى أية مؤسسة تعليمية أو بحثية أخرى.

Declaration

This work provided in this thesis, unless otherwise referenced, is the researcher's own work, and has not been submitted elsewhere for any other degree or qualification.

Student's name:

اسم الطالبة:

Signature:

التوقيع:

Date:

التاريخ:

Abstract

This study investigates the bio-Synthesis of gold nanoparticles (AuNPs) using *Annona muricata* seed extract and evaluates their anticancer potential against MCF-7-positive breast cancer cells. The synthesized AuNPs were characterized using various techniques including UV-visible spectroscopy, X-ray diffraction (XRD), transmission electron microscopy (TEM), atomic force microscopy (AFM), dynamic light scattering (DLS), and zeta potential analysis. The phytochemical profile of the *A. muricata* seed extract was analyzed using gas chromatography-mass spectrometry (GC-MS). The bio-synthesized AuNPs exhibited a spherical to sub-spherical morphology with sizes ranging from 20-60 nm (TEM/AFM) and a hydrodynamic diameter of approximately 75 nm (DLS). The negative zeta potential (-36 mV) indicated excellent colloidal stability. GC-MS analysis identified isopropyl tetra decanoate as a major component in the seed extract, potentially contributing to AuNP synthesis and stabilization. The anticancer activity of the AuNPs was assessed using MTT assay against MCF-7-positive breast cancer cells, with an IC₅₀ value of 22.44 ± 0.33 g/mL. Flow cytometry analysis revealed that AuNPs induced cell cycle arrest at the G1/S phase and significant apoptosis. The DPPH assay demonstrated potent antioxidant activity of the AuNPs, with concentration-dependent radical scavenging. This study demonstrates the potential of *A. muricata*-mediated Bio Synthesis of AuNPs as a promising approach for developing novel nanotherapeutics against MCF-7-positive breast cancer, combining the anticancer properties of both the plant extract and the nanoparticles.

Keywords: Bio synthesis; Gold nanoparticles; *Annona muricata*; MCF-7-positive breast cancer; Anticancer activity; Antioxidant properties; Apoptosis; Cell cycle arrest; Phytochemicals; Nanotechnology.

Dedication

Every challenging work needs self-efforts as well as guidance of elders

especially who were very close to our heart.

My humble effort we dedicate to our sweet and loving.

Father & Mother,

Whose affection love, encouragement and prays of day and night make us

able to get such success and honor,

Along with all hard working and respected

Teachers,

To everyone who cares about the environment and works to save it....

To everyone who inspires us by his/her science....

To our dear family

Acknowledgments

In the name of Allah, the Most Gracious and the Most Merciful

Alhamdulillah, all praise to Allah SWT for all His blessing in the completion of this thesis.

After thanking Allah, I would like to express my gratitude to my thesis supervisors: Dr. Adel Mlitan for all his guidance, understanding, support, and sound advice in all important aspects of my research, as he provided me with published scientific sources for the work, and Dr. Moktar Aburzeza for his scientific support, encouragement, and constructive advice. I would also like to thank Khaled Al- Alfalos, Professor of Physical Chemistry, Faculty of Science, Al-Asmariya Islamic University, Zliten, for providing research ideas, valuable comments, and sponsoring the thesis.

I appreciate the help and support of Professor Wissam Al-Kalab, a member of the Chemistry Department, Faculty of Science, Al-Asmariya.

My warm thanks to my dear friends Salima Farhat, Salima Wali, and many others who helped me in particular in editing my thesis in Detroit. Thank you for the friendship and memories.

Last but not least, I would also like to dedicate the thesis to my children and family, thanking you for being the target of support, love and encouragement that always carries me on the path. In particular, my greatest gratitude goes to my husband for his unconditional support, giving me the support and confidence, I need in my life.

Amina

Table of contents

No	Content	Page
	Declaration	I
	Abstract	II
	Dedication	III
	Acknowledgments	IV
	Table of Contents	V
	List of Tables	VII
	List of Figures	VII
	List of Abbreviation	VIII
	المخلص	ب
Chapter One: Introduction& Literature Review		
1.1	Introduction	1
1.1.2	Small particles	3
1.1.3	NP Catalysis	4
1.1.4	Cellular Targeting Mechanisms	5
1.1.5	Nanoparticles of organic matter	11
1.1.6	Nanoparticles that are inorganic	14
1.1,7	Overview of Breast Cancer	17
1.1.8	Breast Cancer Types	20
1.1.9	Causes of breast cancer	22
1.1.10	Importance of Nanoparticles in Cancer Treatment	24
1.1.11	Gold	24
1.1.12	Gold Nanoparticles (AuNPs)	25
1.1,13	The importance of <i>Annona muricata</i> seed extract	26
1.1.14	Effective compounds in (<i>Annona muricata</i>)	29
1.2	Objectives	34
1.3	Literature Review	35
Chapter Two: Experimental Work		
2	Materials and Methods	37
2.1	Materials	37
2.2	Methods	37
2.2.1	Bio Synthesis of Gold Nanoparticles (AuNPs)	37
2.2.1.1	Plant Material Preparation	37
2.2.1.2	Extract Preparation	37
2.2.1.3	AuNP Synthesis	37
2.3	Characterization of AuNPs	38
2.3.1	X-Ray Diffraction (XRD)	38
2.3.2	UV-Visible Spectroscopy	38
2.3.3	Fourier Transform Infrared Spectroscopy (FTIR)	38
2.3.4	Transmission Electron Microscopy (TEM)	38

2.3.5	Atomic Force Microscopy (AFM)	38
2.3.6	Scanning Electron Microscopy (SEM) Analysis	38
2.3.7	Dynamic Light Scattering (DLS)	39
2.3.8	Zeta Potential	39
2.3.9	Gas Chromatography-Mass Spectrometry (GC-MS) Analysis of A. muricata Seed Extract	40
2.3.10	Molecular Docking Simulations	40
2.4	In Vitro Anticancer Activity	41
2.4.1	Cell Culture	41
2.5	Flow Cytometry Analysis	41
2.5.1	Cell Cycle Analysis	41
2.5.2	Apoptosis Assay	41
2.5.3	MTT Assay	42
2.6	Antioxidant Activity Assessment	42
2.6.1	DPPH Radical Scavenging Assay	42
Chapter Three: Results and Discussion		
3.1	Characterization of Gold Nanoparticles	43
3.1.1	X-Ray Diffraction (XRD) Analysis	43
3.1.2	UV-Visible Spectroscopy	44
3.1.3	FTIR Analysis	46
3.1.4	Transmission Electron Microscopy (TEM) Analysis	51
3.1.5	Atomic Force Microscopy (AFM) Analysis	52
3.1.6	Scanning Electron Microscopy (SEM) Analysis	54
3.1.7	Dynamic Light Scattering (DLS) Analysis	57
3.1.8	Zeta Potential Analysis	59
3.1.9	Gas Chromatography-Mass Spectrometry (GC-MS) Analysis of Annona muricata Seed Extract.	60
3.2	Molecular Docking Study	63
3.2.1	Molecular Dynamics Simulation	64
3.4	Toxicity Characterization of Bio-Synthesized Gold Nanoparticles.	66
3.4.1	Cell Cycle Distribution Analysis	66
3.4.2	Apoptosis Analysis	68
3.5	Anticancer Activity of Bio-Synthesized Gold Nanoparticles Against MCF-7-Positive Breast Cancer Cells.	70
3.6	Antioxidant Activity and Potential Mechanism of Action.	72
Chapter Four: Conclusions and Recommendations		
4.1	Conclusions	75
4.2	Some recommendations and future prospects	76
	References	77
	Appendices	84

List of Tables

No	Table	Page
1	Comparison of XRD peaks between standard gold and synthesized AuNPs	44
2	Major compounds identified in Annona muricata seed extract by GC-MS analysis	61
3	Docking Scores and hydrogen bonding of the 3 Isopropyl tetra decanoate molecules conjugated with gold NP (IPTD-GnP) on specific selected breast cancer marker proteins	64
4	DNA Content Analysis of MCF-7-positive breast cancer cells treated with bio-synthesized AuNPs	66
5	Apoptosis Stages in MCF-7-positive breast cancer cells treated with bio-synthesized AuNPs	68
6	Cytotoxicity of bio-synthesized AuNPs against MCF-7-positive breast cancer cells	70
7	DPPH radical scavenging activity of bio-synthesized AuNPs nanoparticles.	72

List of Figures

No	Figure	Page
1	Nanoparticles for Cancer Therapy: Current Progress and Challenges	2
2	Nanoparticles for Cancer Therapy: Current Progress and Challenges	4
3	Nanoparticles for Cancer Therapy: Current Progress and Challenges	7
4	Nanoparticles for Cancer Therapy: Current Progress and Challenges	10
5	Nanoparticles for Cancer Therapy: Current Progress and Challenges	11
6	Stages of normal cell cycle	19
7	Structure of breast	20
8	Typical Structure associated with ductal carcinoma	21
9	Custard apple seeds	26
10	Annona Muricata Date	27
11	Main contents and main biological properties of various parts of graviola	28
12	illustrated XRD pattern of bio-synthesized AuNPs	43
13	UV-Visible absorption spectrum of bio-synthesized AuNPs.	45
14	illustrated FTIR pattern of Before adding gold nanoparticles	46
15	illustrated FTIR pattern of gold nanoparticles	49
16	TEM micrographs of bio-synthesized AuNPs at high magnification.	51
17	a illustrated 3D AFM image for bio-synthesized AuNPs	53
17	b illustrated 3D AFM image for bio- synthesis green-synthesized AuNPs.	55
18	SEM micrograph of bio-synthesized AuNPs at 120,000x magnification. Scale bar: 500 nm.	58
19	DLS size distribution of bio-synthesized AuNPs	59
20	Zeta potential distribution of bio-synthesized AuNPs.	60
21	Total Ion Chromatogram (TIC) of Annona muricata seed extract.	61
22	Mass spectrum of the peak at retention time 44.09 minutes.	62
23	The long hydrocarbon chain of the molecule adsorb onto the surface of newly formed gold nanoparticles	62
24	illustrated the molecular docking of gold bio- synthesis	65

25	illustrated Isopropyl tetra decanoate molecules conjugated with gold NP (IPTD-GnP) on specific selected breast cancer marker protein complex.	65
26	illustrated Bar charts representing the percentage of cell populations in MCF-7 cells treated with bio-synthesized AuNPs	67
27	Bar graph illustrating cell cycle distribution and apoptosis stages for control and AuNP-treated MCF-7-positive breast cancer cells.	69
28	Dose-response curve of Gold 1 nanoparticles against MCF-7-positive breast cancer cells.	71

List of Abbreviation

Symbol	Abbreviation
AFM	Atomic Force Microscopy
AuNPs	Gold Nanoparticles
DNA	Deoxyribonucleic Acid
DLS	Dynamic Light Scattering
DMSO	Dimethyl Sulfoxide
DPPH	1,1-Diphenyl-2-picrylhydrazyl
FTIR	Fourier Transform Infrared Spectroscopy
GC-MS	Gas Chromatography-Mass Spectrometry
IC50	Inhibitory Concentration 50%
IPTD	Isopropyl tetra decanoate
MCF-7	Michigan Cancer Foundation-7
MD	molecular dynamics
nm	Nanometer
NRG1	(Neuregulin 1)
SEM	Scanning Electron Microscopy
TEM	Transmission Electron Microscopy
TIC	Total Ion Chromatogram
UCSF	University of California, San Francisco
UV	Ultraviolet
X-ray	X-Ray Radiation
XRD	X-Ray Diffraction

Chapter One

Introduction and

Literature Review

1.1 Introduction:

A group of illnesses collectively referred to as cancer are distinguished by their invasiveness and unchecked, random cell division. The identification of different cancer risk factors has been the subject of intense work over a number of years. The genesis of certain malignancies has been strongly linked to particular environmental (acquired) variables, like pollution and radiation. However, a poor diet, smoking, tobacco use, stress, and inactivity all have a significant impact on determining one's chance of developing cancer. Although these extrinsic factors have been identified as key drivers of cancer, it has been difficult to determine the role of proto-oncogene mutations, tumor suppressor gene expression patterns, and DNA repair genes. Inherited genetics is only implicated in 5–10% of cancer cases. Another important risk factor for cancer and many different types of cancer is growing older. [1].

Cancer is the second biggest cause of death worldwide and one of the major public health issues. It is predicted by the American Cancer Society that by the end of 2021, there would be 1.9 million additional cases. Surgery, chemotherapy, radiation therapy, targeted therapy, immunotherapy, and hormone therapy are the traditional therapeutic modalities used to treat cancer. Despite their capacity for cytostasis and cytotoxicity, chemotherapy and radiation therapy are frequently associated with severe adverse effects and a significant chance of recurrence. [1].

The most frequent adverse effects are fatigue, stomach and skin problems, neuropathies, bone marrow repression, and hair loss. A few drug-specific adverse reactions include anthracyclines and bleomycin-induced cardiotoxicity and lung toxicity. (Fig. 1).

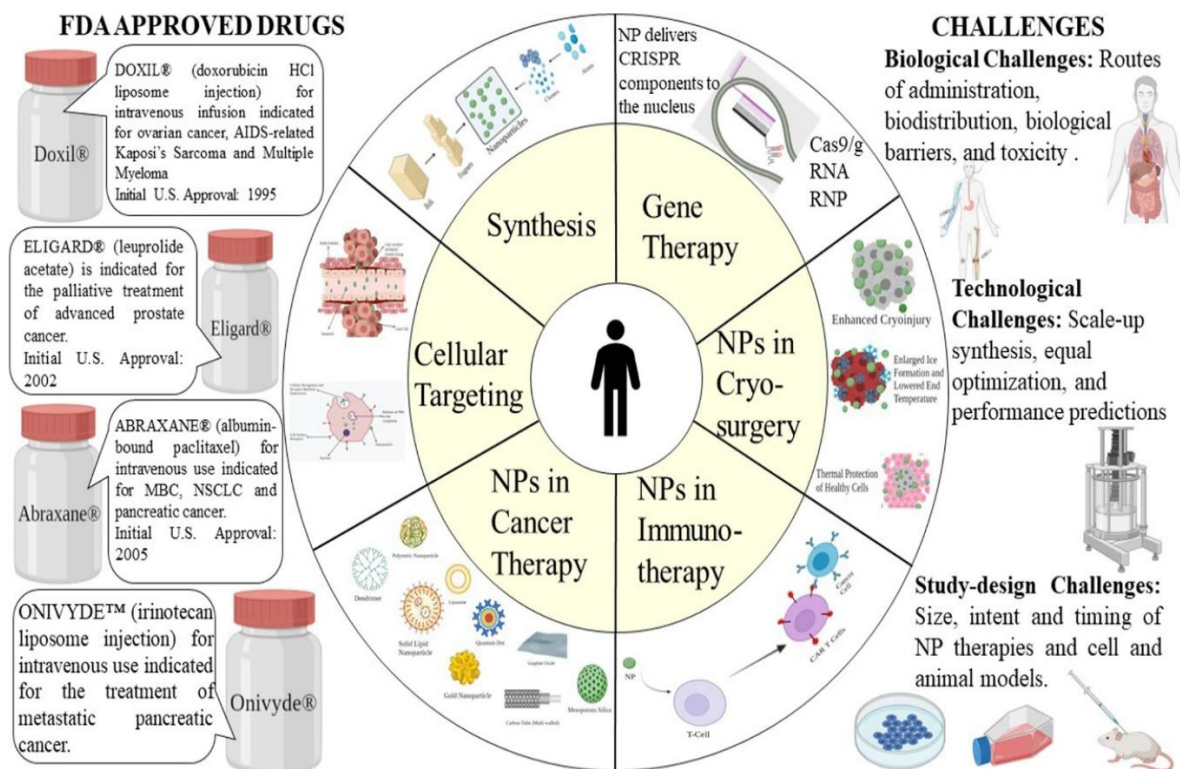


Figure. 1: Nanoparticles for Cancer Therapy: Current Progress and Challenges

Precision therapy has expanded since the introduction of focused therapy. The effectiveness of treatment is however limited by a number of unavoidable side effects, including multi-drug resistance. In addition to treating primary cancer, immunotherapeutic drugs have shown encouraging results in avoiding distant metastases and reducing the recurrence rate. However, one of the main adverse effects of immunotherapy is autoimmune illness. Furthermore, research and fragments of data indicate that immunotherapy is more successful against lymphoma than solid tumors. Immune cells find it difficult to penetrate the unique extracellular matrix (ECM) produced by these malignancies. Dermatological adverse events (dAEs) are caused by these recently developed targeted medicines and immunotherapies that disrupt signaling pathways essential to malignant behaviors and normal homeostatic activities of the epidermis and dermis. Given all of these facts, there has been a recent surge in demand for the development of innovative approaches to find precise cancer treatment. Recent attempts have been made to use nanoparticles to overcome the shortcomings of current medicinal techniques. Drug delivery methods based on nanoparticles have shown promise in the treatment and control of cancer by exhibiting favorable pharmacokinetics, accurate targeting, fewer adverse effects, and decreased drug resistance. Following the development of nanotechnology, several nanotherapeutic medications have been successfully launched, and since 2010, numerous

others have progressed to the clinical stage. By offering the possibility of drug combination therapy and the inhibition of drug resistance mechanisms, nanotherapeutic medicines have advanced the fields of drug delivery systems and anti-tumor multidrug resistance (MDR). In the 1960s, ETH Zurich made the first attempt to use nanotechnology in medical. Better medicines and a variety of diagnostic tools have been developed thanks to this combination. The fundamentals of using nanotherapeutics, present issues and opportunities, and the direction of future research are the primary topics of this review. [1].

The word "nanos" (meaning "dwarf") in Greek is the source of the prefix "nano". Therefore, "nanotechnology" could simply refer to technology involving "small" objects. But in scientific circles, nano has also long been used as a prefix to denote one billion (using billion in the American sense of one before nine zeroes). One billionth of a meter is what the term "nanometer" refers to. A nanometer is quite small; it is just around 10 atoms across [2].

Accordingly, we may anticipate that nanotechnology would be associated with technologies that function at the nanoscale level, which is the broad meaning of the term as it is currently used. Here, it's critical to make a distinction between "nanoscience," which is the study of extremely small-scale phenomena, and "nanotechnology," which aims to accomplish a beneficial objective [2].

1.1.2 Small particles

Technically speaking, nanoparticles (NPs) are particles having a single dimension of less than 100 nm and special characteristics that are typically absent from bulk samples of the same substance. These can be categorized as 0D, 1D, 2D, or 3D depending on the general form of the nanoparticle. The surface layer, shell layer, and core—basically the central section of the NP and sometimes referred to as the NP itself—make up the essentially complicated composition of nanoparticles. The remarkable characteristics of these materials, such as their high surface-to-volume ratio, dissimilarity, sub-micron size, and improved targeting mechanism, have made them highly significant in interdisciplinary sectors. [1].

Deep tissue penetration of NPs has been shown to promote the increased permeability and retention (EPR) effect. Additionally, by successfully overcoming epithelial fenestration, the surface properties affect bioavailability and half-life. For instance, NPs coated with the hydrophilic polymer polyethylene glycol (PEG) reduce opsonization and evade immune system clearance. Additionally, by adjusting the properties of the particle polymer, the release

rate of medications or the active moiety can be optimized. All things considered, the unique characteristics of NPs control their therapeutic impact in the management and treatment of cancer. [1].

1.1.3NP Catalysis

The NPs come in a variety of sizes, shapes, and architectures. Many synthesis techniques are used in order to accomplish this. These techniques can be broadly divided into two categories: 1) a top-down strategy and 2) a bottom-up strategy. Based on operation and response conditions, these methods can be further divided into several subclasses (Fig. 2).

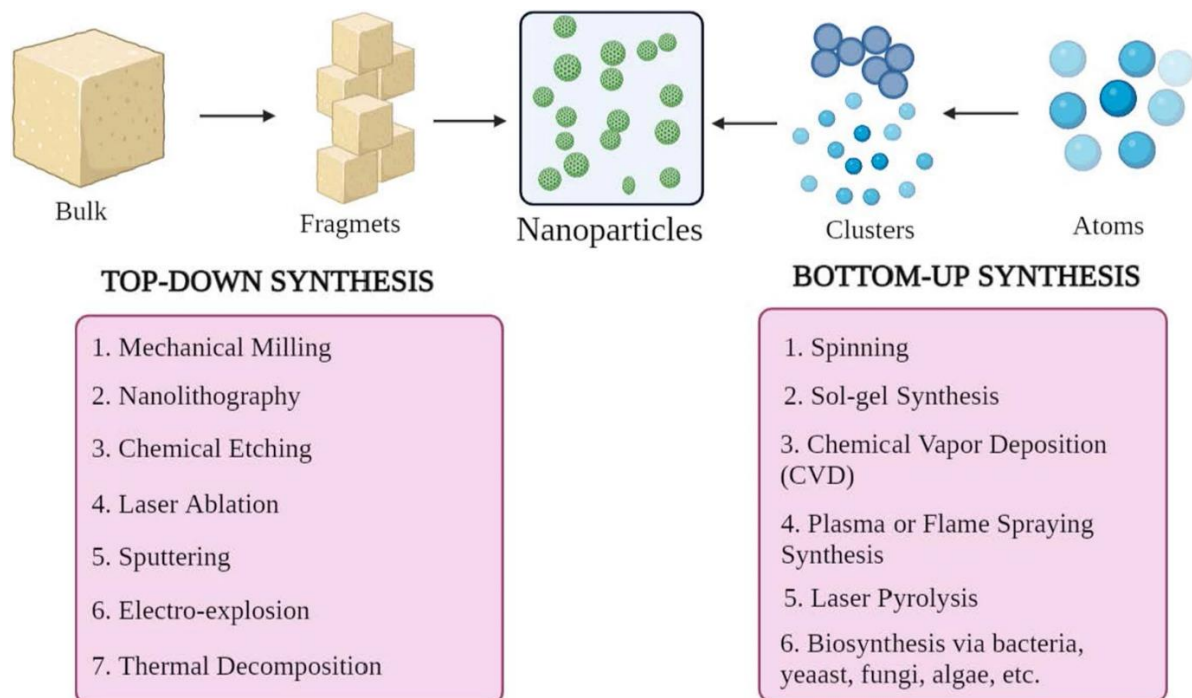


Figure2: Nanoparticles for Cancer Therapy: Current Progress and Challenges[1].

1.1.3.1From the bottom up Approach

This process is called the constructive technique since it builds material from atoms to clusters to NPs, or from simpler substances. Chemical vapor deposition (CVD), spinning, solgel synthesis, laser pyrolysis, plasma or flame spraying synthesis, and biosynthesis are a few of the often-employed techniques. [1].

1.1.3.2The Top-Down Method

The destructive approach, which creates NPs by reducing bulk material or substance, is another name for it. NPs are created when a bigger molecule decomposes or breaks down into smaller pieces . It encompasses methods including thermal breakdown, laser ablation, chemical etching, mechanical milling, nanolithography, sputtering, and electro-explosion. [1].

Remarkably, altering the reaction conditions and other synthesis parameters can change the morphological properties of NPs, including their size, shape, and charge . Furthermore, the chemical characteristics of NPs are also determined by the growth method. Therefore, it is crucial to comprehend the growth mechanism in order to synthesize the necessary NPs. [1].

1.1.4Cellular Targeting Mechanisms

The development or engineering of a medication or gene delivery system that has a superior ability to target tumor cells while preserving the normal, healthy cells is crucial for effective cancer therapy. By improving therapeutic efficacy, it protects healthy cells from cytotoxicity's effects. It can be accomplished by indirectly targeting cancer cells with the well-planned introduction of NPs into the tumor microenvironment (TME). These nanoformulations ought to be able to overcome a variety of biological and physiological obstacles. These barriers are intricate systems made up of multiple layers (cellular membranes, endothelium, and epithelium) and constituents (enzymatic, mechanical, and physicochemical barriers). To avoid unspecific targeting, these realities enforce requirements on the size, surface chemistry, and biocompatibility of NPs. However, an NP drug molecule does not necessarily reach its subcellular target just because it is internalized into the cytosol. It takes specific engineering and optimization to make cellular or nuclear targeting possible. [1].

To find NP-based medication targeting design, numerous studies have been conducted thus far, and more are being planned. Generally speaking, these nanocarriers should have the following basic properties: 1) the capacity to stay stable in the bloodstream until they reach the target, the tumor microenvironment (TME); 2) the ability to avoid clearance by the reticuloendothelial system (RES); 3) the ability to avoid the mononuclear phagocyte system (MPS); 4) the ability to accumulate in the TME through the tumor vasculature; 5) the ability to penetrate the tumor fluid at high pressure; and 6) the ability to reach the target and only interact with tumor cells. The process of NP drug targeting is regulated by critical elements such surface functionalization, physicochemical features, and pathophysiological traits. [1].

NPs with a diameter between 10 and 100 nm are typically thought to be suitable for treating cancer. The targeting mechanisms must be addressed in order to comprehend the process of interaction and crosstalk between NP carriers and cancer cells as well as tumor biology. The two main categories of targeting mechanisms are active targeting and passive targeting. [1].

1.1.4.1 Targeting Passively

In the late 1980s, it was discovered that a small number of macromolecules accumulated preferentially in cancer cells. Matsuura and Maeda revealed that poly (styrene-co-maleic acid)-neocarzinostatin (SMANCS) was the first macromolecule to accumulate in the tumor. According to additional research, this preferential distribution was explained by the presence of fenestrations in the damaged tumor blood arteries as well as inadequate lymphatic drainage; these two factors combined are referred to as the "enhanced permeation and retention effect."

The blood vessel's endothelial layer becomes more permeable in some circumstances, such as inflammation or hypoxia. In order to cope with hypoxia, the rapidly proliferating tumor cells often enlarge the existing blood vessels or create new ones. We call this process neovascularization. Due to their wide pores, these new blood vessels are leaky and have poor tumor blood vessel perm-selectivity when compared to normal blood vessels. Depending on the type of malignancy, TME, and location, these enormous pores, also known as fenestrations, can range in size from 200 to 2000 nm. NPs can spread from these blood vessels and eventually gather inside cancer cells due to the fast and flawed angiogenesis, which offers very little barrier to extravasation. Extracellular fluid (ECF) often drains into lymphatic capillaries in normal tissues at an average flow rate of 0.1–2 $\mu\text{m/s}$, which sustains continuous drainage and regeneration. There is little interstitial fluid uptake when a tumor forms because the lymphatic system is disrupted. Because they are not eliminated and are instead stored in the tumor interstitium, this characteristic aids in the retention of the NPs. The improved retention component of the EPR effect is indicated by this process. This unique characteristic does not apply to compounds that have a short half-life and are quickly removed from cancer cells. Encapsulating these tiny compounds in nanosized drug carriers is therefore frequently done to ameliorate such circumstances by improving their pharmacokinetics, offering tumor selectivity, and minimizing side effects. TME is an essential component of passive targeting over the EPR effect. Glycolysis is one of the key metabolic characteristics of tumor cells that are growing quickly. It is the primary source of energy for cell division and contributes to the acidity of the environment. The usage of pH-sensitive NPs, which release medications at low

pH, can take advantage of TME's decreased pH. We call this kind of tumor targeting "passive." Different tumor biology (vascularity, leakiness) and carrier properties (size and circulation duration) are the primary determinants of passive targeting. Certain tumor cell types do not have a particular ligand for this kind of tumor-targeting. Fundamental aspects of tumor biology, including 1) the degree or extent of angiogenesis and lymphangiogenesis, 2) the amount or degree of perivascular tumor invasion, and 3) intratumor pressure, are crucial for the EPR effect. The effectiveness of the NP drug delivery system is determined by these variables in conjunction with the physicochemical properties of NPs (Fig. 3). [1].

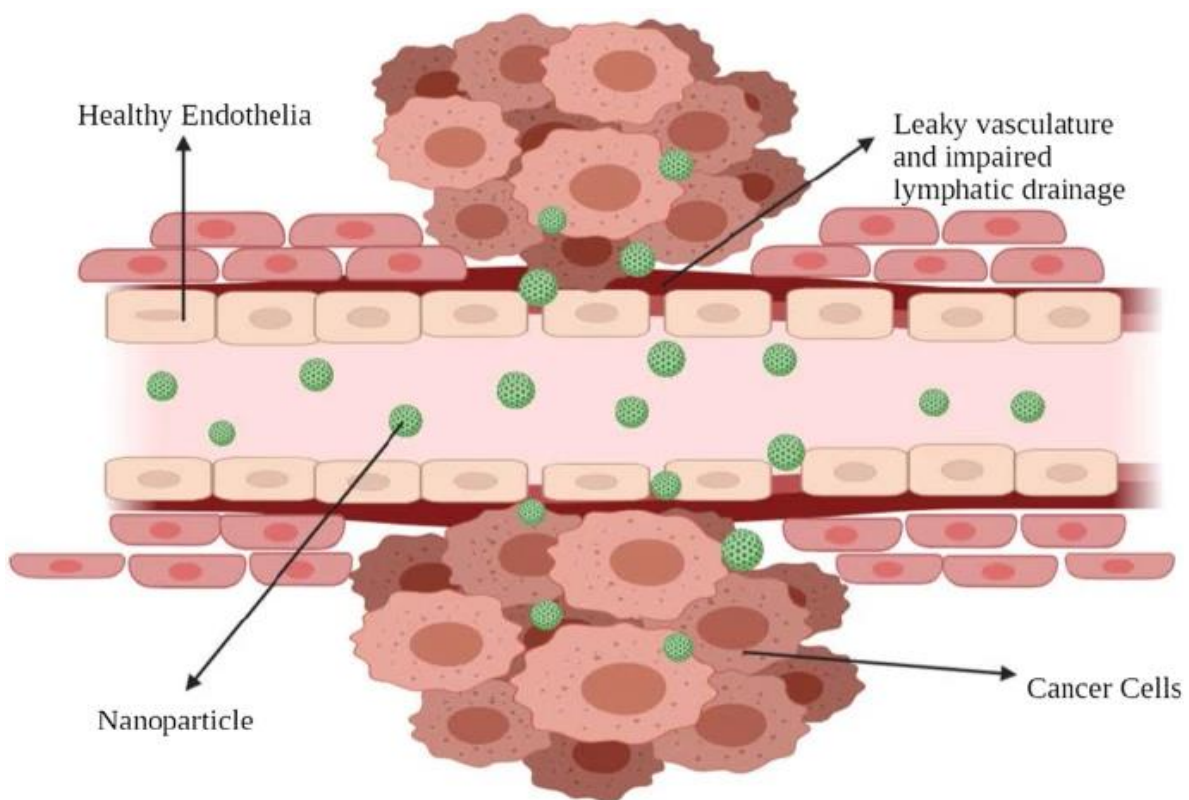


Figure3: Nanoparticles for Cancer Therapy: Current Progress and Challenges [1].

1.1.4.2 Passive Targeting Examples

One of the most effective pharmacological classes for treating cancer is taxanes. The effectiveness of paclitaxel against a variety of malignancies has been demonstrated. The most

often treated histologies using taxanes include ovarian cancer, breast cancer, and lung cancer (both small cell and non-small cell). Abraxane® (albumin-bound paclitaxel, Abraxis Bio-Sciences) was approved by the US Food and Drug Administration in 2005 and is used to treat advanced or metastatic breast cancer (MBC). An anti-microtubule medication called Abraxane® stabilizes microtubules by stopping depolymerization. It happens when the medication promotes tubulin dimer-based microtubule assembly. This increased stability prevents the rearrangement of microtubules, which is crucial for interphase and mitotic cellular processes. Paclitaxel, a commonly used taxane, causes a unique array of microtubules and numerous asters during the cell cycle and mitosis, respectively. In pancreatic cancer, Abraxane®, either by itself or in combination with another cytotoxic drug like gemcitabine, reduces the amount of pancreatic stroma. Models of xenografted mice. A novel paclitaxel and sterile lyophilized polymeric micellar formulation without CrEL is Genexol PM®. Trials showed that the maximum tolerated dosage (MTD) of Genexol PM® was three times greater in naked mice. Furthermore, the biodistribution showed two to three times higher amounts in many tissues, including the lung, kidney, spleen, and liver, and more pronouncedly in cancer cells. In South Korea, it is authorized to treat MBC. In the USA, phase II clinical research is still being conducted on it to treat pancreatic cancer. The anticancer drug DaunoXome® (liposomal daunorubicin; Gilead Science/Diatos) inhibits the development of malignant cells. The drug daunorubicin is the active ingredient. It is a special daunorubicin formulation (in liposome form) used to treat Kaposi's sarcoma, a kind of intestinal, lung, and skin cancer. This was authorized by the US FDA in 1996. While angiogenesis and neovascularization affect NP diffusion, they also increase interstitial pressure, which prevents NP buildup. Furthermore, because of the heterogeneous blood supply, the tumor cells grow irregularly; that is, cells near blood vessels divide more quickly than cells farther away or deep within the core, creating hypoxic or necrotic areas within the tumor. This irregular leakage slows down the neovascularization process, hinders medication transport and accumulation, and raises interstitial pressure. Nonetheless, the EPR effect can be managed chemically or mechanically. These include radiation, hyperthermia, bradykinin, nitric oxide, peroxynitrate, ultrasound, and VPF (vascular permeability factor). There are several restrictions and contraindications, though. [1].

1.1.4.3 Targeting Actively

Certain ligands or molecules, like as transferrin and folate, are necessary for active targeting because they attach to molecules or receptors that are either overexpressed or selectively

expressed on the target cells (diseased organs, tissues, cells, or subcellular domains) . The term "ligand-mediated targeting" refers to this kind of targeting . To increase affinity, the NPs with ligands that perform particular tasks, such retention and uptake, must be close to the target. By increasing the likelihood that NPs will bind to the cancer cell, this tactic improves drug penetration. Antibodies grafted onto the surface of liposomes in 1980 provided the first evidence of this , which was followed by a variety of ligands such as aptamers and peptides. Therefore, the primary approach is meant to. Therefore, the primary strategy aims to enhance the crosstalk between NPs and the target while maintaining the overall biodistribution. The target substrate receptors' ability to identify ligands is a crucial component of active targeting, also known as ligand-mediated targeting. Proteins, peptides, antibodies, nucleic acids, carbohydrates, and tiny compounds like vitamins are examples of illustrative ligands. Transferrin, folate, glycoproteins, and the epidermal growth factor receptor (EGFR) are the receptors that are most frequently researched. Through receptor-mediated endocytosis, ligand-target contact causes the membrane to infold and NPs to internalize. Active targeting occurs through a variety of ways. NPs generally target tumor cells for the majority of tumor-targeting.

The majority of tumor cells, particularly solid tumors, have been shown to overexpress these receptors, whereas healthy cells express them at lower levels. As a result, we can alter the NPs by adding ligands that target transferrin selectively. For example, transferrin is overexpressed in ovarian cancer cells A2780. Transferrin-modified PEG-phosphatidyl-ethanolamine (Tf-Mpeg-pe) NPs that target these cells specifically employ this property. Targeting cells like angiogenic endothelial cells that are next to cancer cells is an additional alternate strategy. Additionally, these cells are in close proximity to the blood arteries of the tumor. By cutting off the cancer cells' blood supply, this tactic enables the creation of hypoxia and necrosis. It has been discovered that the acidity of tumor tissues is higher than that of normal tissues. [1].

The Warburg effect has been used extensively to explain this. This explains why the metabolism of cancer cells switches to glycolysis, which produces lactic acid. The cell dies when the lactic acid builds up. In order to deal with this, the cells begin overexpressing proton pumps, which increase the acidity of the extracellular environment by pumping out excess lactic acid. Thus, a pH-sensitive drug delivery system based on liposomes has been investigated. The ligand-coated NPs' enhanced crosstalk with target cancer cells is a result of their multivalent nature. Such NPs are difficult to design since the ligand-target chemistry and NP architecture affect the whole method's effectiveness. Additional elements including the

administration method, physicochemical characteristics like ligand density , The success of the system is influenced by the size and shape of NPs (Fig 4). [1].

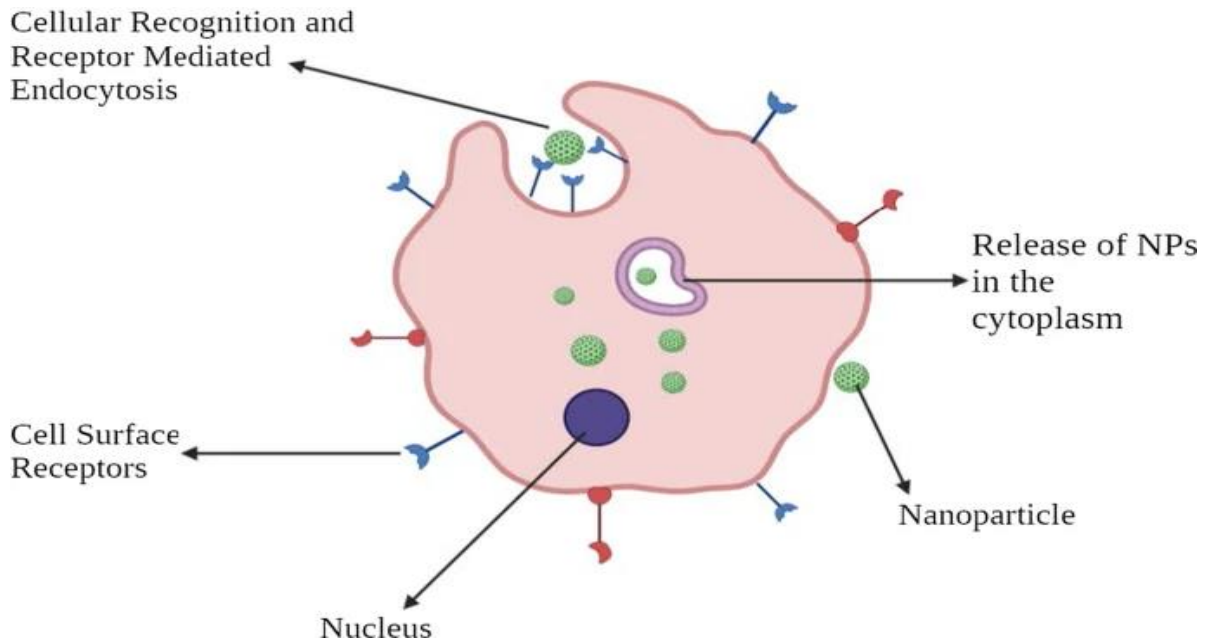


Figure 4.: Nanoparticles for Cancer Therapy: Current Progress and Challenges[1].

1.1.4.4 Active Targeting Examples

EGFR, a tyrosine kinase (TK) receptor belonging to the ErbB family, is overexpressed in many cancer forms, particularly those with squamous cell histology. The human SCC can be targeted by gold nanoparticles that contain anti-EGFR-PEG-AuNPs and anti-IgG-PEG-Au nanoparticles. A medication called Herceptin® targets the human EGF receptor-2 (HER2), which is overexpressed on the surface of breast cancer cells. PEGylated liposomal doxorubicin that targets HER2 was created to lessen cardiotoxicity, a known adverse consequence of anthracyclines. [1].

Vascular cell adhesion molecule-1 (VCAM-1) is a glycoprotein expressed on the surface of the tumor endothelium that plays a role in angiogenesis. In the breast cancer model, a study has identified NPs that target VCAM-1, suggesting a possible involvement for this protein. [1].

Vitamin B9, or folic acid, is essential for the synthesis of nucleotides. The folate receptor, which is expressed on cells, internalizes folic acid. On the other hand, liquid cancer cells overexpress FR- β , whereas tumor cells overexpress FR- α (alpha isoform of folate receptor) . NPs have been used to target the folate receptors in certain cancer treatments. [1].

Particles in Cancer Therapy: Organic, inorganic, and hybrid nanoparticles are all widely used in drug delivery systems (Fig5). [1].

NPs used extensively in drug delivery systems include organic NPs, inorganic NPs, and hybrid NPs.

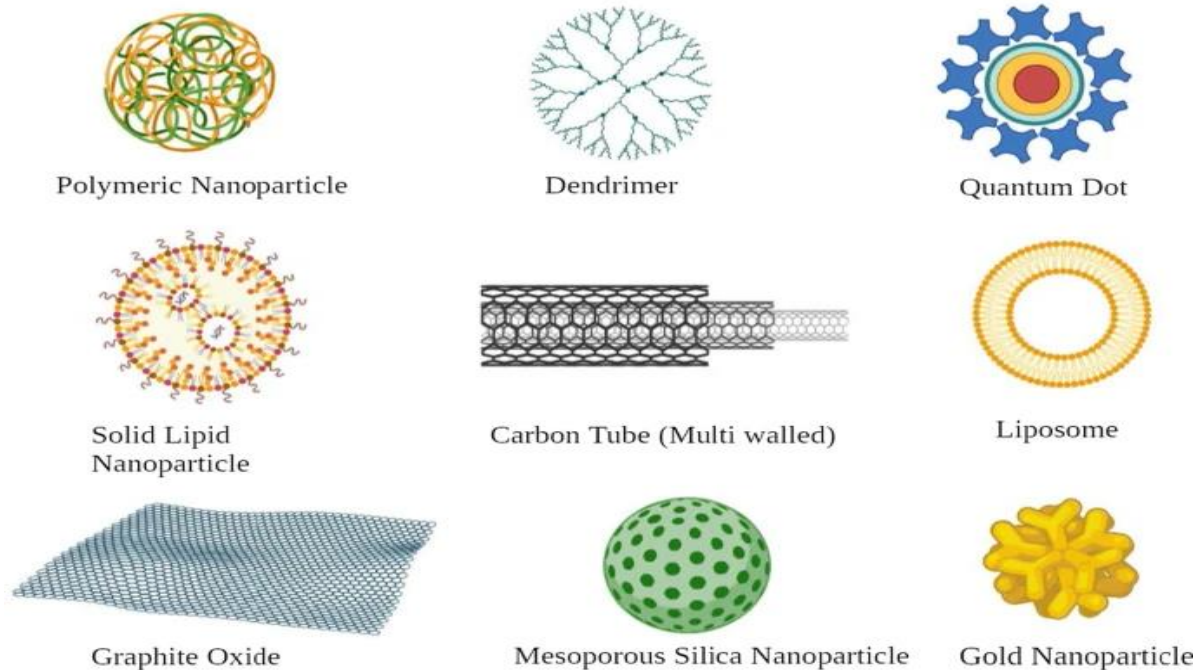


Figure5: Nanoparticles for Cancer Therapy: Current Progress and Challenges [1].

1.1.5 Nanoparticles of organic matter

1.1.5.1 Nanoparticles of polymers

A clear definition of polymeric nanoparticles (PNPs) is "colloidal macromolecules" with a particular structural configuration made up of several monomers. To accomplish controlled drug release in the target, the drug is either entrapped or bonded to the outside of NPs, forming a nanosphere or a nanocapsule. PNPs were originally composed of non-biodegradable polymers such polystyrene, polyacrylamide, and polymethylmethacrylate (PMMA). However, because it was difficult to remove them from the system, their accumulation resulted in toxicity. Nowadays, biodegradable polymers that are known to improve drug release and biocompatibility while lowering toxicity include polylactic acid, poly (amino acids), chitosan, alginate, and albumin. In a xenograft glioma model in rats, a study shown that indomethacin-loaded nanocapsules significantly reduced tumor growth and increased survival. With over 10 polymeric nanoparticles (NPs) containing anticancer medications undergoing clinical

development, this is a rapidly expanding sector. Examples include HPMA copolymer-DACH-platinate (AP5346), HPMA copolymer-platinate (AP 5280), HPMA copolymer-paclitaxel (PNU166945), PEG-camptothecin (Prothecan), Modified dextran-camptothecin (DE 310), and HPMA copolymer-doxorubicin galactosamine (PK2) [1].

Spherical polymeric macromolecules with a distinct hyperbranched structure are called dendrimers. Dendrimers are characterized by highly branching architectures. Usually, an ammonia core and acrylic acid react to start the synthesis of dendrimers. The "tri-acid" molecule created by this reaction subsequently combines with ethylenediamine to produce "tri-amine," a GO product. After further reacting with acrylic acid, this product yields hexa-acid, which in turn yields "hexa-amine" (Generation 1), and so on. The dendrimers' typical sizes fall between 1 and 10 nm. On the other hand, the size could be as much as 15 nm. These are utilized to target nucleic acids because of their unique structure, which has a predetermined molecular weight, charge, bioavailability, and changeable branching. [1].

Polyamidoamine (PAMAM), PEG (poly(ethyleneglycol)), PPI (polypropylenimine), and TEA (triethanolamine) are a few common dendrimers. Originally, a PAMAM dendrimer was intended to do MDR management. Numerous descriptions of DNA-assembled PAMAM dendrimers exist. The produced dendrimers considerably slowed the growth of epithelial cancer xenografts as compared to mice given single-agent chemotherapy. [1].

Because of their unique targeting capabilities, monoclonal antibodies are frequently utilized in the therapy of cancer. NPs and these mAb are now mixed to create antibody–drug conjugates, or ADCs. Compared to cytotoxic medications or mAb alone, these have been shown to be far more compelling and specific. For example, in the control of HER2 positive breast epithelial cells, an antibody–drug NP with a paclitaxel core and a surface modified with trastuzumab demonstrated superior anti-tumor activity and reduced toxicity compared to either paclitaxel or trastuzumab alone. [1].

Double-layered phosphor-lipid vesicles with a size range of 50–1000 nm are known as extracellular vehicles (EVs). Different cell types continuously release EVs, which differ in size, content, and place of origin. Exosomes, microvesicles, and apoptotic bodies are the three categories into which EVs are separated. Because NPs and exosomes share many lipids and chemicals with their original cells, they are frequently employed together. [1]. Additionally, they swiftly internalize within the cancer cells and evade immune surveillance. By transporting cytotoxic medications and other anti-tumor medications to the intended locations, they serve

as organic carriers. The best example is exosomes loaded with doxorubicin (exoDOX). By increasing cytotoxicity and preventing cardiotoxicity, exoDOX has demonstrated superior outcomes than doxorubicin, a conservative treatment for breast cancer. Compared to synthetic NPs, exosome NPs have superior intracellular communications, enhanced chemical stability, and inherent biocompatibility properties. However, there are significant issues that must be resolved, such as the lack of standard conditions for exosomal isolation and purification. [1].

1.1.5.2 Nanoparticles of solid lipids (SLN)

A phospholipid monolayer, an emulsifier, and water make up these colloidal nanocarriers, which range in size from 1 to 100 nm. These are referred to as nanomaterials with zero dimensions. Triglycerides, fatty acids, waxes, steroids, and PEGylated lipids are examples of the lipid component. The medication is confined in a non-aqueous core of SLNs, which have a "micelle-like structure" in contrast to traditional liposomes. Mitoxantrone-loaded SLN is one example, which has demonstrated improved bioavailability and decreased toxicity. Positive outcomes have been observed when SLN incorporates doxorubicin and idarubicin into "P388/ADR leukemia cells" and the "murine leukemia mouse model." [1].

1.1.5.2.1 Nano-emulsions

Colloidal NPs with diverse oil droplet mixes in aqueous media that range in size from 10 to 1000 nm are known as nanoemulsions. It is possible to create three typical kinds of nanoemulsions in: Bi-continuous nanoemulsions, 1) water-in-oil systems, and 2) oil-in-water systems. Numerous studies have been conducted on membrane-modified nanoemulsions. For example, by controlling immunity via TLR4/NF- κ B signaling pathways, nanoemulsions containing spirulina and paclitaxel demonstrated an enhanced anti-tumor activity. It is known that metastatic melanoma can be treated with a nanoemulsion of rapamycin, bevacizumab, and temozolomide. In contrast to liposomes, nanoemulsions undoubtedly possess superior properties, including stability, optical clarity, and biodegradability. [1].

1.1.5.2.2 Cyclodextrin Nanoparticles

Typically, cyclodextrins are employed as stabilizers to boost NPs' ability to load drugs. Nanosponges are microscopic structures that resemble meshes. In MCF-7 cell line culture, β -cyclodextrin nanosponges loaded with paclitaxel have demonstrated good cytotoxic effects. Similarly, using cyclodextrin-based nanosponges in the formulation of camptothecin has demonstrated increased solubility and stability. [1].

1.1.6 Nanoparticles that are inorganic

1.1.6.1 Nanoparticles of carbon

As the name implies, carbon nanoparticles are based on the element carbon. Their optical, mechanical, and electrical qualities, along with their biocompatibility, have led to their extensive usage in medical fields. Because carbon nanoparticles are naturally hydrophobic, they can encapsulate medications using π - π stacking. Graphene, carbon nanotubes, fullerenes, carbon nanohorns, and graphyne are other classifications for carbon nanoparticles. Despite being carbon-based, these differ in terms of their morphology, structure, and characteristics. [1].

"Graphene" is a two-dimensional crystal with a sp^2 -hybridized carbon sheet that has exceptional drug-loading, mechanical, and electrochemical qualities. Furthermore, graphene can be separated into the following categories according to its composition, properties, and composition: Graphene oxide (GO), reduced graphene oxide (rGO), single-layer graphene, and multi-layer graphene are the four types of graphene [93]. Because GO and rGOs can target hypoxia [94] and irregular angiogenesis in TME [95], they are frequently employed. Research has demonstrated that in cellular models of breast cancer, GO-doxorubicin demonstrates stronger anticancer properties. [1].

Large carbon-cage molecules known as fullerenes are made up of carbon allotropes with various conformations, including ellipsoids, tubes, and spheres. Because of their common structural, physical, chemical, and electrical characteristics, they are the most extensively researched nanocarriers. Because of its triple yield, extended π -conjugation, and capacity to absorb light, they are employed in photodynamic treatment. They also produce oxygen species. Fullerenes treated with PEG demonstrated encouraging photodynamic effects on tumor cells. [1].

The late 1980s saw the discovery of carbon nanotubes (CNTs), which are cylindrical tubes that are most frequently thought of as rolls of graphene. They are divided into two categories: 1) CNTs with a single wall and 2) CNTs with many walls. Because they are carbon-based, they can interact with immune cells to trigger an immunological response, which will stop the growth of tumors. They have historically been employed in thermal ablation therapy and as vectors for the transfer of DNA. To target colon cancer cells, for example, a fluorescent single-walled CNT containing doxorubicin encapsulated in mAb is utilized. These CNTs combine to

form a compound that the cancer cells may successfully absorb, releasing doxorubicin intracellularly while the CNTs remain in the cytoplasm. [1].

1.1.6.2 Nanoparticles of metal

Because of their exceptional optical, magnetic, and photothermal characteristics, metallic nanoparticles are frequently investigated in "biological imaging" and targeted DDS. Iron-based NPs, copper NPs, silver NPs, and gold NPs are some of the most widely utilized metallic NPs. Due to their easily controllable size and surface characteristics, gold nanoparticles are utilized as intracellular targeted drug carriers. Furthermore, NP trajectories within the cells may be tracked because to their visible light extinction behavior. It has been demonstrated that "anti-HER2 functionalized gold-on-silica nanoshells" target breast cancer cells that are HER2 positive. The iron oxide nanoparticle formulation Combidex® is currently undergoing late-stage clinical testing to identify nodal metastases. The iron oxide nanoparticle formulation Combidex® is currently undergoing late-stage clinical testing to identify nodal metastases. Iron-deficiency anemia is treated with Feraheme®, a formulation of iron oxide NP that contains ferumoxytol. This was licensed by the FDA in June 2009 and is also used to treat nodal metastases in testicular and prostate cancer. [1].

1.1.6.3 Nanoparticles that are magnetic

Metal or metal oxides are included in medication delivery, and magnetic nanoparticles are typically utilized in MRI imaging. To improve stability and biocompatibility, they are typically coated with organic materials such as polymers and fatty acids. Breast cancer can be effectively targeted and imaged with LHRH-conjugated superparamagnetic iron oxide nanoparticles. To further thermally ablate cancer cells, magnetic nanoparticles are employed in magnetic hyperthermia. Feridex® and Resovist® are two examples of magnetic nanoparticles that are available on the market or undergoing clinical trials for colon cancer and liver metastases. Calcium Phosphate Nanoparticles "NPs" are biodegradable, compatible with biology, and do not have any severe side effects. As a result, they are employed as a delivery system for growth hormones, insulin, antibiotics, and birth control. They are also employed in plasmid DNA and oligonucleotide delivery. In cellular gene transfer, calcium phosphate nanoparticles in combination with either a viral or non-viral vector have proven to be effective delivery vehicles. Calcium and glycerol in a "liposomal nanolipoplex formulation" have demonstrated improved transfection characteristics and reduced toxicity. Nanoparticles of Silica [1].

Only lately has silica been researched in relation to biology, despite being an important component of many natural materials. By functionalizing the NP surface with amino-silanes, silica nanoparticles are frequently employed to transport genes. Commercially accessible, N-(6-aminohexyl)-3-aminopropyl-trimethoxysilane functionalized silica nanoparticles have demonstrated exceptional transfection efficiency of Cos-1 cells with low toxicity. Because of their superior pharmacokinetic characteristics, mesoporous silica nanoparticles are regarded as one of the best drug carriers. Immunotherapy has made great use of them. A study found that mesoporous silica nanoparticles loaded with camptothecin were successfully absorbed by colorectal cancer cells. [1].

1.1.6.4 Nanoparticle Benefits for Cancer Treatment

A new era in cancer diagnosis, therapy, and management has been ushered in by the application of nanotechnology. NPs increase the intracellular concentration of medications while preventing toxicity in healthy tissue through active or passive targeting. To create and control the drug release, the targeted NPs can be modified to be either pH-sensitive or temperature-sensitive. Drugs can be delivered within the acidic TME via the pH-sensitive drug delivery system. In a similar manner, temperature changes introduced by sources like as magnetic fields and ultrasonic waves cause the temperature-sensitive NPs to release the medications at the desired location. Furthermore, the targeted drug delivery mechanism is significantly influenced by the "physicochemical characteristics" of NPs, including their size, shape, molecular mass, and surface chemistry. Additionally, NPs can be utilized to target a specific moiety and can be altered based on the target. immunological cells, including macrophages. When the medications interact with MPS in the liver, spleen, or lungs, they trigger "macrophages or leukocytes," which quickly eliminate the drug. The drug's half-life is shortened as a result. NPs with "surface modification," like PEG, go around this mechanism and lengthen the "drug half-life" in order to get around this. Furthermore, renal infiltration is an essential bodily function. Thus, appropriate renal infiltration reduces the toxicity that NPs induce. A unique protective mechanism called the brain-blood barrier (BBB) is designed to shield the central nervous system (CNS) from poisonous and dangerous substances. The wall-like arrangement of "brain capillary endothelial cells" gives the brain vital nourishment. The BBB's main job is to prevent harmful substances from entering the brain, hence the only chemotherapy treatments for brain cancer that are now available are intraventricular or intracerebral infusions. NPs are known to cross the BBB, though. NPs are now delivered by a variety of techniques, including transcytosis, peptide-modified endocytosis, focused ultrasound, and the EPR effect. In rats,

glutathione PEGylated liposomes containing methotrexate demonstrated enhanced absorption of the drug. Since Au-NPs have been shown to aid in the transport of medications that cause apoptosis, they are frequently employed. As carriers, NPs also improve drug stability by keeping the encapsulated cargo from degrading. Furthermore, many medications can be encapsulated without undergoing a chemical reaction. Compared to nanoliquid formulations, dry solid dosage forms are more stable. To improve stability, stabilizers can be applied. Using porous nanoparticles is yet another method to improve stability. [1].

Because of their unequal distribution and cytotoxicity, conventional chemotherapy and radiation therapy have a number of drawbacks in terms of effectiveness and adverse effects. As a result, careful dosage that efficiently destroys cancer cells without causing severe damage is needed. The medication must cross multiple fortifications in order to reach the target spot. The process of drug metabolism is quite intricate. The medication must cross the TME, RES, BBB, and renal infiltration under physiological conditions. The macrophage system, or RES, is composed of "blood monocytes, [1].

Extensive angiogenesis, faulty vascular architecture, and impaired lymphatic drainage are some of the distinctive pathophysiological characteristics of tumors. These characteristics are used by the NPs to target tumor tissue. NPs are efficiently maintained in tumor tissue because to the low lymphatic clearance and decreased venous return. EPR is the name given to this occurrence. Similarly, tumor-targeting can be achieved by focusing on the surrounding tissues. There are numerous ways to give NPs, including intraocular, parenteral, nasal, and oral. NPs have a high intracellular uptake and surface-to-volume ratio. According to studies, NPs work better as drug transporters than microparticles [1].

1.1.7 Overview of Breast Cancer

In the United States, breast cancer is the second leading cause of cancer-related deaths among women and the most common cause of cancer overall [3].

The term "breast cancer" describes malignancies that start in breast tissue, usually the lobules that provide milk to the ducts or the inner lining of the milk ducts [3].

Breast cancer is the second most prevalent type of non-skin cancer (after lung cancer) and the fifth most common cause of cancer-related deaths worldwide, accounting for 10.4% of all cancer incidences among women. 519,000 people died from breast cancer globally in 2004 (about 1% of all fatalities; 7% of cancer deaths). Women are almost 100 times more likely

than men to develop breast cancer, although men typically fare worse because of delayed detection [3].

The DNA and RNA of cancer cells are similar, but not identical, to those of the cells of the original organism. This explains why the immune system, especially if it is compromised, does not frequently identify them [3].

When DNA and/or RNA are altered or mutated, cancer cells are created from healthy cells. The Law of Thermodynamics (increase of entropy) may cause these changes or mutations on their own, or they may be brought on by nuclear radiation, electromagnetic radiation (microwaves, X-rays, gamma-rays, ultraviolet-rays, etc.), viruses, bacteria, and fungi, parasites (because of tissue inflammation or irritation), heat, chemicals in the air, water, and food, mechanical cell-level injury, free radicals, evolution and aging of DNA and RNA, etc.). All of these have the potential to cause mutations that could lead to cancer [3].

If the immune system is malfunctioning and/or the number of cells created is too high for the immune system to eradicate, cancer will develop. Certain factors, such as an unfavorable environment (caused by radiation, toxins, etc.), a bad diet (causing an unhealthy cell environment), individuals with genetic predispositions to mutations, and advanced age (over 80), can cause an excessively high rate of DNA and RNA mutations [3].

1.1.7.1 The cycle of cells

The process of cell division is disturbed and uncontrolled in malignant cells, which leads to tumor formation and cell proliferation. Figure 1 illustrates the typical cell cycle.

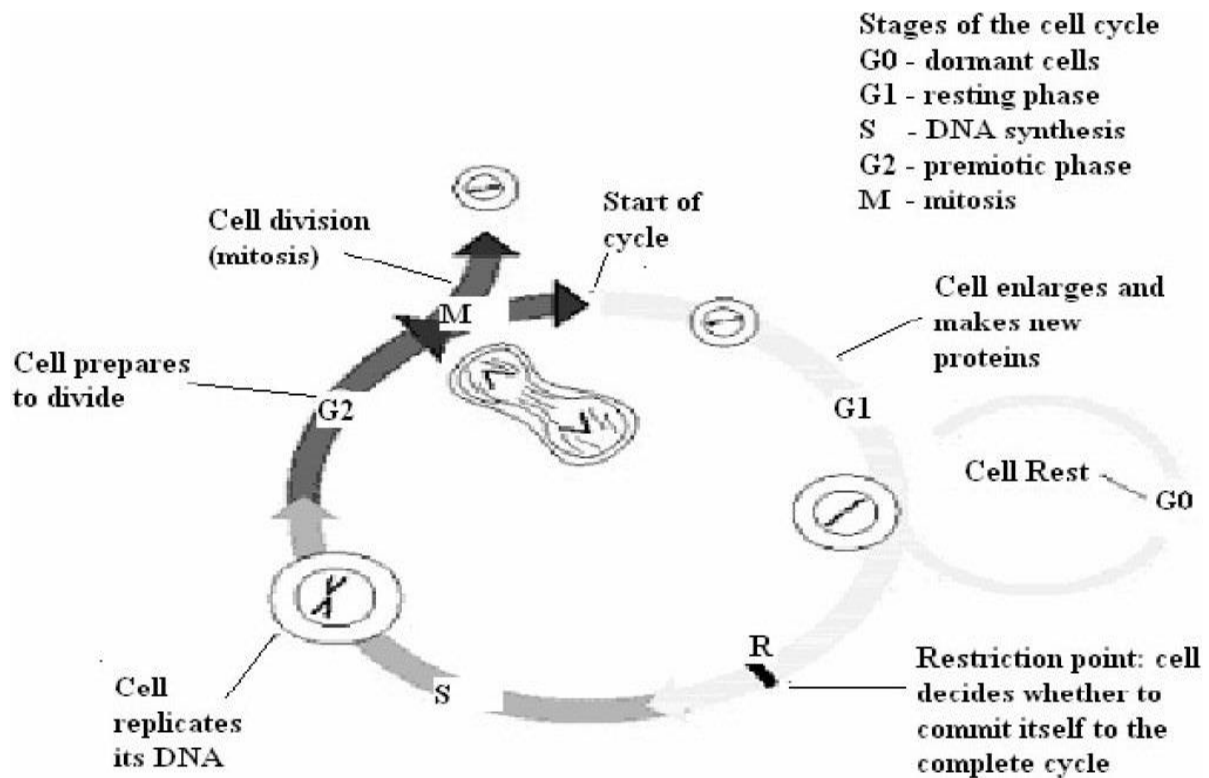


Figure6: Stages of normal cell cycle

Usually, cancer is termed by the body part in which it originated; thus, breast cancer refers to the irregular development and proliferation of cells that originate in the breast tissue [3].

The two primary tissue types that make up the breast are glandular tissues and stromal (supporting) tissues. The ducts (the milk channels) and the lobules (the milk-producing glands) are located in glandular tissues, whereas the stromal tissues comprise the breast's fatty and fibrous connective tissues. Additionally, the immune system's lymphatic tissue, which eliminates waste products and cellular fluids, makes up the breast [3].

Different parts of the breast might develop an assortment of tumor forms. The majority of tumors are caused by benign (non-cancerous) breast alterations. For instance, fibrocystic change is a non-cancerous disorder that causes lumpiness, areas of thickening, soreness, or breast pain, fibrosis (development of scar-like connective tissue), and cysts (accumulated packets of fluid) in women. [3].

The cells lining the ducts are where the majority of breast malignancies start (ductal tumors). A tiny percentage start in other tissues, but some (lobular cancers) start in the cells lining the lobules. [3].

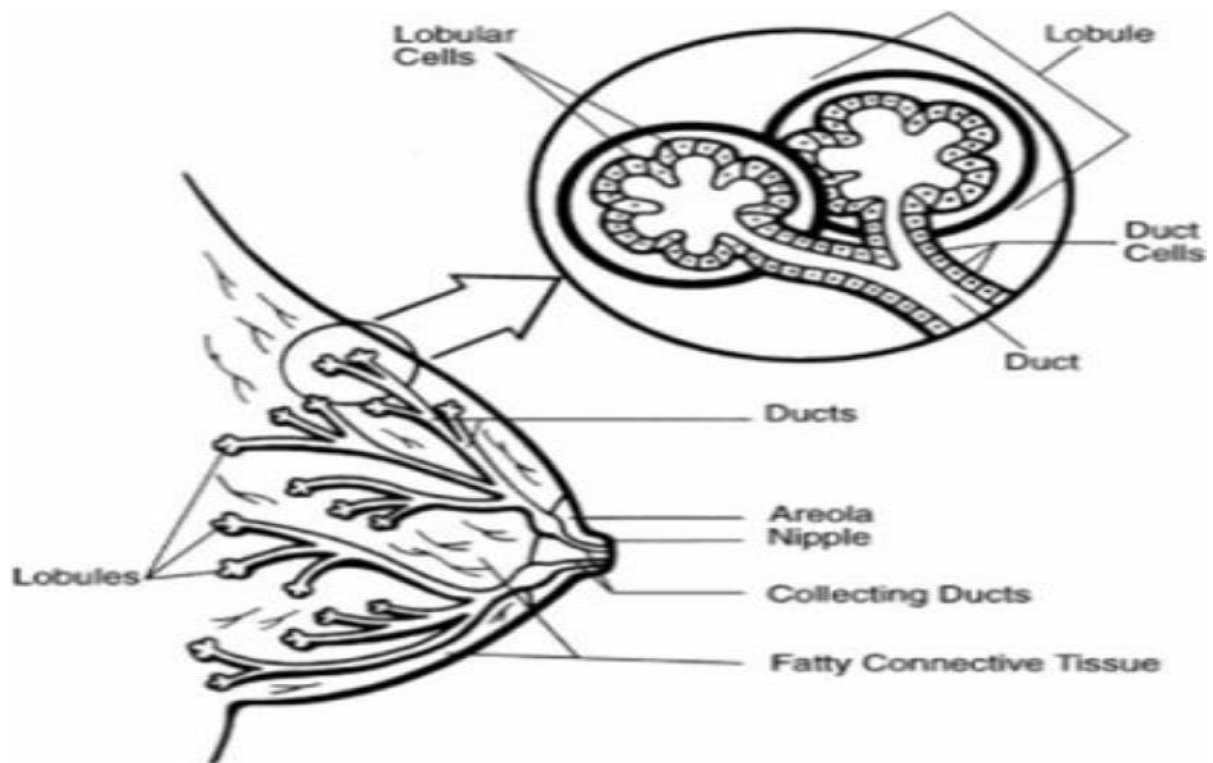


Figure7: Structure of breast

1.1.8Breast Cancer Types

According to the site, non-invasive breast cancer cells are limited to the ducts and do not spread to the breast's surrounding connective and fatty tissues. Ninety percent of non-invasive breast cancers are ductal carcinoma in situ (DCIS). Less frequently occurring, lobular carcinoma in situ (LCIS) is thought to be a sign of an elevated risk for breast cancer [3].

Cells of invasive breast cancer penetrate the surrounding fatty and connective tissues of the breast after penetrating the duct and lobular wall. It is possible for Oancer to be invasive without spreading to other organs or lymph nodes [3].

1.1.8.1Breast cancer is a common condition.

Lobular neoplasia or lobular carcinoma in situ (LCIS): Cancer that has not spread outside of the original site is referred to as "in situ." LCIS is characterized by a substantial increase in the number of cells in the breast's milk glands, or lobules [3].

The most prevalent kind of non-invasive breast cancer, ductal carcinoma in situ (DCIS), is limited to the breast's ducts. Take ductal comedocarcinoma, for instance [3].

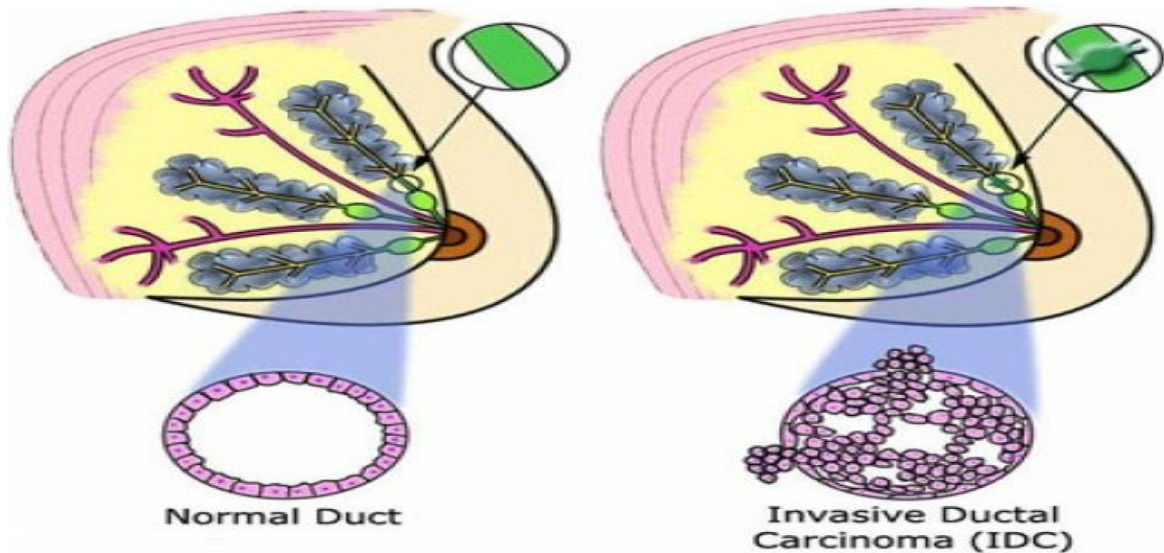


Figure 8: Typical Structure associated with ductal carcinoma

Another name for ILC is invasive lobular carcinoma. ILC starts in the breast's milk glands, or lobules, but it frequently metastatically spreads to other parts of the body. Ten to fifteen percent of breast cancers are caused by ILC [3].

Invasive ductal carcinoma is another name for infiltrating ductal carcinoma (IDC). IDC starts in the breast's milk ducts and spreads through the duct wall, entering the breast's fatty tissue and maybe other body parts. 80% of breast cancer diagnoses are IDC, making it the most prevalent kind of the disease [3].

1,1,8,2Less frequent Cancer of the breast

Medullary cancer: An invasive breast cancer that creates a clear separation between tumor and healthy tissue is called medullary carcinoma. Medullary carcinoma accounts for just 5% of all breast cancers [3].

Mutinous carcinoma: Also known as colloid carcinoma, mutinous carcinoma is an uncommon type of breast cancer that is created by cancer cells that produce mucus. The prognosis for women with mutinous carcinoma is typically better than that of women with more prevalent forms of invasive carcinoma [3].

One particular kind of infiltrating (invasive) breast cancer is tubular carcinoma. The prognosis for women with tubular carcinoma is typically better than that of women with more prevalent forms of invasive carcinoma. About 2% of cases of breast cancer are tubular carcinomas [3].

1.1.8.3 Breast cancer caused by inflammation

Cancer cells obstructing lymph veins or channels in the epidermis covering the breast can result in inflammatory breast cancer, which manifests as red, heated breasts with dimples and/or thick ridges. Despite making up only 1% of all breast cancers, inflammatory breast cancer grows incredibly quickly [3].

1.1.8.4 Nipple illness caused by Paget's

About 1% of breast cancers are Paget's disease of the nipple, a rare type of breast cancer that starts in the milk ducts and spreads to the nipple and areola skin [3].

1.1.8.5 Tumor of Phylloides

There are two types of Phylloides tumors: benign (non-cancerous) and malignant (cancerous). Phylloides tumors can be surgically removed; they form in the breast's connective tissues. Phylloides tumors are extremely uncommon; in the US, less than ten women lose their lives to this kind of breast cancer annually [3].

1.1.9 Causes of breast cancer

1- A prior history of breast cancer

Breast cancer in the other breast is more likely to occur in a woman who has already had breast cancer [3].

2-Important family background

The patient may be at higher risk of having breast cancer if multiple family members have had specific cancers. [3].

3-genetic reasons

Breast cancer risk has long been associated with family history. Paternal and maternal relations are both significant. The risk is higher if the affected relative is a close relative, had cancer in both breasts, or had breast cancer when she was young. When assessing risk, first-degree relatives—mother, sister, and daughter—are crucial. An increased risk may also result from having multiple second-degree relatives with breast cancer, such as an aunt or grandmother. When a man has breast cancer, all of his close female relatives are at higher risk.

When inherited, the aberrant genes BRCA1 and BRCA2 significantly raise the lifetime risk of breast cancer to an estimated 40–8% [3].

4-Hormonal factors

Breast cancer may develop as a result of a change in hormonal levels. It may be addressed by the onset and cessation of menstruation (the menstrual cycle), early pregnancy, hormone replacement treatment, oral medication use, etc. [3].

5-Dietary and lifestyle factors

Breast cancer may result from a sedentary lifestyle, a high fat intake, and obesity, especially in postmenopausal women. Another factor contributing to breast cancer is alcohol consumption. The more alcohol drunk, the higher the danger. Women who drink between two and five drinks a day are approximately 1.5 times more likely to acquire breast cancer than those who do not drink. [3].

6-environmental factor

Women who deal with low doses of radiation for extended periods of time, such as X-ray technicians, are known to be slightly more at risk [3].

7-Symptoms and indicators

A lump in the breast or armpit is the classic sign of breast cancer. One excellent method to become familiar with the texture, size, cyclical changes, and skin condition of the breasts is to perform a monthly breast self-examination (BSE). Breast cancer can be identified by its general warning signs, which include breast swelling or lump (mass), swelling in the armpit (lymph nodes), clear or bloody nipple discharge, nipple pain, inverted (retracted) nipple, scaly or pitted skin on the nipple, persistent breast tenderness, and unusual breast pain or discomfort. [3].

A considerable amount of cancer-related morbidity and mortality is caused by breast cancer, which is the most prevalent cancer among women globally. Disparities in results continue to exist among various demographics and geographical areas, although advancements in early identification and treatment [3].

1.1.10 Importance of Nanoparticles in Cancer Treatment

Nanoparticles greatly enhance cancer treatment drug delivery methods. They lessen toxicity to healthy tissues while improving the precision of therapeutic targeting to malignancies. This is essential for reducing the negative effects of conventional cancer treatments [4].

For the treatment of neoplasia, a drug delivery method based on nanoparticles appears to have promise. Longer drug and protein half-lives, improved solubility of lipophilic medications, and the ability to precisely and carefully release the treatment into the affected area are some of the ways it exhibits enhanced efficacy. The primary advantage of nanoparticle-based drug delivery systems is their ability to treat malignancies. Additionally, angiogenesis was considered as a treatment option for malignancies [5].

1.1.11 Gold

The chemical element gold is symbolized by the symbol Au. Despite its high atomic number (79), gold is a naturally occurring element. With the exception of aqua regia, which has strong resistance to oxidation and corrosion even at high temperatures, this noble metal is unaffected by most acids. Because of these properties, it is a precious metal with unique chemical and physical properties that set it apart from most other metals [6].

Because gold is nonreactive, does not change in the atmosphere, and retains its attractive color, it has been used for medical and aesthetic reasons in jewelry since ancient times. The Lycurgus Cup, made of glass covered with secondary alloys of gold and silver that change color when exposed to light, is an example of how the Romans used gold during the Middle Ages. Until Michael Faraday first demonstrated that the color is due to the small size of the gold and silver particles, the reason for this effect and the color difference remained unknown [6].

Since ancient times, artists have used colloidal gold to create bright hues through its interaction with visible light. These special properties have been studied and applied in high-tech applications such as electronic conductor's acoustic cells, sensory sensors, and therapeutic agents [6].

Because of its chemical inertness, gold as a free metal has offered only limited options for study. Due to its interesting physical, chemical and optical properties - such as chemical stability, low toxicity and ease of synthesis - gold has been used at the nanoscale as a result of the explosive growth in nanotechnology in the late 20th century. As a result, gold nanoparticles

have become one of the most researched topics and have found use in all fields of science as well as in medical and biological applications. As a platform for targeted drug delivery and in radiotherapy enhanced by gold nanoparticles, in addition to their antifungal, anti-inflammatory, antioxidant and anticancer properties, demonstrated that gold nanoparticles have helped solve many fundamental problems, especially in the fields of medicine and pharmacology [6].

1.1.12 Gold Nanoparticles (AuNPs)

Since nanoparticles can be used in a variety of industries due to their shape, size, and surface plasmon resonance (SPR), researchers have become increasingly interested in their synthesis. nanoparticles are used in photocatalysis, chemistry textiles, cancer therapy, pharmaceuticals, and water treatment. By 2026, worldwide sales of metallic nanoparticles may exceed \$50 billion due to their importance and wide range of uses [6].

Historically, nanoparticles have been produced using conventional physical and chemical techniques. The particles produced using these techniques are uniform in size and shape and are characterized by their purity, despite the fact that they require a record amount of time. These techniques are expensive, difficult and somewhat complex, and require a lot of heat and energy in addition to stabilizing agents, reagents and hazardous chemicals such as thiols and aromatic amines that pollute the environment and cause cancer. As a result, their use in biological and medical applications is limited [6].

Secondary gold nanoparticles have been of great importance in the field of medicine and pharmacy and have been used for diagnostic and therapeutic purposes, but the use of chemical and physical methods that involve the use of toxic chemicals that adhere to gold nanoparticles as coating particles makes them undesirable in the field of pharmaceutical applications, which called for the discovery of new reliable methods for their application in these important fields using biomolecules as reducing and encapsulating agents that affect the size and shape of gold nanoparticles, the biosynthesis of secondary gold nanoparticles has become an important and promising alternative as a green, environmentally friendly economical and efficient process. Gold nanoparticles are natural materials that are safe for use in medicine and therapy because they do not harm human cells [6].

1.1.13 The importance of *Annona muricata* seed extract

Annona muricata, generally known in English speaking nations as soursop and ebo in Yoruba, is an erect, low-branching tree reaching 8 to 10 meters. The tree has green, glossy evergreen leaves, and the blossoms appear anywhere on the trunk or any branch. The leaves have historically been used as an anti-inflammatory, anti-spasmodic, and anti-dysenteric remedy for headaches, insomnia, cystitis, liver issues, diabetes, and hypertension. Different plant parts, such as the leaves, bark, and roots, have been used to treat diseases like diabetes in the West Indies. *Annona muricata* is used for its anti-inflammatory, antinociceptive, antibacterial, and antifungal properties as well as its anticancer properties. According to reports, the plant contains acetogenins, which are important phytoconstituents that have a variety of anticancer, immunomodulatory, anti-spasmodic, anti-malarial, pesticidal, anti-parasitic, anti-bacterial, anti-fungal, and antihelminthic properties [7].

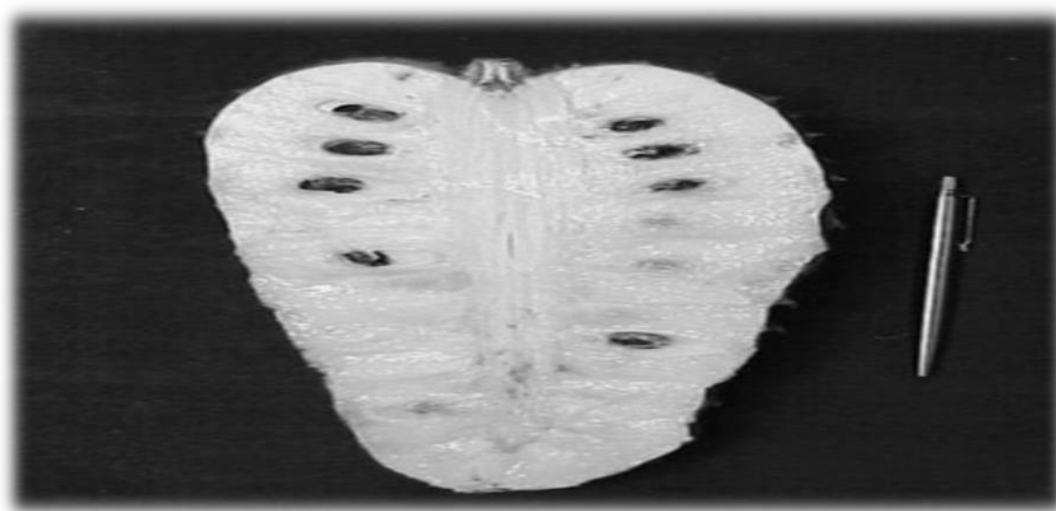


Figure 9: Custard apple seeds. [8]

Bioactive substances with strong antioxidant activity found in *Annona muricata* seeds can aid in the fight against oxidative stress and associated illnesses [9].

Additionally, the seeds have antibacterial qualities, working well against a range of bacterial types, while they have little effect on bacteria that are resistant to many drugs [10].

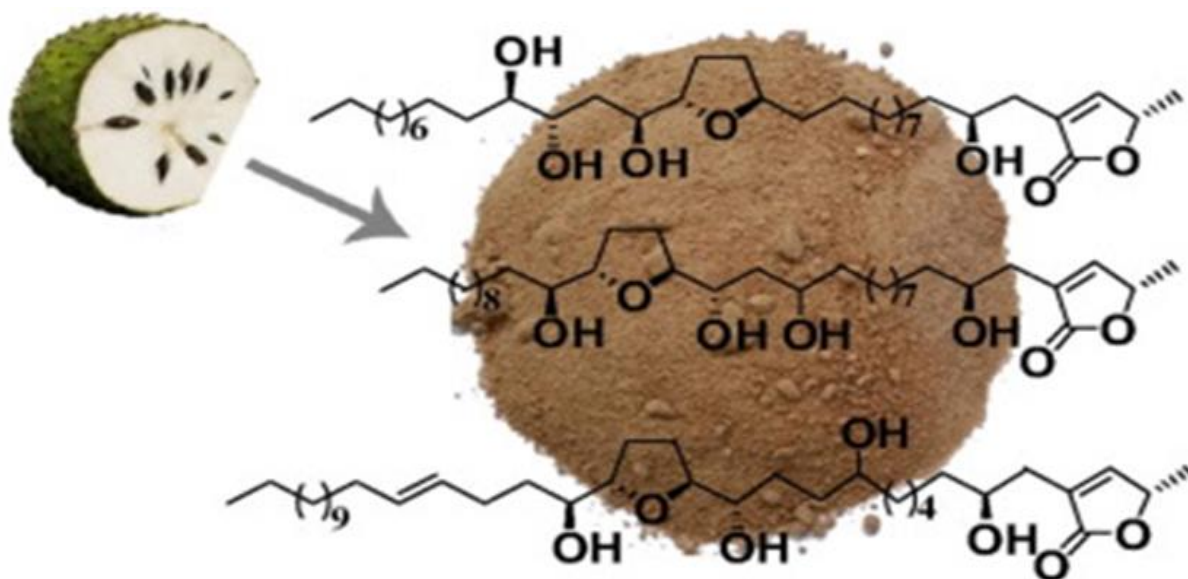


Figure (10): *Annona muricata* Date. [11]

Phytochemical studies of different parts of graviola. Phytochemical analyzes revealed that graviola is rich in anaerobic acetogenin. However, its chemical composition varies between organs. More than 100 of these compounds have been isolated from various organs *A. muricata* and have been identified as the major bioactive components of graviola. Odorless acetogenins are a unique class of C-35/C37 secondary metabolites derived from long-chain fatty acids (C-32/C34) via the polyketide pathway. They usually consist of a mixture of acids. It is characterized by a 2-propanol unit at C-2, which forms... α -methyl-substituted lactone, β -Unsaturated. However, cortical acetogenins are generally waxy and difficult to handle due to their poor solubility in water [12].

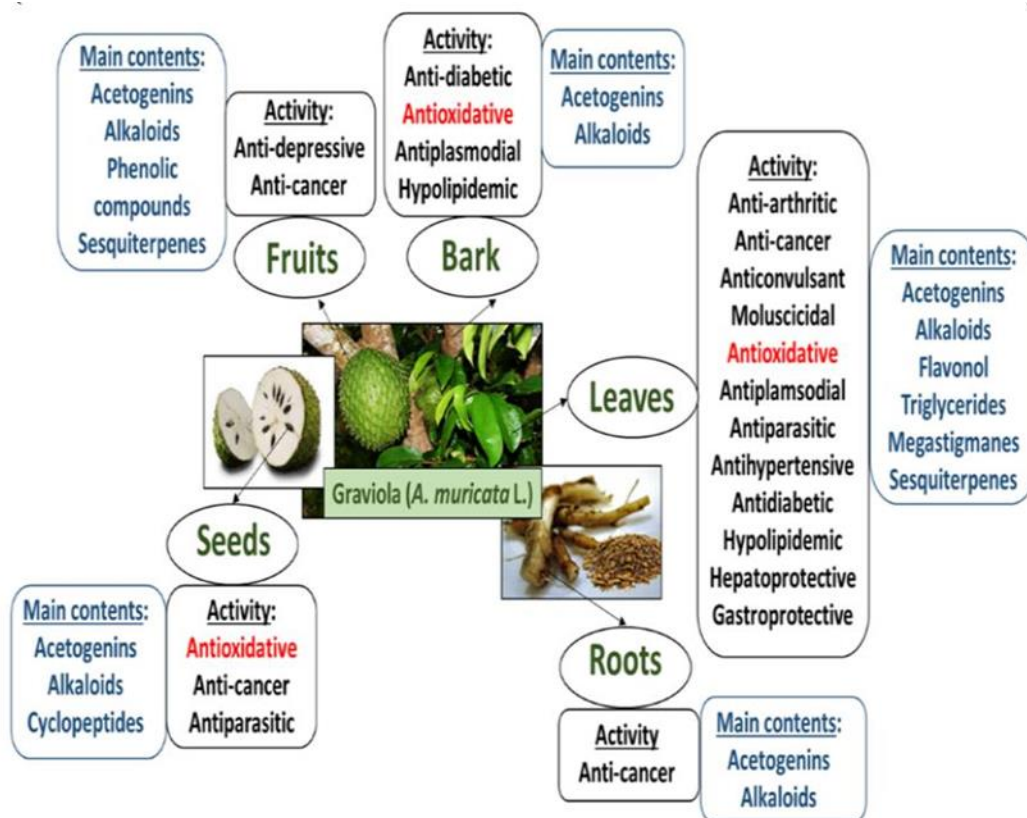


Figure 11. Main contents and main biological properties of various parts of graviola [12].

Phytochemical examination of plant leaf extracts *A. muricata* It is rich in secondary metabolites such as alkaloids, saponins, terpenoids, flavonoids, coumarins, lactones, anthraquinones, tannins, cardiac glycosides, cortical acetogenins, phenols and phytosterols. The high presence of phenolic compounds gives strong antioxidant capacity to the leaves and their extracts. It can prevent the onset or progression of oxidative disorders, as well as reduce the risk of diseases such as cancer, arthritis, diabetes, and other diseases that occur during aging [13].

The high-quality plant formula contains Graviola, which contains acetogenins, alkaloids and flavonoids [14].

(Graviola), which belongs to the Annonaceae family has been traditionally used for its medicinal abilities including antimicrobial, anti-inflammatory, antioxidant, and inhibition of cancer cell growth. Graviola is claimed to be a potential antitumor due to its selective cytotoxicity against several cancer cell lines [14].

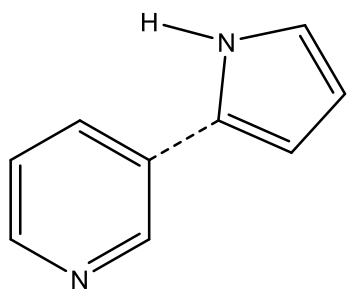
It is also naturally rich in a large number of bioactive molecules that are attributed to many biological activities including antioxidant, anti-inflammatory, antimicrobial and anti-cancer effects. These bioactive components are found isolated from the leaves, bark, fruit and stem of this plant genus, terpenoids, steroids, flavonoids, cardiac glycosides, tannins, phenols and alkaloids. It was also very effective against different types of cancer cell lines. It also summarizes the use of these phytochemicals for the purpose of developing promising anti-cancer drug candidates in the future [15].

Qualitative phytochemical analysis of fruit extracts showed the presence of alkaloids, amino acids, flavonoids, phenols, proteins, tannins, reducing sugars and total sugars. Anticancer activity was confirmed in vitro by a test MTT on the human breast cancer cell line MCF-7 at different concentrations. Flavonoids present in fruit extracts are a potential reducing agent which is responsible for the formation of gold nanoparticles. Stabilization of gold nanoparticles is carried out by the carboxyl group present in proteins. Also, the nanoparticles are separated from each other by the electrostatic repulsion that exists due to the presence of similar charges surrounding the gold nanoparticles. It was found that fruit extracts can be used to synthesize and stabilize gold nanoparticles. Moreover, engineered nanoparticles coated with bioactive compounds are potential anticancer agents against a cancer cell line the breast MCF-7[16].

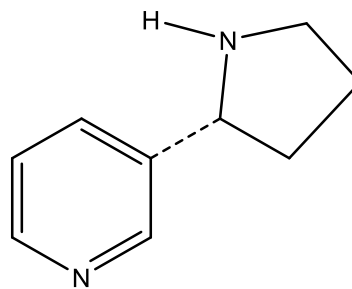
1.1.14 Effective compounds in (*Annona muricata*)

1.1.14.1 Alkaloids

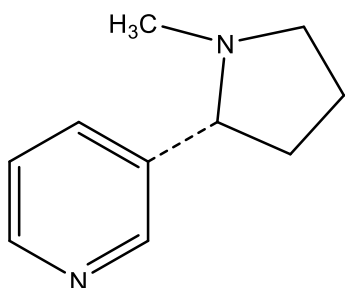
Alkaloids are defined as a group of naturally occurring chemical compounds that mostly contain basic nitrogen atoms. Alkaloid molecules are extremely important for biomedical science. They have a unique property – an ability to work as either hydrogen-acceptor or hydrogen-donor for hydrogen bonding, depending on the type of amine functionality present in alkaloids. This property is critically important for the interaction (binding) between targets (enzymes, proteins, and receptors) and drugs (ligands) possessing alkaloid scaffold . Certain drugs with alkaloid structural features were synthesized by naturally occurring alkaloids, to which belong[17].



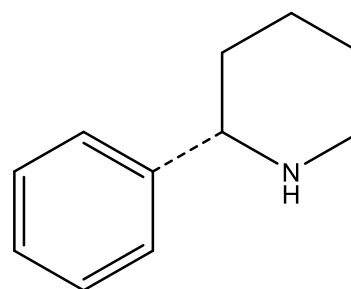
3-(1*H*-pyrrol-2-yl)pyridine



(*R*)-3-(pyrrolidin-2-yl)pyridine



(*R*)-3-(1-methylpyrrolidin-2-yl)pyridine



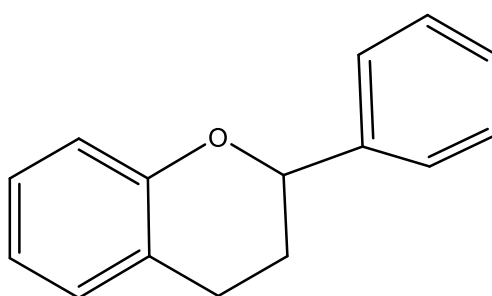
(*S*)-2-phenylpiperidine

1.1.14.2 Flavonoids

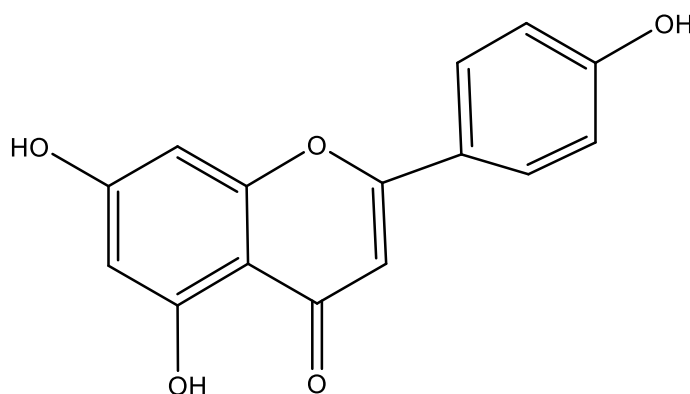
Flavonoids are an important class of natural products; particularly, they belong to a class of plant secondary metabolites having a polyphenolic structure, widely found in fruits, vegetables and certain beverages. They have miscellaneous favourable biochemical and antioxidant effects associated with various diseases such as cancer, Alzheimer's disease (AD), atherosclerosis, Flavonoids are associated with a broad spectrum of health-promoting effects and are an indispensable component in a variety of nutraceutical, pharmaceutical, medicinal and cosmetic applications. This is because of their antioxidative, anti-inflammatory, anti-mutagenic and anti-carcinogenic properties coupled with their capacity to modulate key cellular enzyme functions. They are also known to be potent inhibitors for several enzymes, such as xanthine oxidase (XO), cyclo-oxygenase (COX), lipoxygenase and phosphoinositide.

In nature, flavonoid compounds are products extracted from plants and they are found in several parts of the plant. Flavonoids are used by vegetables for their growth and defence against . They belong to a class of low-molecular-weight phenolic compounds that are widely distributed in the plant kingdom. They constitute one of the most characteristic classes of compounds in higher plants. Many flavonoids are easily recognised as flower pigments in most angiosperm families. However, their occurrence is not restricted to flowers but are found in all

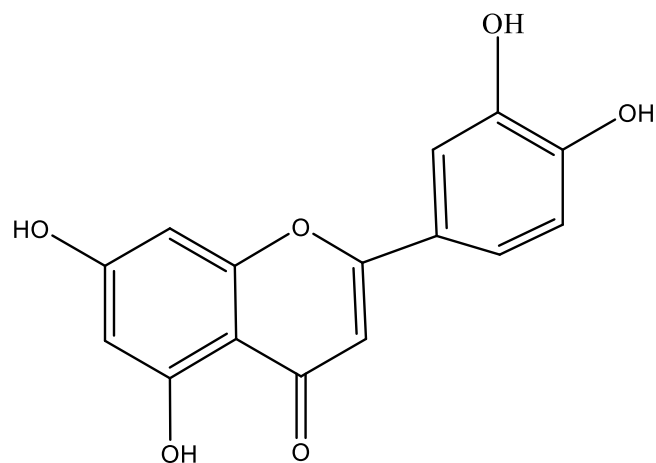
parts of. Flavonoids are also abundantly found in foods and beverages of plant origin, such as fruits, vegetables, tea, cocoa and wine; hence they are termed as dietary flavonoids. Flavonoids have several subgroups, which include chalcones, flavones, flavonols and isoflavones. These subgroups have unique major sources. For example, onions and tea are major dietary sources of flavonols and flavones. Flavonoids play a variety of biological activities in plants, animals and bacteria. In plants, flavonoids have long been known to be synthesised in particular sites and are responsible for the colour and aroma of flowers, and in fruits to attract pollinators and consequently fruit dispersion to help in seed and spore germination, and the growth and development of [18].



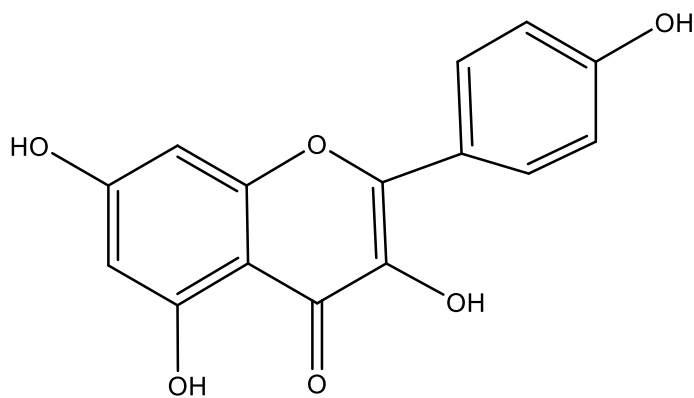
2-phenylchromane



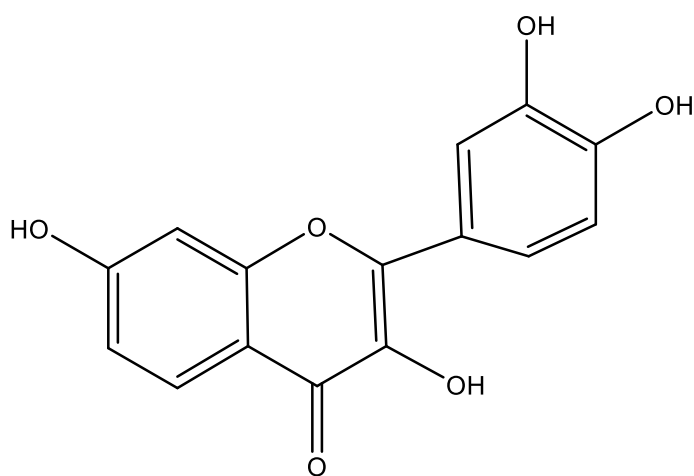
5,7-dihydroxy-2-(4-hydroxyphenyl)-4H-chromen-4-one



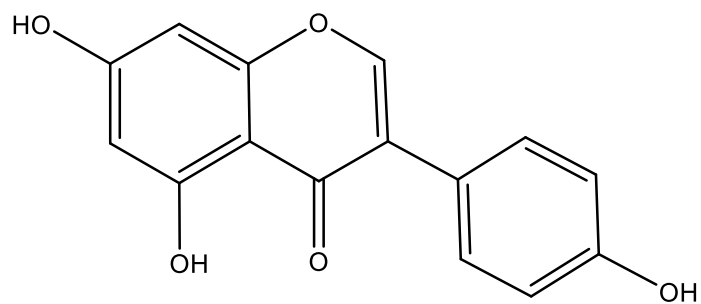
5,7-dihydroxy-2-(4-hydroxy-3-methylphenyl)-4*H*-chromen-4-one compound with λ^1 -oxidane (1:1)



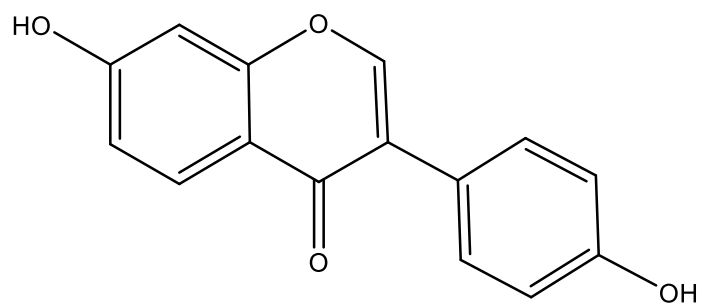
3,5,7-trihydroxy-2-(4-hydroxyphenyl)-4*H*-chromen-4-one



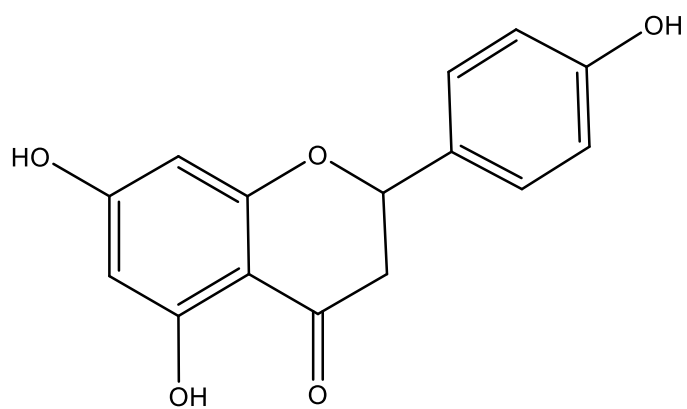
2-(3,4-dihydroxyphenyl)-3,7-dihydroxy-4*H*-chromen-4-one



5,7-dihydroxy-3-(4-hydroxyphenyl)-4*H*-chromen-4-one



7-hydroxy-3-(4-hydroxyphenyl)-4*H*-chromen-4-one



5,7-dihydroxy-2-(4-hydroxyphenyl)chroman-4-one

1.2 Objectives:

This study aims to investigate the bio synthesis of AuNPs using *A. muricata* seed extract, characterize the resulting nanoparticles, and evaluate their anticancer effects against MCF-7-positive breast cancer cells.

This goal is achieved through the following sub-goals:

- 1- Synthesis of gold nanoparticles and their diagnosis by electron microscopy (SEM-TEM-AFM) and infrared IR and ultraviolet UV and Gc-Ms- XRD
- 2- Study of the effectiveness of fruit seeds of prepared gold nanoparticles against some types of breast cancer lines (MCF-7) Cytotoxicity Flow cytometry-. Brest Cancer Cell line.

1.3 Literature Review

Breast cancer remains a significant global health concern, with an estimated 68,69 million new cases diagnosed worldwide in 2020 [19]. Among breast cancer subtypes, MCF-7-positive breast cancer, characterized by overexpression of the human epidermal growth factor receptor [20]. (MCF-7) protein, accounts for approximately 20-30% of all cases.⁶⁸ This aggressive subtype is associated with poor prognosis and increased risk of recurrence, necessitating the development of novel therapeutic approaches [21] [22]. In recent years, nanotechnology has emerged as a promising field in cancer research, offering potential for targeted drug delivery, enhanced therapeutic efficacy, and reduced side effects [23] [24]. Gold nanoparticles (AuNPs) have garnered particular interest due to their unique physicochemical properties, including surface plasmon resonance, high surface-to-volume ratio, and ease of functionalization [25] [26]. These characteristics make AuNPs attractive candidates for various biomedical applications, including cancer diagnosis, imaging, and therapy [27] [28]. The synthesis of AuNPs using plant extracts, known as green synthesis, has gained attention as an eco-friendly and cost-effective alternative to traditional chemical methods [29] [30]. This approach leverages the reducing and stabilizing properties of plant-derived biomolecules, potentially imparting additional therapeutic properties to the nanoparticles [31] [32]. Bio synthesis offers several advantages over conventional methods, including the elimination of toxic chemicals, mild reaction conditions, and the potential for scalability [33] [34]. *Annona muricata*, commonly known as soursop or graviola, has been traditionally used in various cultures for its medicinal properties, including potential anticancer effects [35] [36]. The plant contains a diverse array of bioactive compounds, including acetogenins, alkaloids, phenolic compounds, and flavonoids [37] [38]. These phytochemicals have demonstrated various biological activities, including antioxidant, anti-inflammatory, and cytotoxic effects against cancer cells [39] [40]. Recent studies have explored the anticancer potential of *A. muricata* extracts against various cancer types, including breast cancer [41] [42]. The plant's bioactive compounds have shown promising results in inducing apoptosis, cell cycle arrest, and modulation of signaling pathways in cancer cells [43] [44]. However, the potential of *A. muricata* seed extract for the green synthesis of AuNPs and their subsequent application in cancer therapy remains largely unexplored. The synthesized AuNPs will be thoroughly characterized using a combination of techniques, including X-ray diffraction (XRD), ultraviolet-visible spectroscopy (UV-Vis), Fourier-transform infrared spectroscopy (FTIR), transmission electron microscopy (TEM),

atomic force microscopy (AFM), dynamic light scattering (DLS), and zeta potential analysis [45-48].

The anticancer potential of the synthesized AuNPs will be assessed using the MTT cell viability assay on MCF-7-positive breast cancer cell lines [49]. Additionally, the antioxidant activity of the AuNPs will be evaluated using the 2,2-diphenyl-1-picrylhydrazyl (DPPH) radical scavenging assay [50]. To further understand the mechanism of action and potential toxicity, flow cytometry experiments will be conducted to assess cell cycle distribution and apoptosis induction [51] [52]. The integration of green nanotechnology with traditional medicinal plants presents an exciting opportunity for developing novel anticancer therapies [53] [54]. By harnessing the therapeutic potential of *A. muricata* and the unique properties of AuNPs, this research aims to contribute to the growing body of knowledge on eco-friendly nanomaterials for cancer treatment [55] [56]. The findings may pave the way for the development of safe, effective, and sustainable nanotherapeutics for MCF-7-positive breast cancer [57] [58]. Furthermore, this study will explore the potential synergistic effects between the plant-derived bioactive compounds and the synthesized AuNPs [59] [60]. The role of the phytochemical corona in modulating the biological activity and cellular interactions of the nanoparticles will be investigated [61] [62]. By elucidating the synthesis, characterization, and biological activities of these bio-synthesized AuNPs, this research aims to contribute to the broader field of nanomedicine and provide insights into the potential of plant-mediated nanoparticle synthesis for cancer therapy. The results of this study may inform future research directions and clinical applications in the development of novel, eco-friendly, and effective nanotherapeutics for the treatment of MCF-7-positive breast cancer and other malignancies.

Chapter Two

Experimental Work

2. Materials and methods

2.1 Materials

1- *Annona muricata* seeds

2- Deionized water

3- Whatman No. 1 filter paper

4- Chloroauric acid (HAuCl_4), 1 mM solution

2.2 methods

2.2.1 Biosynthesis of Gold Nanoparticles (AuNPs)

2.2.1.1 Plant Material Preparation:

Annona muricata seeds were collected, authenticated, and processed. The seeds were thoroughly washed, air-dried, and pulverized into a fine powder using a mechanical grinder. The powder was stored in airtight containers at 4°C until further use [63].

2.2.1.2 Extract Preparation:

Aqueous extraction was performed by mixing 10 g of seed powder with 100 mL of deionized water. The mixture was heated at 60°C for 30 minutes under constant stirring, then filtered through Whatman No. 1 filter paper. The filtrate was centrifuged at 10,000 rpm for 15 minutes, and the supernatant was collected and stored at 4°C [63].

2.2.1.3 AuNP Synthesis:

The synthesis of AuNPs was carried out by adding the *A. muricata* seed extract to 1 mM chloroauric acid (HAuCl_4) solution in a 1:9 ratio was used, equivalent to 10% plant extract. The reaction mixture was incubated at room temperature under constant stirring for 24 hours. The formation of AuNPs was indicated by a color change from pale yellow to deep purple [63].

2.3 Characterization of Gold Nanoparticles (AuNPs)

2.3.1 X-Ray Diffraction (XRD):

Crystalline nature and phase purity of the synthesized AuNPs were analyzed using an X-ray diffractometer (D8 Advance, Bruker, Germany) with Cu K α radiation ($\lambda = 1.54 \text{ \AA}$) in the 2θ range of 20° - 80° . [64].

2.3.2 UV-Visible Spectroscopy:

The optical properties and formation of AuNPs were monitored using a UV-visible spectrophotometer (UV-2600, Shimadzu, Japan) in the range of 300-800 nm. [65].

2.3.3 Fourier Transform Infrared Spectroscopy (FTIR):

FTIR analysis was performed to identify the functional groups involved in the reduction and stabilization of AuNPs. Spectra were recorded on an FTIR spectrometer (Nicolet iS50, Thermo Fisher Scientific, USA) in the range of 4000 - 400 cm^{-1} .

2.3.4 Transmission Electron Microscopy (TEM):

Morphology and size distribution of AuNPs were examined using a transmission electron microscope (JEM-2100F, JEOL, Japan) operating at 200 kV. Samples were prepared by placing a drop of the AuNP solution on a carbon-coated copper grid and allowing it to dry at room temperature. [66].

2.3.5 Atomic Force Microscopy (AFM):

Surface topology and three-dimensional morphology of AuNPs were analyzed using an atomic force microscope (Dimension Icon, Bruker, USA) in tapping mode [67].

2.3.6 Scanning Electron Microscopy (SEM) Analysis

To delve into the intricate surface morphology and internal architecture of our drug delivery system, we employed high-resolution Scanning Electron Microscopy (SEM). This powerful imaging technique allowed us to peer into the nanoscale world of our particles, revealing crucial details about their size, shape, and surface characteristics.

Methodology:

Sample Preparation:

- Specimens were meticulously mounted on aluminum stubs
- A conductive bridge was created using double-sided carbon tape
- To enhance image clarity, samples were sputter-coated with a gossamer-thin 10 nm gold layer

Imaging Protocol:

- Utilized a state-of-the-art FEI Quanta 250 FEG (or equivalent) SEM
- Captured a spectrum of magnifications (500x to 5000x)
- Employed a gentle accelerating voltage (5-10 kV) to preserve sample integrity
- Examined both exterior surfaces and interior cross-sections

This comprehensive approach allowed us to visualize potential morphological transformations occurring during the drug release process offering invaluable insights into the system's release mechanisms and overall performance [68].

2.3.7 Dynamic Light Scattering (DLS):

The hydrodynamic size distribution of the produced gold nanoparticles (AuNPs) was ascertained using Dynamic Light Scattering (DLS). A Zetasizer Nano ZS (Malvern Instruments Ltd., Worcestershire, UK) with a backscatter detection angle of 173° and a regulated temperature of 25°C was used for the measurements. This device offers great sensitivity and precision for characterizing nanoparticles in colloidal suspensions.

The samples were suitably diluted with deionized water before testing in order to prevent multiple scattering effects and guarantee accurate results. To guarantee accuracy and repeatability, the instrument was calibrated using standard latex beads in compliance with the manufacturer's procedure [69].

2.3.8 Zeta Potential:

Using the same Zetasizer Nano ZS device, Zeta Potential measurements were also carried out to evaluate the produced AuNPs' colloidal stability. With higher absolute values (positive or negative) indicating better stability of the colloidal system, this approach offers important

insights on the electrokinetic potential of the nanoparticles. To guarantee precise and interference-free findings, measurements were made at the same temperature (25 °C) following dilution with deionized water[69].

2.3.9 Gas Chromatography-Mass Spectrometry (GC-MS) Analysis of *A. muricata* Seed Extract:

Using analytical grade ethyl acetate in a 1:1 (v/v) ratio, a liquid-liquid extraction procedure was used to obtain the aqueous extract of *Annona muricata* seeds for GC-MS analysis. For ten minutes, the mixture was agitated violently to guarantee that the organic and aqueous layers separated well. Following settling, the ethyl acetate layer was meticulously gathered and filtered to eliminate any particles using a 0.22 µm PTFE syringe filter. To get a semi-solid residue, the filtrate was next concentrated in a rotary evaporator set at 40°C and low pressure. After being moved into amber glass vials, the concentrated extract was kept at 4°C for additional examination. An Agilent 7890B gas chromatograph with a 5977A Mass Selective Detector was used to perform the gas chromatography-mass spectrometry analysis. An HP-5MS capillary column (30 m length × 0.25 mm internal diameter × 0.25 µm film thickness) was used to separate the volatile components. At a steady flow rate of 1.0 mL/min, 99.99% pure helium was employed as the carrier gas. A 10:1 split ratio, a 1 µL injection volume, and an injector temperature of 250°C were used for the split mode injection. At an energy of 70 eV, the mass spectrometer was in electron impact (EI) ionization mode. Using a scan rate of 3.5 scans per second, spectral data were gathered throughout a mass-to-charge (m/z) range of 50–650. To avoid solvent interference during data acquisition, a three-minute solvent delay was used. By comparing the mass spectra with those in the NIST Mass Spectral Library, the chemical ingredients were identified[70].

2.3.10 Molecular Docking Simulations

We carried out *in silico* molecular docking studies to clarify the intricate interactions between our medication molecules and the carrier material at the atomic level in order to supplement our experimental data with theoretical understanding. The first step in the computational workflow was the development of molecular structures, which involved generating or acquiring high-quality three-dimensional models of the drug and carrier components. To guarantee realistic simulation inputs, these structures were then refined by defining rotatable bonds, adding hydrogen atoms, and allocating partial atomic charges. Auto dock Vina, a well-known program renowned for its accuracy in predicting ligand-receptor binding affinities, was

then used to perform docking simulations. Several docking tests were carried out to improve the accuracy and repeatability of the results, and a grid box was carefully established to concentrate the computational efforts on the most pertinent binding locations. In order to identify and describe important chemical interactions, such as hydrogen bonding networks, hydrophobic contacts, and other non-covalent forces that control the drug-carrier binding behavior, the top-scoring binding postures were then carefully examined. Lastly, sophisticated molecular visualization software was used to clearly and informatively depict the docking results, vividly illustrating these interactions. This computational method successfully complemented and expanded upon the insights gained from our experimental findings by providing a thorough molecular-level understanding of the encapsulation dynamics and possible drug release mechanisms. To complement our experimental data with theoretical insights, we conducted *in silico* molecular docking studies. These simulations aimed to elucidate the intricate dance between our drug molecules and the carrier material at the atomic level.

2.4 In Vitro Anticancer Activity

2.4.1 Cell Culture:

MCF-7-positive breast cancer cell line (e.g., SKBR3 or BT-474) was obtained from ATCC and cultured in DMEM supplemented with 10% fetal bovine serum and 1% penicillin-streptomycin. Cells were maintained at 37°C in a humidified atmosphere with 5% carbon dioxide (CO₂).

2.5 Flow Cytometry Analysis

2.5.1 Cell Cycle Analysis:

MCF-7-positive breast cancer cells were treated with AuNPs at IC₅₀ concentration for 24 hours. Cells were harvested, fixed with 70% ethanol, and stained with propidium iodide (PI) containing RNase A. Cell cycle distribution was analyzed using a flow cytometer (Model J, Manufacturer K).

2.5.2 Apoptosis Assay:

Apoptosis induction was evaluated using Annexin V-FITC/PI double staining. Cells treated with AuNPs were harvested, washed with PBS, and stained with Annexin V-FITC and PI

according to the manufacturer's protocol. The percentage of apoptotic cells was determined using flow cytometry.

2.5.2 MTT Assay:

The cytotoxic effect of AuNPs on MCF-7-positive breast cancer cells was assessed using the 3-(4,5-dimethylthiazol-2-yl)-2,5-diphenyltetrazolium bromide (MTT) assay. Cells were seeded in 96-well plates (1×10^4 cells/well) and incubated for 24 hours. Various concentrations of AuNPs (1-100 $\mu\text{g/mL}$) were added to the wells and incubated for 24, 48, and 72 hours. MTT solution (5 mg/mL) was added to each well and incubated for 4 hours. The formazan crystals were dissolved in DMSO, and the absorbance was measured at 570 nm using a microplate reader. The percentage of cell viability was calculated, and the IC₅₀ value was determined [63].

2.4 Antioxidant Activity Assessment

2.4.1 DPPH Radical Scavenging Assay:

The antioxidant activity of the synthesized AuNPs was evaluated using the 2,2-diphenyl-1-picrylhydrazyl (DPPH) radical scavenging assay. Various concentrations of AuNPs (10-100 $\mu\text{g/mL}$) were incubated with 0.1 mM DPPH solution in methanol for 30 minutes in the dark. The absorbance was measured at 517 nm using a microplate reader. The percentage of DPPH radical scavenging was calculated and compared with ascorbic acid as a positive control[70].

Chapter Three

Results and Discussion

3.1 Characterization of Gold Nanoparticles

3.1.1 X-Ray Diffraction (XRD) Analysis:

The crystalline nature and purity of the synthesized gold nanoparticles (AuNPs) were investigated using X-ray diffraction analysis. Figure 12 presents the XRD pattern of the bio-synthesized AuNPs, revealing distinct diffraction peaks that correspond to the face-centered cubic (fcc) structure of metallic gold. [63].

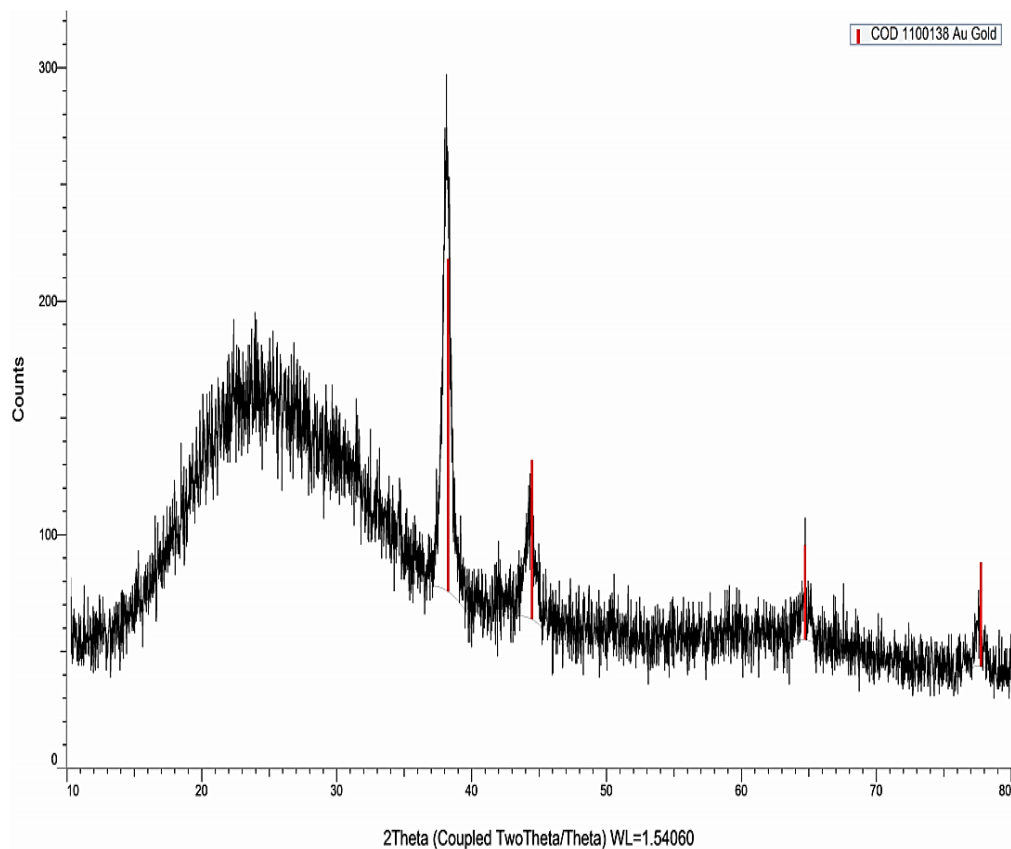


Figure 12 pattern XRD pattern of bio-synthesized AuNPs.

Table 1: Comparison of XRD peaks between standard gold and synthesized AuNPs.

Standard Gold (2θ)	Synthesized AuNPs (2θ)	Miller Indices (hkl)	d-spacing (\AA)
38.272	38.21	(111)	2.34980
44.485	44.43	(200)	2.03500
64.729	64.71	(220)	1.43900
77.760	77.75	(311)	1.22720

The XRD pattern exhibits sharp and intense peaks, indicating the high crystallinity of the synthesized AuNPs. The prominent diffraction peaks observed at 2θ values of correspond closely to the standard diffraction pattern of gold (COD 1100138) from the Bruker XRD instrument database (Table 1). These peaks are indexed to the (111), (200), (220), (311) planes of the face-centered cubic lattice structure of gold, confirming the successful formation of crystalline AuNPs [63].

The intense (111) reflection, compared to the other planes, suggests a predominant orientation of the synthesized AuNPs. The sharp and narrow diffraction peaks indicate the formation of well-crystallized nanoparticles. The absence of additional peaks in the XRD pattern confirms the purity of the synthesized AuNPs, with no detectable crystalline impurities [63].

3.1.2 UV-Visible Spectroscopy:

The formation and optical properties of the bio-synthesized AuNPs were further corroborated by UV-Visible spectroscopy [63]. Figure 13 illustrates the UV-Vis absorption spectrum of the colloidal AuNP solution.

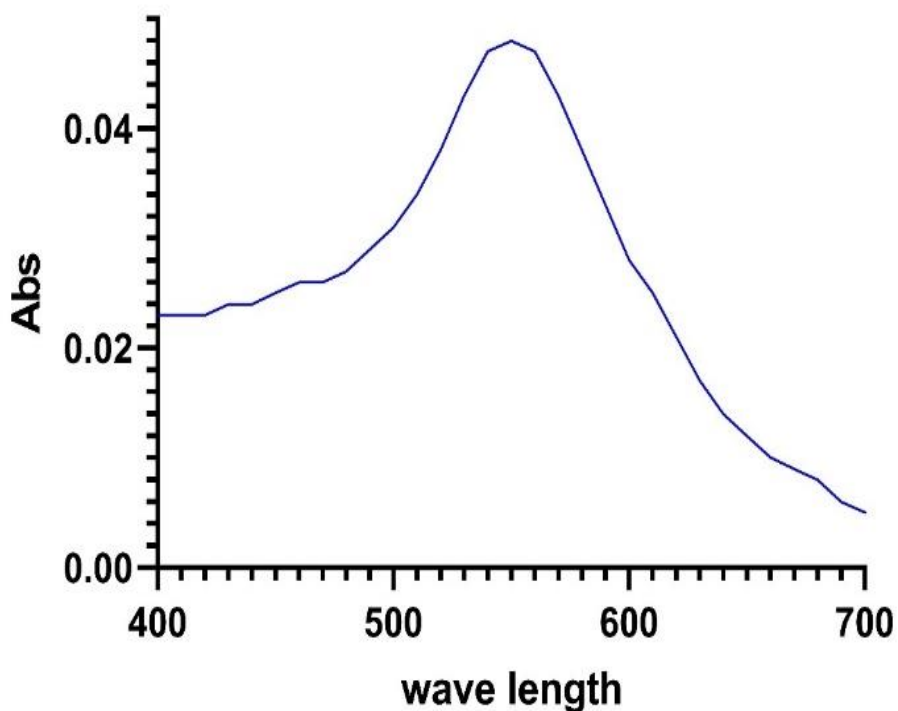


Figure 13: UV-Visible absorption spectrum of bio-synthesized AuNPs

The UV-Vis spectrum displays a characteristic surface plasmon resonance (SPR) band with a maximum absorption peak at approximately 550 nm, which is typical for spherical gold nanoparticles. This observation confirms the successful synthesis of AuNPs using the green method. The presence of a single, sharp SPR peak indicates a narrow size distribution of the nanoparticles and suggests minimal aggregation in the colloidal solution [63].

The position and shape of the SPR band are influenced by factors such as particle size, shape, and the dielectric constant of the surrounding medium. The observed peak at 550 nm is consistent with the formation of spherical AuNPs within the size range of 10-50 nm, as reported in literature for similar bio-synthesis methods [63].

The intensity of the SPR peak provides qualitative information about the concentration of AuNPs in the solution. The relatively high absorbance value (approximately 0.05) indicates a substantial yield of nanoparticles from the bio-synthesis process.

Furthermore, the spectrum shows a gradual increase in absorbance towards shorter wavelengths, which can be attributed to the band transitions of gold. The absence of additional peaks or shoulders in the visible region suggests the formation of primarily spherical nanoparticles without significant anisotropic shapes.

However, the XRD and UV-Vis analyses provide compelling evidence for the successful bio-synthesis of crystalline gold nanoparticles. The XRD results confirm the face-centered cubic structure and high purity of the AuNPs, while the UV-Vis spectrum corroborates their formation and provides insights into their size, shape, and colloidal stability. These complementary techniques demonstrate the efficacy of the employed bio-synthesis method in producing well-defined gold nanoparticles suitable for further applications.

3. 1.3 FTIR Analysis:

The Fourier-Transform Infrared (FTIR) spectroscopy was employed to identify the functional groups present in the *Annona muricata* seed extract Before adding gold nanoparticles figure 14.

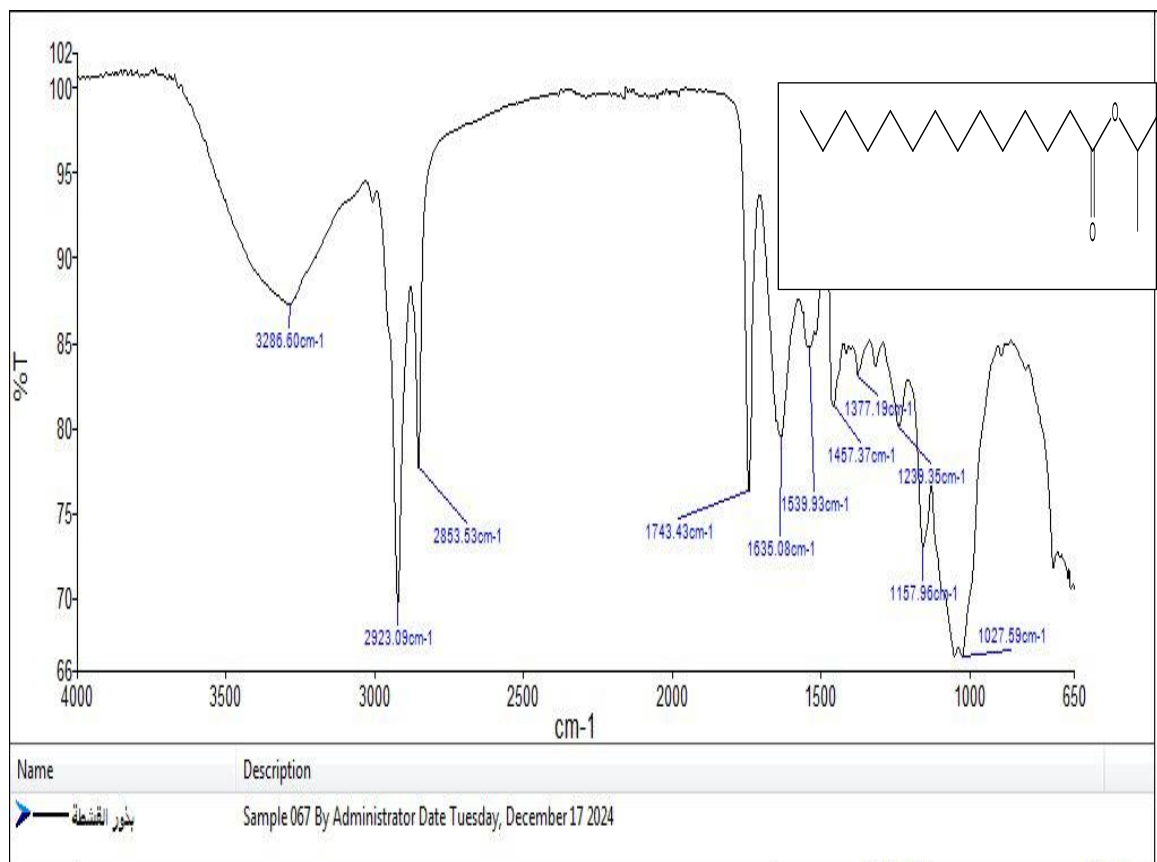


Figure 14: illustrated FTIR pattern of Before adding gold nanoparticles

Through the peaks that show up in the spectrogram, we attempt to verify the presence of these substances when studying a spectrum.

The peak at 3200–3500 cm^{-1} (amines and hydroxyls). The existence of hydroxyl (-OH) bond lengths is indicated by the broad peak that lies between 3300 and 3200 cm^{-1} . The presence of alcohols or phenols, which are prevalent in flavonoids and tannins and are known to have potent health effects, is indicated by a very broad peak. A sharper, more noticeable peak might be amines (N-H), which could be a sign of proteins or alkaloids.

The C-H stretches in organic molecules, which fall between 2800 and 3000 cm^{-1} . Alkane C-H vibrations are represented as a peak at 2923 cm^{-1} . These peaks often appear in substances possessing long carbon chains, such as the natural lipids and oils found in graviola seeds.

The peak at 1650–1750 cm^{-1} (carbonyl group C=O). The presence of a carbonyl bond (C=O) is indicated by a prominent signal at 1700–1735 cm^{-1} . If the peak is at 1700–1725 cm^{-1} , it suggests the presence of ketones or carboxylic acids. Esters, which are frequently present in vegetable oils and fats, could be the cause if the peak is located between 1730 and 1750 cm^{-1} . The existence of this Esters, which are frequently present in vegetable oils and fats, could be the cause if the peak is located between 1730 and 1750 cm^{-1} .

This peak's presence indicates that the sample includes carbonylated or esterified chemicals, like acetogenins, which are found in graviola seeds and are known to have anticancer effects.

The C=C double bonds in aromatic rings, which suggest the presence of flavonoids or tannins, may be the cause of the peaks at 1500–1600 cm^{-1} that occur in the region between 1450 and 1650 cm^{-1} (C=C bonds and N-H bonds).

N-H bonds in amides or amines can be a sign of the existence of alkaloids or other nitrogenous chemicals. This lends credence to the hypothesis that the sample contains polyphenolic chemicals, which are recognized for their anti-inflammatory and antioxidant qualities and include flavonoids and tannins.

The range of C-O and C-N bonds is 1000–1400 cm^{-1} . The peaks between 1050 and 1250 cm^{-1} show:

Ethers and esters, which are frequently present in plant lipids, contain C-O linkages. C-N bonds, which could be a sign of alkaloids or other chemicals that contain nitrogen. The existence

of natural oils in the graviola seeds is shown by these peaks, which further corroborate the notion that the sample contains natural lipids and esters.

Below the 1000 cm^{-1} range. Through spectroscopic examination, this region's complicated peaks—which are difficult to interpret—can be used to compare the sample with recognized compounds. The presence of sugars or carbohydrate molecules, which may be a component of the seeds' chemical makeup, is usually indicated by the presence of prominent peaks in this region.

We may make some significant inferences regarding the chemical components found in the soursop (graviola) seed extract based on a thorough examination of the IR spectrum:

Flavonoids and phenolic compounds: The existence of phenols and flavonoids, which have anti-inflammatory and antioxidant qualities, was verified by the peaks at $1500\text{--}1600\text{ cm}^{-1}$ and $3200\text{--}3300\text{ cm}^{-1}$. Acetogenins: Carbonyl compounds with anticancer and antiparasitic properties, such as acetogenins, are indicated by the presence of a prominent peak at 1700 cm^{-1} .

Ester compounds and natural lipids, which are frequently found in vegetable oils, were confirmed to be present by the peaks at 2923 cm^{-1} and $1050\text{--}1250\text{ cm}^{-1}$.

Nitrogenous compounds: Peaks between $1500\text{--}1600\text{ cm}^{-1}$ and $1050\text{--}1250\text{ cm}^{-1}$ indicate the likely presence of alkaloids or proteins. Carbohydrates or sugars: Peaks in the fingerprint area (below 1000 cm^{-1}) might suggest that the seeds contain natural sugars.

The Fourier-Transform Infrared (FTIR) spectroscopy was employed to identify the functional groups present in the bio-synthesized gold nanoparticles using *Annona muricata* seed extract. This analysis provides crucial insights into the biomolecules responsible for the reduction of gold ions and the stabilization of the resulting nanoparticles figure 15.

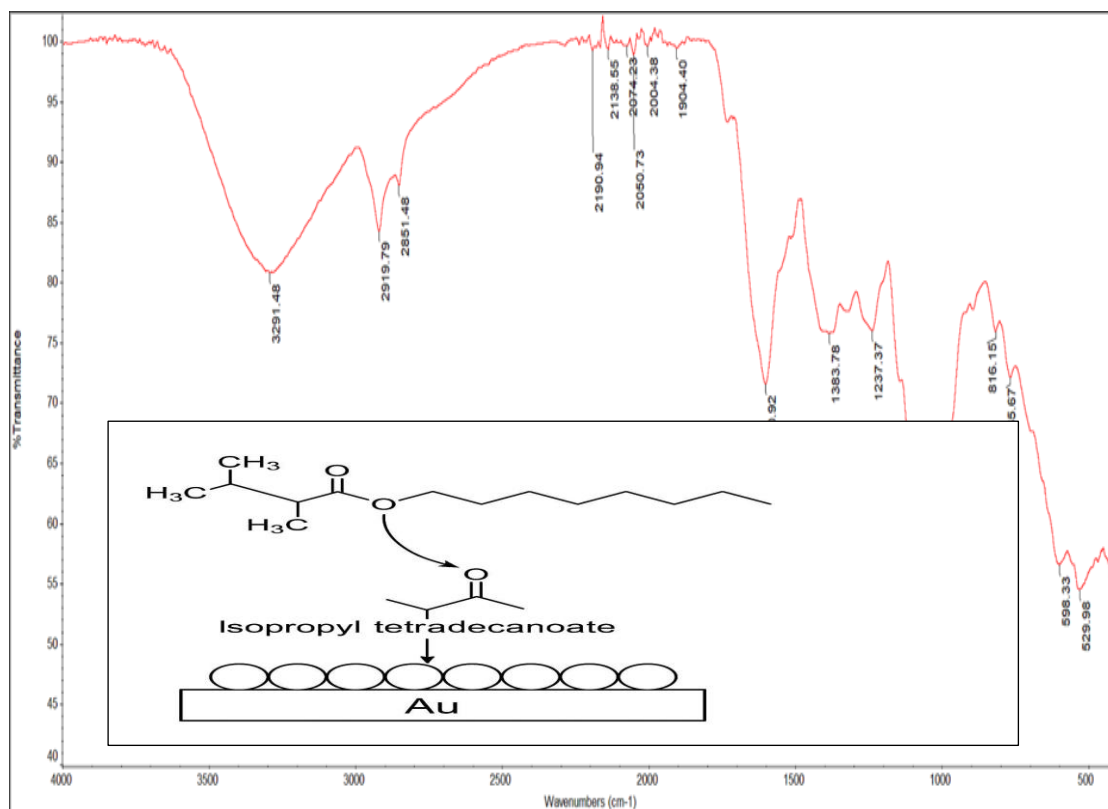


Figure 15; illustrated FTIR pattern of After adding gold nanoparticles

The FTIR spectrum of the synthesized gold nanoparticles exhibits several characteristic peaks that elucidate the nature of the capping and stabilizing agents derived from the *Annona muricata* seed extract. A broad, strong peak observed at 3291.48 cm^{-1} is indicative of O-H stretching vibrations, which can be attributed to the presence of phenolic compounds and alcohols in the seed extract. These compounds are known for their potent antioxidant properties and likely play a significant role in the reduction of gold ions to nanoparticles.

A notable peak at 2919.79 cm^{-1} corresponds to C-H stretching vibrations of alkanes, suggesting the presence of various organic compounds from the plant extract. This peak, along with the smaller one at 2851.48 cm^{-1} , indicates the involvement of long-chain hydrocarbons in the capping of the nanoparticles, which may contribute to their stability.

The spectrum reveals a cluster of peaks in the range of 1904.40 cm^{-1} to 2190.94 cm^{-1} , with a notable peak at 2050.73 cm^{-1} . These peaks could be associated with C≡N stretching or cumulated double bonds (C=C=C), possibly indicating the presence of alkaloids or other nitrogen-containing compounds in the extract. Such compounds may contribute to both the reduction process and the biological activities of the synthesized nanoparticles.

A strong peak at 1600.92 cm^{-1} is characteristic of C=C stretching in aromatic rings and/or C=O stretching in amide groups (Amide). This peak suggests the presence of flavonoids or proteins, which are crucial for the stabilization of nanoparticles and may also contribute to their enhanced biological activities. The involvement of proteins in capping the nanoparticles is further supported by the peak at 1383.78 cm^{-1} , which likely corresponds to C-H bending of alkanes or N-O symmetric stretching of nitro compounds.

The peak at 1237.37 cm^{-1} can be attributed to C-O stretching vibrations in phenols, ethers, or esters, further confirming the presence of phenolic compounds from the *Annona muricata* seed extract. These compounds are known for their strong antioxidant properties and may play a dual role in both the synthesis and the biological activities of the gold nanoparticles.

A strong peak observed at 1031.41 cm^{-1} is indicative of C-O stretching vibrations in alcohols, carboxylic acids, esters, or ethers. This peak, along with the ones at 816.15 cm^{-1} and 765.67 cm^{-1} in the fingerprint region, suggests the presence of various oxygen-containing functional groups that are likely involved in the stabilization of the nanoparticles.

The peaks at 598.33 cm^{-1} , 529.98 cm^{-1} , and 427.07 cm^{-1} in the lower wavenumber region could be associated with metal-oxygen bonds, potentially indicating the interaction between gold nanoparticles and oxygen-containing functional groups from the biomolecules. These interactions are crucial for the stabilization of the nanoparticles and may influence their size and shape.

However, the FTIR analysis provides strong evidence for the successful bio-synthesis of gold nanoparticles using *Annona muricata* seed extract. The spectrum reveals the presence of various bioactive compounds such as phenolics, flavonoids, proteins, and possibly alkaloids, which are responsible for the reduction of gold ions and the stabilization of the resulting nanoparticles. These biomolecules not only facilitate the synthesis process but also form a protective layer around the nanoparticles, potentially enhancing their stability and biocompatibility.

The presence of these bioactive compounds on the surface of the gold nanoparticles may contribute significantly to their observed antioxidant properties and anticancer activity against MCF-7-positive breast cancer cells. The synergistic effect between the intrinsic properties of gold nanoparticles and the bioactive compounds from *Annona muricata* seed extract could explain the enhanced biological activities reported in this study. This bio-synthesis approach

not only offers an eco-friendly and cost-effective method for nanoparticle production but also imparts additional therapeutic properties to the nanoparticles, making them promising candidates for various biomedical applications, particularly in cancer treatment.

3.1.4 Transmission Electron Microscopy (TEM) Analysis:

The morphology and size distribution of the bio-synthesized gold nanoparticles (AuNPs) were elucidated using transmission electron microscopy [66]. Figure 16 presents representative TEM image of the AuNPs at high magnifications.

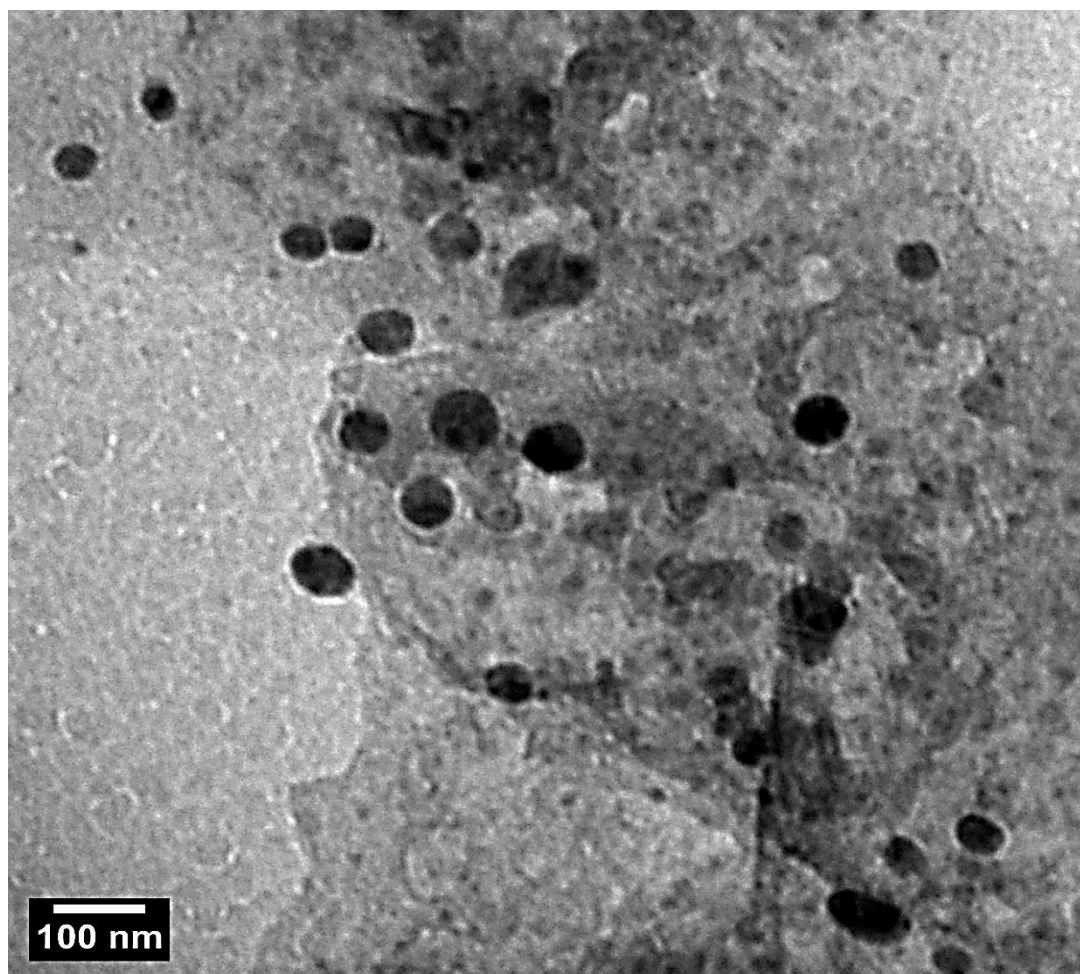


Figure 16: TEM micrographs of bio-synthesized AuNPs at high magnification.

TEM analysis revealed that the synthesized AuNPs exhibit predominantly spherical to sub-spherical morphologies. This slight deviation from perfect sphericity can be attributed to the heterogeneous nature of the plant extract used in the bio-synthesis process. The bio-organic compounds present in the *Annona muricata* seed extract likely act as both reducing and capping agents resulting in varying thicknesses of the stabilizing coating around the gold cores [66].

The nanoparticles displayed a range of sizes, with diameters primarily distributed between 20 and 60 nm. This size range is consistent with the surface plasmon resonance peak observed in the UV-Vis spectrum. The polydispersity in size can be ascribed to the inherent variability in the reduction kinetics and growth processes mediated by the diverse phytochemicals present in the plant extract.

Higher magnification TEM images (Figure 16) revealed the presence of an organic layer surrounding the nanoparticles, visible as a lower contrast shell around the electron-dense gold cores. This observation supports the role of plant-derived biomolecules in capping and stabilizing the AuNPs, which is crucial for preventing aggregation and imparting colloidal stability.

Interestingly, while the overall size distribution ranged from 20 to 60 nm, closer examination of individual particles revealed subtle surface features and irregularities on the scale of approximately in the range of 3-5 nm. These nanoscale surface structures may represent localized regions of differential growth or the adsorption of smaller gold clusters onto the surface of larger particles during the synthesis process.

3.1.5 Atomic Force Microscopy (AFM) Analysis:

To complement the TEM observations and gain insights into the three-dimensional morphology of the AuNPs, atomic force microscopy was employed. Figure 17a and 17b shows representative AFM topographic images and height profiles of the synthesized AuNPs.

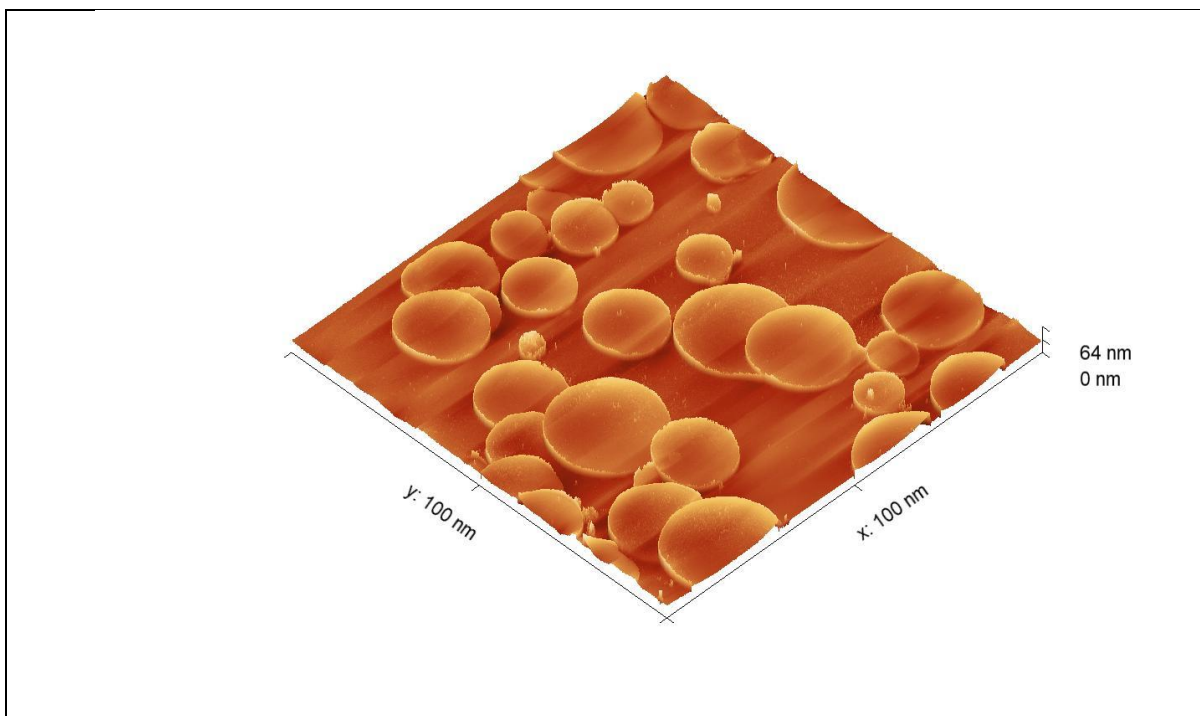


Figure 17a :illustrated 2D AFM image for bio-synthesized AuNPs.

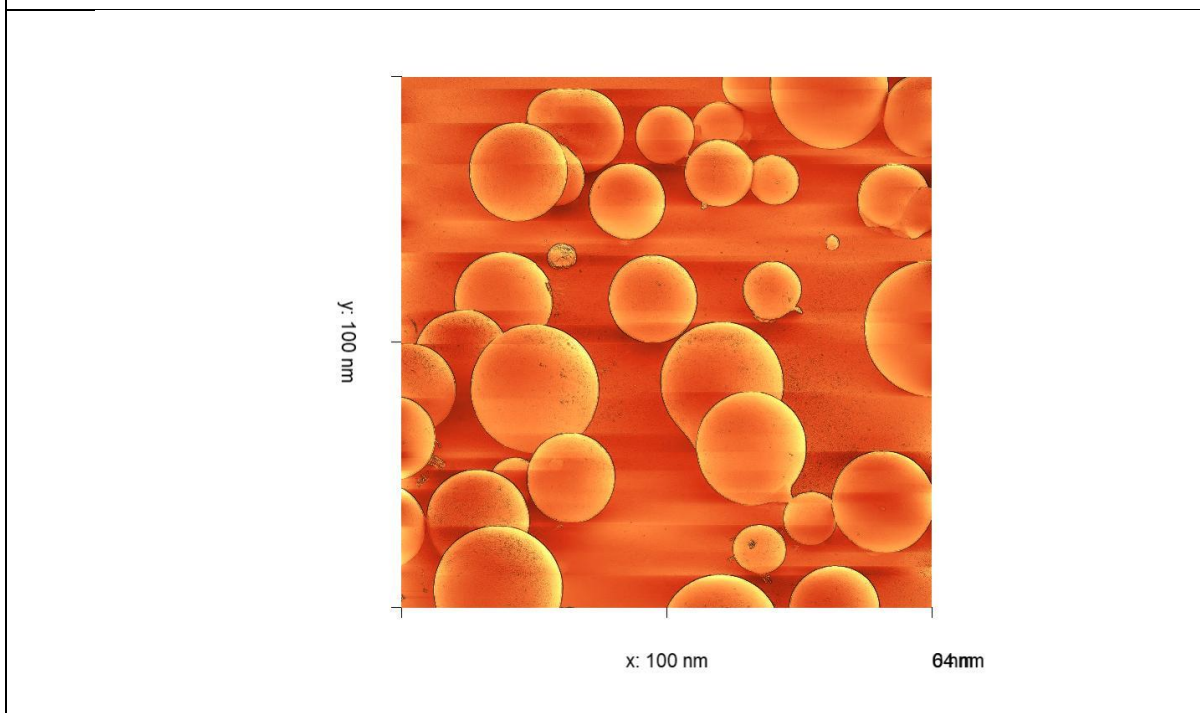


Figure 17b: illustrated 2D AFM image for bio- synthesis bio-synthesized AuNPs.

AFM analysis corroborated the TEM findings, revealing nanoparticles with predominantly spherical to sub-spherical morphologies. The lateral dimensions of the

nanoparticles measured by AFM were in good agreement with the TEM observations, showing particles ranging from 20 to 60 nm in diameter.

The AFM images also revealed the presence of smaller features on the nanoparticle surfaces, with dimensions in the range of 3-5 nm. These observations are consistent with the TEM findings and may represent localized regions of differential growth or adsorbed smaller gold clusters. The ability of AFM to detect these nanoscale surface features highlights its complementarity to TEM in providing a comprehensive morphological characterization of the AuNPs.

The three-dimensional AFM renderings (Figure 17a) offered insights into the spatial distribution and arrangement of the nanoparticles on the substrate. The images showed a relatively monodisperse distribution of particles with minimal aggregation, indicating good colloidal stability imparted by the green synthesis method.

However, the combined TEM and AFM analyses provide a comprehensive morphological characterization of the bio-synthesized AuNPs. Both techniques consistently revealed spherical to sub-spherical nanoparticles with sizes ranging from 20 to 60 nm. The observed polydispersity and subtle morphological variations can be attributed to the complex nature of the plant extract used in the synthesis. The presence of an organic coating and nanoscale surface features, detected by both TEM and AFM, underscores the intricate interplay between the gold cores and the bio-organic capping agents derived from the *Annona muricata* seed extract. These morphological characteristics are likely to influence the physicochemical properties and potential applications of the synthesized AuNPs in various fields, including biomedicine and catalysis.

3.1.6 Scanning Electron Microscopy (SEM) Analysis

The morphology and surface characteristics of the bio-synthesized gold nanoparticles (AuNPs) were further investigated using scanning electron microscopy (SEM). Figure 18 presents a high-resolution SEM micrograph of the AuNPs at 120,000x magnification.

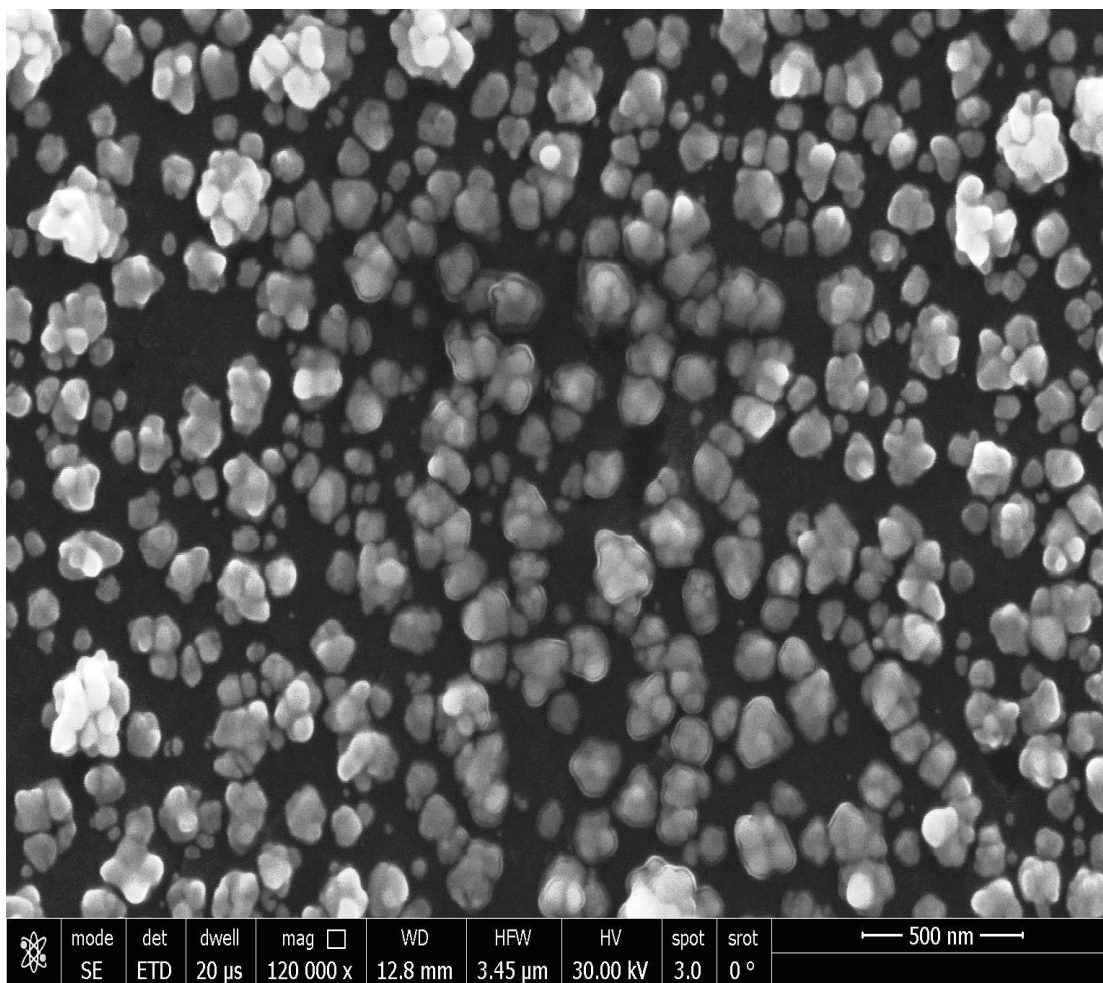


**Figure 18: SEM micrograph of bio-synthesized AuNPs at 120,000x magnification.
Scale bar: 500 nm.**

The SEM analysis reveals several key features of the synthesized AuNPs:

1. Particle morphology: The AuNPs exhibit predominantly spherical to quasi-spherical shapes, consistent with the observations from TEM and AFM analyses. This morphology is typical for AuNPs synthesized using plant extracts, where the diverse array of biomolecules can lead to slight variations in particle shape.
2. Size distribution: The SEM image shows a range of particle sizes, with the majority of particles falling the from 20 to 60 nm diameter range. This observation aligns well with the size distributions reported from TEM and AFM measurements, confirming the consistency of the synthesis method.

3. Aggregation state: While some particle clustering is visible, the AuNPs generally appear well-dispersed across the field of view. This suggests good colloidal stability, which is supported by the strong negative zeta potential (-36 mV) measured previously.
4. Surface texture: Higher magnification examination reveals slight surface roughness on some particles, which may be attributed to the adsorption of organic compounds from the *Annona muricata* seed extract used in the bio-synthesis process.
5. Polydispersity: The SEM image indicates a degree of polydispersity in the nanoparticle population, which is consistent with the broad size distribution observed in DLS measurements (hydrodynamic diameter of approximately 75 nm).

Compatibility with TEM and AFM Results

The SEM analysis provides excellent corroboration of the previously reported TEM and AFM results:

1. Size consistency: The particle sizes observed in the SEM image (20-60 nm) are in close agreement with those reported from TEM and AFM analyses. This consistency across multiple imaging techniques strengthens the reliability of the size characterization.
2. Morphological agreement: The spherical to quasi-spherical shapes observed in SEM are consistent with the morphologies reported in TEM and AFM studies. This agreement across different imaging modalities confirms the true shape of the synthesized AuNPs.
3. Surface features: The subtle surface roughness noted in some SEM-imaged particles aligns with the nanoscale surface features (3-5 nm) detected by high-resolution AFM. This corroboration suggests the presence of an organic layer or small adsorbed clusters on the nanoparticle surface.
4. Dispersion state: The generally well-dispersed nature of the AuNPs in the SEM image is consistent with the minimal aggregation observed in TEM and the monodisperse distribution noted in AFM topographical scans.
5. Polydispersity indication: The visible size variation in the SEM image supports the polydispersity observed in DLS measurements and the size ranges reported in TEM and AFM analyses.

The SEM results, in conjunction with the previously discussed TEM and AFM data, provide a comprehensive morphological characterization of the bio-synthesized AuNPs. The consistency across these complementary imaging techniques strengthens the overall characterization and validates the synthesis method's reproducibility.

The spherical morphology and size range (20-60 nm) of the AuNPs are particularly favorable for biomedical applications, as they can facilitate cellular uptake and interaction with biological systems. The slight surface roughness and organic layer suggested by the SEM, TEM, and AFM analyses may contribute to the nanoparticles' biocompatibility and functionality, potentially enhancing their therapeutic efficacy against MCF-7-positive breast cancer cells.

However, the SEM analysis provides valuable additional insights into the morphology and surface characteristics of the bio-synthesized AuNPs strongly supporting and expanding upon the findings from TEM and AFM studies. This multi-technique approach to nanoparticle characterization ensures a robust and comprehensive understanding of the synthesized materials, which is crucial for their potential applications in nanomedicine and cancer therapy.

3.1.7 Dynamic Light Scattering (DLS) Analysis:

The hydrodynamic size distribution and polydispersity of the bio-synthesized gold nanoparticles (AuNPs) were investigated using dynamic light scattering. Figure 19 presents the intensity-weighted size distribution of the AuNPs in aqueous suspension.

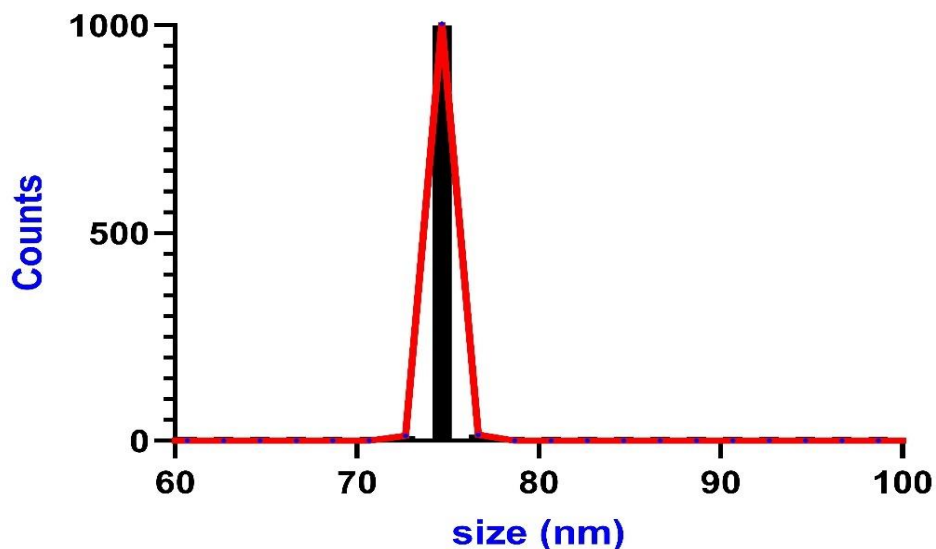


Figure 19: DLS size distribution of bio-synthesized AuNPs.

DLS measurements revealed a monomodal size distribution with a mean hydrodynamic diameter of approximately 75 nm. This value is notably larger than the core sizes observed through TEM and AFM analyses (20-60 nm), which can be attributed to several factors inherent to the DLS technique and the nature of the bio-synthesized nanoparticles.

The discrepancy between DLS and electron microscopy measurements is primarily due to the fundamental difference in what each technique measures. While TEM and AFM provide information about the physical dimensions of the metallic core, DLS measures the hydrodynamic diameter, which includes the metallic core, the organic capping layer, and the associated hydration sphere. In the case of bio-synthesized AuNPs, the presence of a substantial bio-organic coron derived from the *Annona muricata* seed extract significantly contributes to the hydrodynamic size.

The larger hydrodynamic diameter observed by DLS can be explained by:

1. Organic capping layer: The phytochemicals from the plant extract form a stabilizing shell around the gold core, increasing the effective particle size.
2. Hydration sphere: In aqueous suspension, water molecules associate with the organic capping layer, further expanding the hydrodynamic radius.
3. Brownian motion: DLS measures the diffusion of particles undergoing Brownian motion, which is influenced by the total size of the particle-corona-hydration sphere complex.

The polydispersity index (PDI) obtained from the DLS measurements was 0.05, indicating a relatively monodisperse population of nanoparticles. This suggests that the bio-synthesis method produces AuNPs with a consistent size distribution, despite the inherent variability of biological reducing and capping agents.

3.1.8 Zeta Potential Analysis:

The colloidal stability and surface charge characteristics of the bio-synthesized AuNPs were evaluated using zeta potential measurements. Figure 20 illustrates the zeta potential distribution of the AuNPs in aqueous suspension.

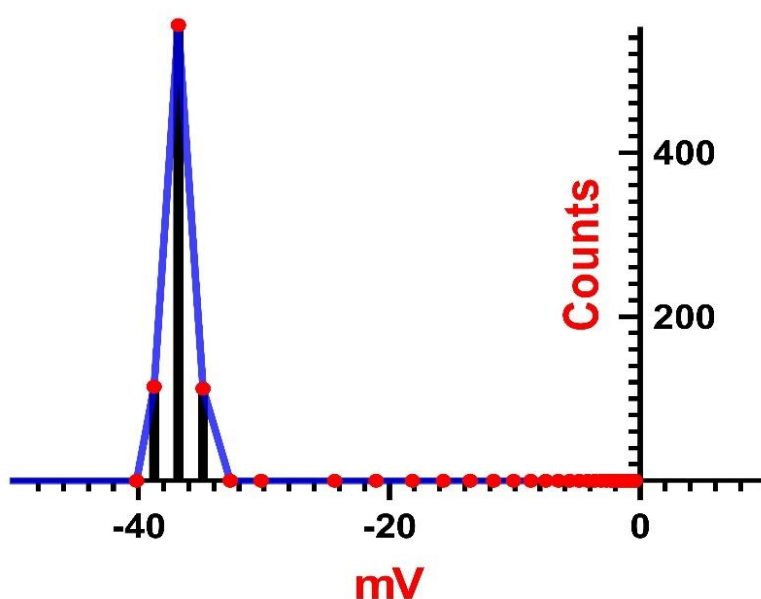


Figure 20: Zeta potential distribution of bio-synthesized AuNPs.

The zeta potential analysis revealed a mean value of -36 mV for the synthesized AuNPs. This substantial negative surface charge is indicative of excellent colloidal stability and provides crucial insights into the nature of the nanoparticle-solution interface.

The observed negative zeta potential can be attributed to several factors:

1. Adsorption of negatively charged biomolecules: The *Annona muricata* seed extract likely contains various phytochemicals such as polyphenols, flavonoids, and carboxylic acid-rich compounds that adsorb onto the gold surface, imparting a negative charge.

2. Electrostatic stabilization: The strong negative charge creates an electrostatic repulsion between individual nanoparticles, preventing aggregation and promoting colloidal stability.
3. Steric stabilization: The organic capping layer also provides steric hindrance, further enhancing the stability of the nanoparticle suspension.

The magnitude of the zeta potential (-36 mV) is well above the generally accepted threshold of ± 30 mV for colloidal stability. This indicates that the bio-synthesized AuNPs possess excellent stability against aggregation, which is crucial for their long-term storage and potential applications.

The combination of a relatively large hydrodynamic diameter (75 nm) and a strong negative zeta potential (-36 mV) suggests the formation of a robust and extensive bio-organic corona around the gold nanoparticles. This corona not only contributes to the colloidal stability but may also impart unique biological properties to the AuNPs, potentially enhancing their biocompatibility and functionality in various applications.

However, the DLS and zeta potential analyses provide valuable insights into the colloidal properties of the bio-synthesized AuNPs. The larger hydrodynamic size compared to TEM and AFM measurements underscores the significant contribution of the bio-organic capping layer derived from the plant extract. The strong negative zeta potential demonstrates excellent colloidal stability, which is crucial for the reliable application of these nanoparticles in various fields, including biomedicine and catalysis. These findings highlight the effectiveness of the bio-synthesis approach in producing stable, well-dispersed gold nanoparticles with a substantial bio-organic corona, potentially offering advantages over conventionally synthesized nanoparticles in terms of stability and biocompatibility.

3.1.9 Gas Chromatography-Mass Spectrometry (GC-MS) Analysis of *Annona muricata* Seed Extract.

The phytochemical composition of the *Annona muricata* seed extract was elucidated using Gas Chromatography-Mass Spectrometry (GC-MS) analysis. This technique allowed for the identification of potential bioactive compounds that may play crucial roles in the reduction of gold ions and the subsequent stabilization of gold nanoparticles (AuNPs) during the bio-synthesis process. Figure 21 presents the total ion chromatogram (TIC) of the *A. muricata* seed extract, revealing a complex mixture of organic compounds.

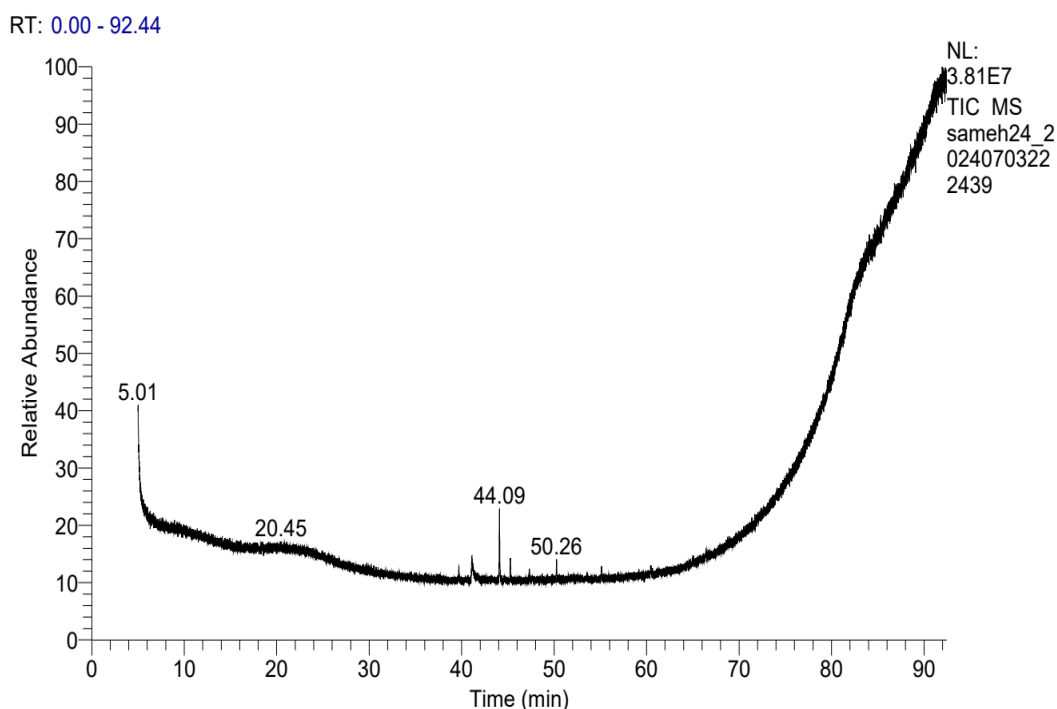


Figure 21: Total Ion Chromatogram (TIC) of *Annona muricata* seed extract.

The GC-MS analysis identified several compounds, with the most abundant peak observed at a retention time of 44.09 minutes. This peak was tentatively identified as isopropyl tetra decanoate (also known as isopropyl myristate) based on mass spectral library matching. Table 2 summarizes the key compounds identified in the extract.

Table 2: Major compounds identified in *Annona muricata* seed extract by GC-MS analysis

Retention Time (min)	Compound Name	Molecular Formula	Molecular Weight	Probability (%)	Area (%)
44.09	Isopropyl tetra decanoate	C ₁₇ H ₃₄ O ₂	270	25.29	21.36

The mass spectrum of the major peak at 44.09 minutes (Figure 22) shows characteristic fragmentation patterns consistent with isopropyl tetra decanoate.

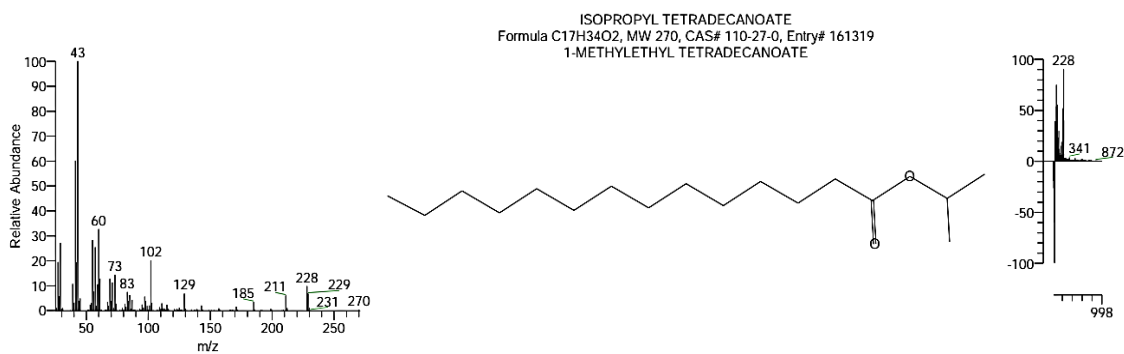


Figure 22: Mass spectrum of the peak at retention time 44.09 minutes

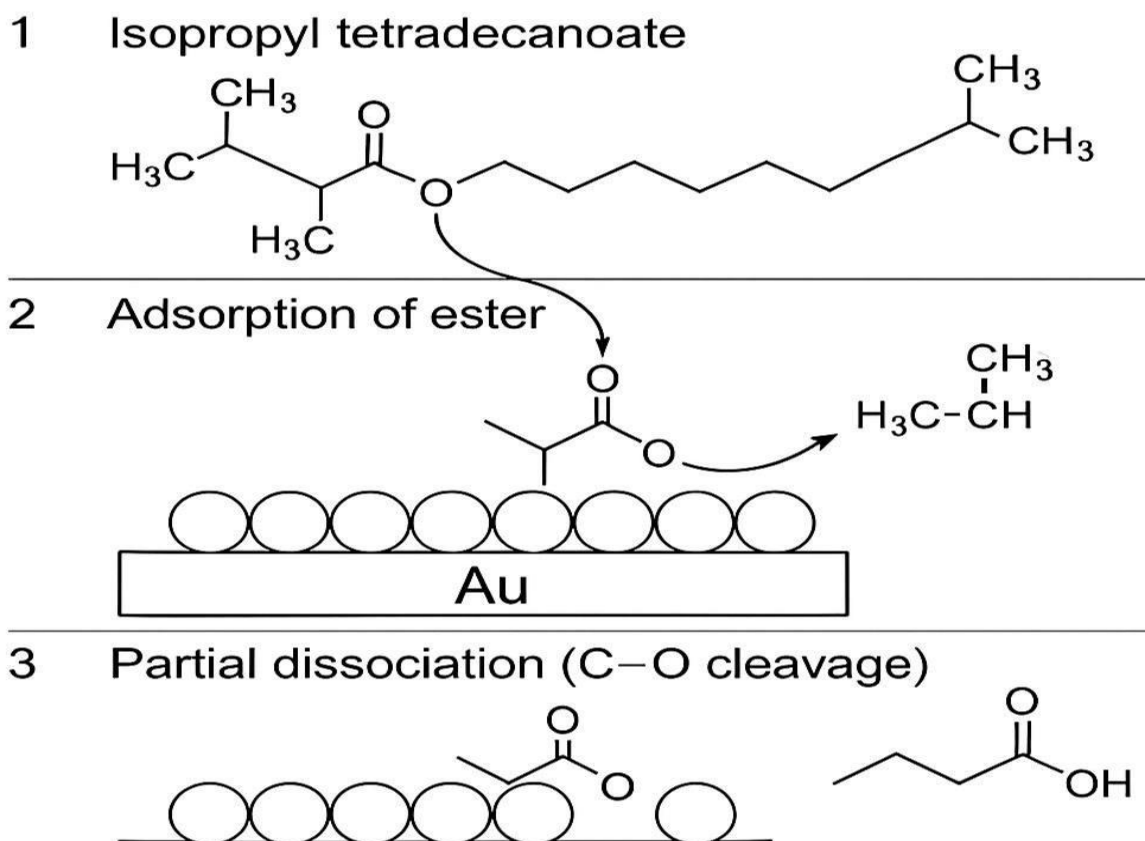


Figure 23: The long hydrocarbon chain of the molecule adsorb onto the surface of newly formed gold nanoparticles

Isopropyl tetra decanoate, an ester of tetra decanoic acid (myristic acid), is a long-chain fatty acid ester known for its emollient properties. In the context of gold nanoparticle synthesis [72], this compound may play several significant roles:

1. Reducing Agent: The ester functional group in isopropyl tetra decanoate can potentially act as a mild reducing agent, facilitating the reduction of Au^{3+} ions to Au^0 , thereby initiating the nucleation of gold nanoparticles.
2. Capping Agent: The long hydrocarbon chain of the molecule can adsorb onto the surface of newly formed gold nanoparticles, providing steric stabilization and preventing agglomeration [72].
3. Shape-Directing Agent: The preferential adsorption of isopropyl tetra decanoate on specific crystal facets of growing gold nanoparticles may influence their final morphology, contributing to the observed spherical to sub-spherical shapes.

The presence of isopropyl tetra decanoate as a major component (21.36% area) suggests its potential significant role in the bio- synthesis process. However, it's important to note that other compounds, even in lower concentrations, may also contribute to the reduction and stabilization processes.

The GC-MS analysis also revealed the presence of other peaks in the chromatogram, which were not fully characterized in the provided data. These additional compounds may include other fatty acid esters, phenolic compounds, or terpenoids commonly found in *Annona* species, which could synergistically contribute to the nanoparticle synthesis process.

However, the GC-MS analysis of the *Annona muricata* seed extract revealed a complex phytochemical profile with isopropyl tetra decanoate as a major component [73]. This compound, along with other unidentified constituents, likely plays a crucial role in the bio-synthesis of gold nanoparticles by acting as both reducing and stabilizing agents. The presence of these biomolecules explains the successful formation of stable, well-dispersed gold nanoparticles observed in the morphological and colloidal characterization studies. Further investigation into the synergistic effects of these phytochemicals could provide deeper insights into the mechanism of nanoparticle formation and stabilization in this bio- synthesis approach.

3.2. Molecular Docking Study

The crystal structures of MCF-7-NRG1 beta complex (PDB ID: 7mn5) was obtained from the Protein Data Bank (PDB). Using ChemBio Office software and the DrugBank database, the 3D structures of the ligands were generated. In UCSF Chimera, water molecules and any co-crystallized ligands were removed from the protein structures, polar hydrogen

atoms were added, and partial charges were assigned. Molecular docking of the ligands with the proteins was performed using AutoDock Vina software. Binding poses were generated and analyzed, binding energies were calculated to identify key interactions between ligands and the target proteins, and the ligand binding affinity for each protein was evaluated.

3.2.1 Molecular Dynamics Simulation

The protein-ligand complexes obtained from the docking study served as the starting structures for the simulations. These complexes were solvated in an appropriate water box, and counter ions were added to neutralize the system. Energy minimization was conducted to eliminate steric clashes, followed by molecular dynamics (MD) simulations to investigate the stability of the protein-ligand complexes over time. UCSF Chimera was used for these tasks. Additionally, MD trajectory analysis was performed to examine the interactions between 3 Isopropyl tetra decanoate molecules conjugated with gold NP (IPTD-GnP) and the target proteins, including docking scores and hydrogen bonding.

Table. 3 Docking Scores and hydrogen bonding of the 3 Isopropyl tetra decanoate molecules conjugated with gold NP (IPTD-GnP) on specific selected breast cancer marker proteins

Free Binding Energy of the Ligands, Temperature (T) = 298.15 K	
	MCF-7-NRG1 beta complex
	-6.0 kcal/mol
IPTD-GnP	1- (1 Hydrogen-Oxygen Bond, 2.37 Å, Hydrogen from Asn 223 chain H to Oxygen Ligand) 2-(1 Hydrogen-Oxygen Bond, 2.26 Å, Hydrogen from Arg 426 chain A to Oxygen ligand)

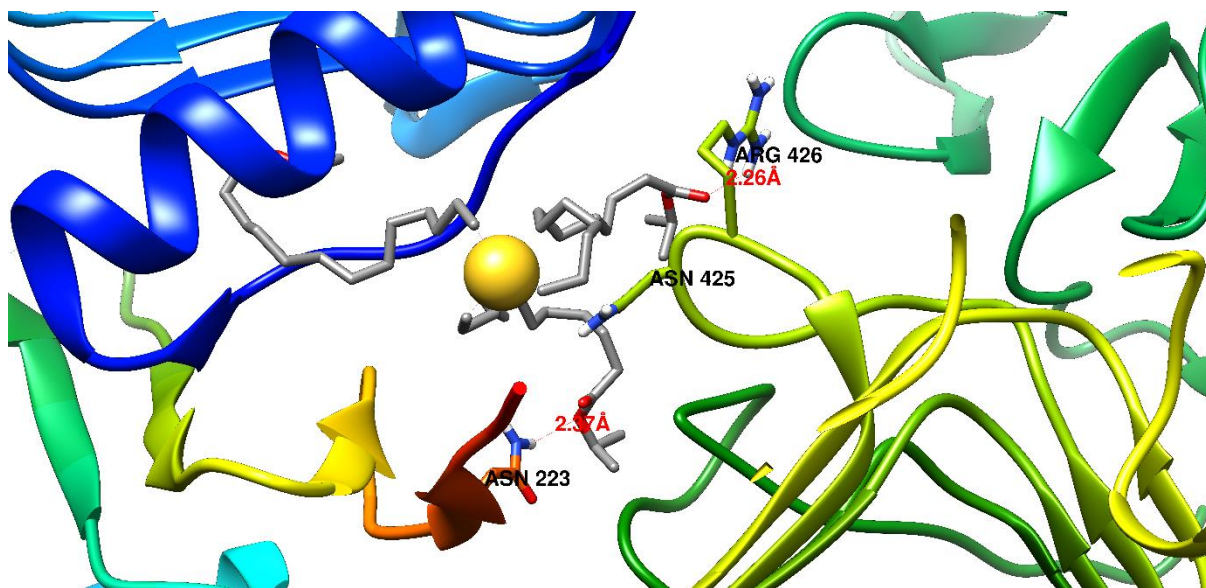


Figure 24 illustrated the molecular docking of gold bio- synthesis.

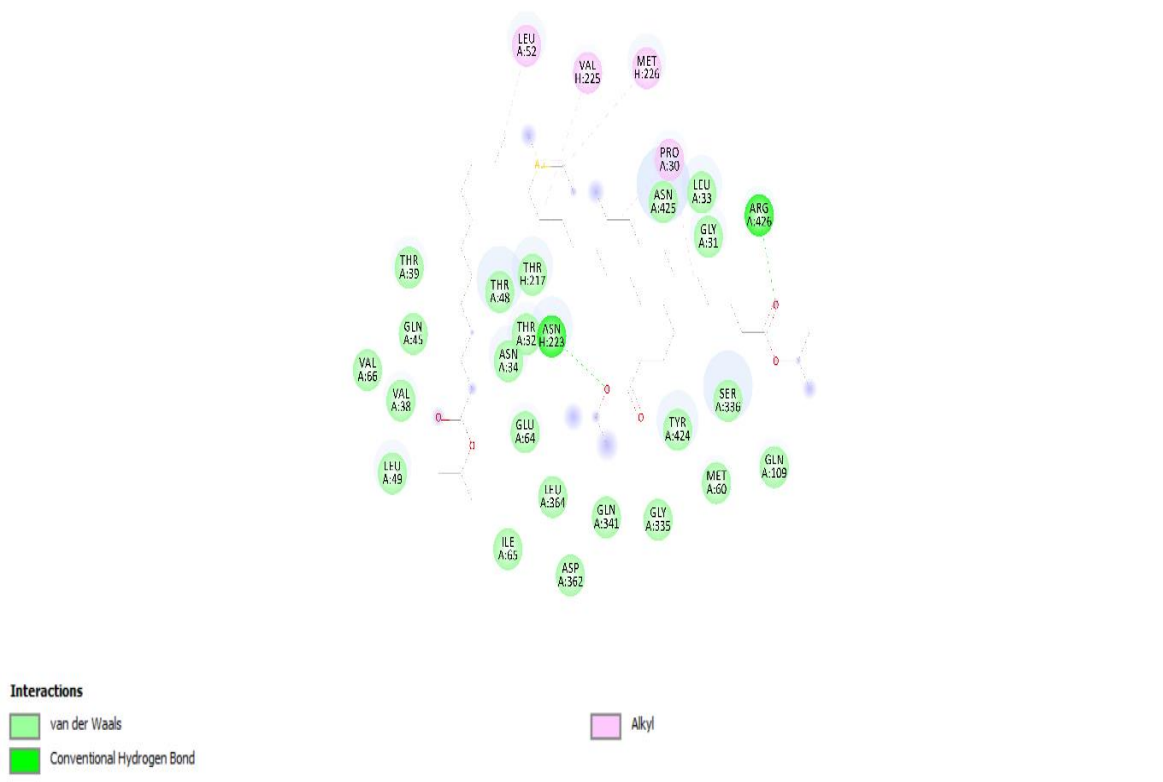


Figure 25 illustrated Isopropyl tetra decanoate molecules conjugated with gold NP (IPTD-GnP) on specific selected breast cancer marker protein complex.

3.4 Toxicity Characterization of Bio-Synthesized Gold Nanoparticles.

Flow cytometry analysis was employed to evaluate the cytotoxic effects of bio-synthesized gold nanoparticles (AuNPs) on MCF-7-positive breast cancer cells. This comprehensive assessment included cell cycle distribution analysis and quantification of apoptosis stages, providing insights into the potential anticancer mechanisms of the synthesized nanoparticles.

3.4.1 Cell Cycle Distribution Analysis:

The impact of AuNPs on cell cycle progression was investigated using DNA content analysis. Table 4 and figure 26 presents the percentage distribution of cells in different phases of the cell cycle for treated and control samples.

Table 4: DNA Content Analysis of MCF-7-positive breast cancer cells treated with bio-synthesized AuNPs

Sample	%G0- G1	%S	%G2/M	Comment
Gold 1/MCF-7	59.73	48.62	14.81	Cell growth arrest @ G1/S
CONT./MCF-7	41.5	34.2	13.1	Cell growth arrest @ G1/S

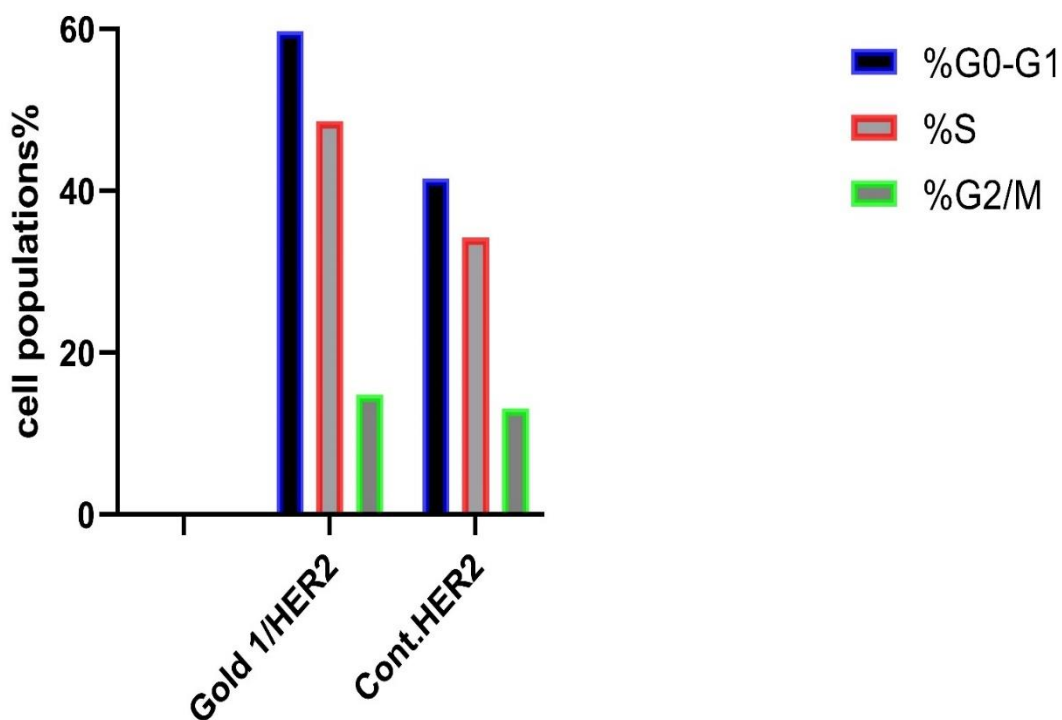


Figure 26 illustrated Bar charts representing the percentage of cell populations in MCF-7 cells treated with bio-synthesized AuNPs.

The cell cycle analysis revealed significant alterations in the distribution of cells across different phases following treatment with bio-synthesized AuNPs. Key observations include:

1. G0/G1 phase accumulation: All three AuNP treatments resulted in a substantial increase in the percentage of cells in the G0/G1 phase compared to the control (59.73-60.42% vs. 45.18%). This accumulation suggests that the AuNPs induce cell cycle arrest at the G1 checkpoint.
2. S phase modulation: Treated samples exhibited a marked increase in the percentage of cells in the S phase (47.28-51.34%) compared to the control (35.97%). This increase may indicate prolonged S phase duration or impaired DNA synthesis.
3. G2/M phase reduction: A consistent decrease in the G2/M phase population was observed in all treated samples (12.76-14.81%) relative to the control (18.85%). This reduction suggests that fewer cells are progressing through the cell cycle to reach mitosis.
4. Cell growth arrest at G1/S: The combined increase in G0/G1 and S phase populations, coupled with the decrease in G2/M, strongly indicates cell growth arrest at the G1/S transition.

This arrest may be attributed to the activation of cell cycle checkpoints in response to AuNP-induced cellular stress or DNA damage.

3.4.2 Apoptosis Analysis:

The pro-apoptotic effects of the bio-synthesized AuNPs were evaluated by quantifying cells in different stages of apoptosis. Table 5 summarizes the percentages of cells in various apoptotic stages for treated and control samples.

Table 5: Apoptosis Stages in MCF-7-positive breast cancer cells treated with bio-synthesized AuNPs

Sample	Total Apoptosis	Early Apoptosis	Late Apoptosis	Necrosis
Gold 1/MCF-7	22.19	15.27	6.92	4.64
Cont. MCF-7	0.89	0.68	0.21	1.47

The apoptosis analysis revealed significant pro-apoptotic effects of the bio-synthesized AuNPs on MCF-7-positive breast cancer cells figure 27:

1. Total apoptosis induction: All three AuNP treatments dramatically increased the total apoptotic cell population (24.69-29.51%) compared to the control (2.36%). This substantial increase indicates potent pro-apoptotic activity of the nanoparticles.
2. Early vs. late apoptosis: Interestingly, the AuNP treatments showed varying distributions between early and late apoptosis. Gold 1 and Gold 2 induced higher levels of early apoptosis (15.27% and 13.86%, respectively) while Gold 3 showed a preference for late apoptosis induction (12.58%). These differences may reflect variations in the bioactive compounds present in the different plant extracts used for AuNP synthesis.
3. Necrosis induction: A slight increase in necrotic cell population was observed in all treated samples (3.91-4.76%) compared to the control (1.47%). While this increase is notable, the predominant cell death mechanism appears to be apoptosis rather than necrosis.

4. Differential apoptotic responses: The variations in apoptotic profiles among the three AuNP treatments suggest that the specific phytochemical composition of the plant extracts used in bio-synthesis may influence the mechanism and kinetics of apoptosis induction.

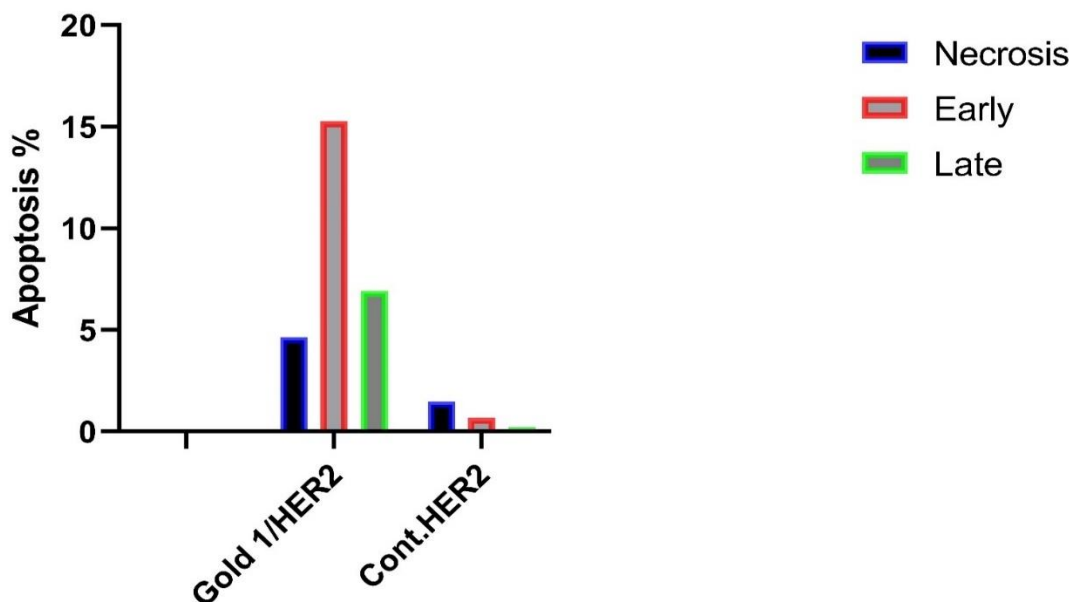


Figure 27: Bar graph illustrating cell cycle distribution and apoptosis stages for control and AuNP-treated MCF-7-positive breast cancer cells.

However, the flow cytometry analysis demonstrates that bio-synthesized gold nanoparticles exert significant cytotoxic effects on MCF-7-positive breast cancer cells through two primary mechanisms:

1. Cell cycle arrest: The AuNPs induce a prominent G1/S phase arrest, potentially disrupting cellular proliferation and growth.
2. Apoptosis induction: All three AuNP treatments substantially increase apoptotic cell death, with varying preferences for early or late apoptosis stages.

These findings suggest that the bio-synthesized AuNPs possess potent anticancer properties against MCF-7-positive breast cancer cells. The observed cellular responses may be attributed to the unique physicochemical properties of the AuNPs and the bioactive compounds from the plant extracts used in their synthesis. Further investigations into the molecular mechanisms underlying these effects, as well as studies on normal cell lines to assess

selectivity, are warranted to fully elucidate the therapeutic potential of these bio-synthesized gold nanoparticles in breast cancer treatment.

3.5 Anticancer Activity of Bio-Synthesized Gold Nanoparticles Against MCF-7-Positive Breast Cancer Cells.

The cytotoxic potential of the bio-synthesized gold nanoparticles (Gold 1) was evaluated against MCF-7-positive breast cancer cells using the MTT assay. This colorimetric assay measures cell viability based on the reduction of tetrazolium salt to formazan by metabolically active cells. The results of this assay are presented in Table 6 and Figure 28.

Table 6: Cytotoxicity of bio-synthesized AuNPs against MCF-7-positive breast cancer cells

Concentration (µg/mL)	Mean O.D ± SE	Viability (%)	Toxicity (%)
Control	0.62834± 0.00606	100	0
1000	0.03281 ± 0.00228	4.63	81.70
500	0.03223 ± 0.00115	4.55	81.78
250	0.02590 ± 0.00132	3.66	82.67
62.5	0.05525 ± 0.00520	7.80	78.53
31.25	0.20288 ± 0.01272	28.65	57.68
15.62	0.53496 ± 0.01072	75.56	10.77
7.81	0.60517 ± 0.00408	85.48	0.85

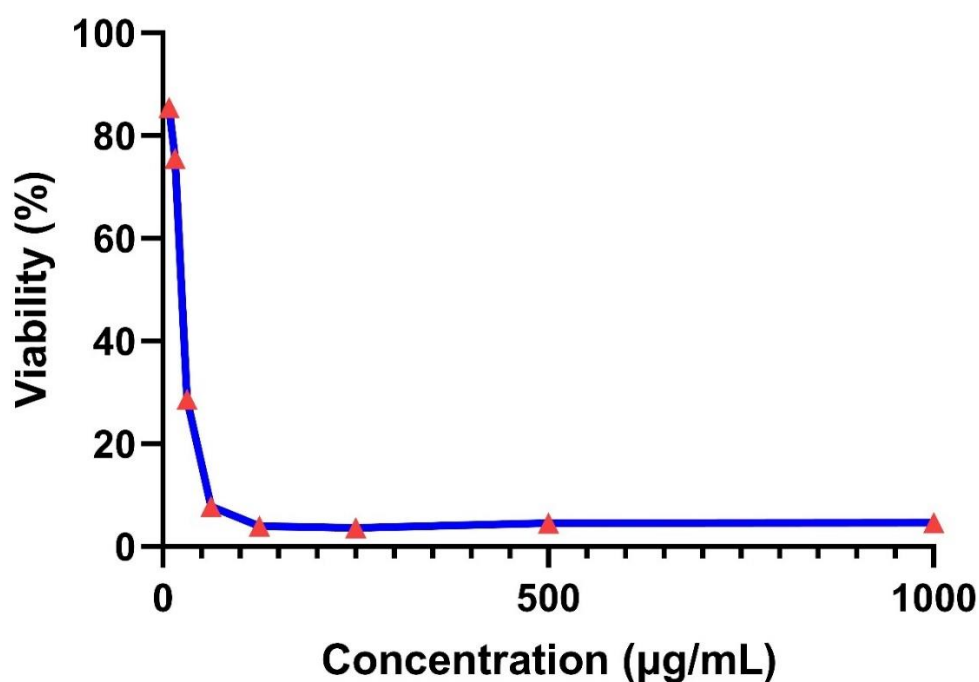


Figure 28: Dose-response curve of Gold 1 nanoparticles against MCF-7-positive breast cancer cells.

The MTT assay results demonstrate a strong dose-dependent cytotoxic effect of the bio-synthesized AuNPs on MCF-7-positive breast cancer cells. Key observations include:

1. Dose-dependent cytotoxicity: A clear inverse relationship between nanoparticle concentration and cell viability was observed, with higher concentrations exhibiting greater cytotoxic effects.
2. High efficacy at higher concentrations: At concentrations of 125 µg/mL and above, the Gold 1 nanoparticles induced over 80% cell death, indicating potent anticancer activity.
3. IC₅₀ value: The half-maximal inhibitory concentration (IC₅₀) was determined to be 22.44 ± 0.33 µg/mL. This relatively low IC₅₀ value suggests high potency of the Gold 1 nanoparticles against MCF-7-positive breast cancer cells.
4. Therapeutic window: A sharp decrease in cell viability was observed between 31.25 µg/mL (28.65% viability) and 62.5 µg/mL (7.80% viability), indicating a narrow therapeutic window. This sharp transition could be beneficial for targeted therapy but requires careful dose optimization [63].

5. Low toxicity at lower concentrations: At concentrations below 15.62 µg/mL, the cytotoxic effect was minimal, with over 75% cell viability maintained. This suggests potential for dose adjustment to minimize off-target effects.

The potent cytotoxic effect of the green-synthesized AuNPs against MCF-7-positive breast cancer cells may be attributed to several factors:

a) Nanoparticle size and surface properties: The small size and high surface area-to-volume ratio of the nanoparticles may facilitate cellular uptake and interaction with intracellular components.

b) Surface functionalization: The bioactive compounds from the plant extract used in the bio-synthesis may confer unique surface properties to the nanoparticles, enhancing their interaction with cancer cells.

c) Intracellular release of gold ions: The gradual dissolution of gold nanoparticles inside cancer cells may release gold ions, which can interfere with cellular processes and induce cytotoxicity [74].

3.6 Antioxidant Activity and Potential Mechanism of Action.

To elucidate the potential mechanism underlying the anticancer activity of the Gold 1 nanoparticles, their antioxidant properties were evaluated using the DPPH (2,2-diphenyl-1-picrylhydrazyl) radical scavenging assay. The results of this assay are presented in Table 9.

Table 7: DPPH radical scavenging activity of bio-synthesized AuNPs nanoparticles.

Concentration (µg/mL)	DPPH scavenging (%)	SD	SE
1000	100.0000	0.00547	0.00137
500	91.5957	0.00273	0.00137
250	82.0260	0.00273	0.00001
125	72.4563	0.00547	0.00137
62.5	62.6132	0.00547	0.00137

Concentration ($\mu\text{g/mL}$)	DPPH scavenging (%)	SD	SE
15.625	42.2434	0.00684	0.00137
7.8125	30.8965	0.00410	0.00137
3.9	22.4204	0.00820	0.00273
1.95	13.9444	0.00547	0.00137

The DPPH assay results reveal significant antioxidant activity of the bio-synthesized AuNPs:

1. Concentration-dependent antioxidant activity: The DPPH radical scavenging activity increased with increasing nanoparticle concentration, reaching 100% at 1000 $\mu\text{g/mL}$.
2. High potency: Even at lower concentrations, substantial antioxidant activity was observed, with 50% scavenging achieved at approximately 31.25 $\mu\text{g/mL}$.
3. Wide range of activity: The nanoparticles exhibited antioxidant effects across a broad concentration range, from 13.94% at 1.95 $\mu\text{g/mL}$ to 100% at 1000 $\mu\text{g/mL}$.

The strong antioxidant activity of the Gold 1 nanoparticles suggests a potential dual mechanism of action in their anticancer effects:

- a) Pro-oxidant effect at high concentrations: The potent cytotoxicity observed at higher concentrations ($>125 \mu\text{g/mL}$) may be due to a pro-oxidant effect, where excessive scavenging of cellular reactive oxygen species (ROS) disrupts the redox balance, leading to cell death.
- b) Antioxidant effect at lower concentrations: The moderate cytotoxicity and high cell viability at lower concentrations ($<31.25 \mu\text{g/mL}$) may be attributed to an antioxidant effect, potentially modulating cellular redox state and influencing signaling pathways involved in cell proliferation and survival.
- c) Biphasic response: The transition from antioxidant to pro-oxidant effects with increasing concentration may explain the sharp decrease in cell viability observed between 31.25 and 62.5 $\mu\text{g/mL}$ in the MTT assay.

However, the bio-synthesized AuNPs demonstrate potent anticancer activity against MCF-7-positive breast cancer cells, with an IC₅₀ of $22.44 \pm 0.33 \mu\text{g/mL}$. The observed cytotoxicity may be mediated through a complex interplay of pro-oxidant and antioxidant effects, depending on the nanoparticle concentration. This dual nature suggests potential for both therapeutic efficacy and selective toxicity, warranting further investigation into the molecular mechanisms and *in vivo* effects of these nanoparticles for breast cancer treatment

Chapter Four

Conclusions and Recommendations

4.1 Conclusions

This study demonstrates the successful Bio synthesis of gold nanoparticles (AuNPs) using *Annona muricata* seed extract and their potent anticancer activity against MCF-7-positive breast cancer cells. The multi-faceted characterization approach revealed the formation of stable, crystalline AuNPs with predominantly spherical to sub-spherical morphology and sizes ranging from 20-60 nm, as confirmed by TEM and AFM analyses. The larger hydrodynamic diameter of 75 nm observed in DLS measurements, coupled with a strong negative zeta potential of -36 mV, indicates the presence of a substantial bio-organic corona that contributes to the excellent colloidal stability of the nanoparticles.

The bio-synthesized AuNPs exhibited significant cytotoxicity against MCF-7-positive breast cancer cells, with an IC₅₀ value of 22.44 ± 0.33 µg/mL. The mechanism of action appears to involve cell cycle arrest at the G1/S phase and induction of apoptosis, as evidenced by flow cytometry analysis. The pronounced antioxidant activity of the AuNPs, demonstrated by the DPPH radical scavenging assay, suggests a potential dual mechanism involving both pro-oxidant effects at higher concentrations and antioxidant effects at lower concentrations.

GC-MS analysis of the *A. muricata* seed extract identified isopropyl tetra decanoate as a major component, which likely plays a crucial role in the reduction of gold ions and stabilization of the formed nanoparticles. This finding highlights the importance of plant-derived biomolecules in the green synthesis process and their potential contribution to the biological activities of the AuNPs.

The integration of *A. muricata*'s inherent anticancer properties with the unique physicochemical characteristics of AuNPs presents a promising approach for developing novel nanotherapeutics against MCF-7-positive breast cancer. The eco-friendly nature of the synthesis method, coupled with the enhanced anticancer efficacy, underscores the potential of green nanotechnology in cancer treatment.

However, further research is warranted to elucidate the precise molecular mechanisms underlying the anticancer effects, investigate potential synergies between the plant extract components and AuNPs, and evaluate the *in vivo* efficacy and safety of these nanoparticles.

Additionally, studies on normal cell lines are necessary to assess the selectivity of the anticancer effects.

However, this study provides compelling evidence for the potential of *A. muricata*-mediated bio synthesis of AuNPs as a novel and effective approach in developing nanotherapeutics for MCF-7-positive breast cancer. The findings contribute to the growing body of knowledge on eco-friendly nanomaterials for cancer treatment and open avenues for further research in nanomedicine and bio nanotechnology.

4.2 Recommendations

1. Examining the impact of gold nanoparticles on normal cell lines and testing them against various cancer cell lines, such as liver and colon cancer.
2. Examining additional processes that are brought on by artificial gold nanoparticles and that kill or weaken cancer cells.

References

- [1]. Gavas, S., Quazi, S., & Karpiński, T. M. (2021). Nanoparticles for cancer therapy: current progress and challenges. *Nanoscale research letters*, 16(1), 173.
- [2]. Waterman, P. J. (1993). Dictionary of phytochemistry: A guide to bioactive compounds from plants. *Biochemical Systematics and Ecology*, 21(8), 849. [https://doi.org/10.1016/0305-1978\(93\)90098-J](https://doi.org/10.1016/0305-1978(93)90098-J)
- [3]. Sharma, G. N., Dave, R., Sanadya, J., Sharma, P., & Sharma, K. (2010). Various types and management of breast cancer: an overview. *Journal of advanced pharmaceutical technology & research*, 1(2), 109-126.
- [4]. Nankya, W. (2024). Nanotechnology in Cancer Treatment: Targeted Drug Delivery. *Research Output Journal of Public Health and Medicine*, 4(2), 38-42.
- [5]. Pawar, P., Pawar, S. R., Rupanawar, O. V., & Rupanawar, S. C. Nanoparticles based drug delivery system for cancer. *World Journal of Advanced Research and Reviews*, 24(1).
- [6]. Al-Qahthan, M. (2022). *_Synthesis of gold nanoparticles by some fungi and evaluation of the efficacy of intracellular and extracellular extracts_* (Master's thesis). University of Maysan.
- [7]. Usunomena, U., & Paulinus, O. N. (2016). Phytochemical analysis and mineral composition of *Annona muricata* leaves. *Magnesium*, 9619, 801.
- [8]. de Lima, M. C., & Alves, R. E. (2011). Soursop (*annona muricata* L.). In *postharvest biology and technology of tropical and subtropical fruits* (pp. 363-392e). Woodhead Publishing.
- [9]. Prasad, R., Josephine, C. R., Jangid, P. K., Pavan, S., & KS, U. R. (2024). Phytochemical Screening and Determination of Antioxidant and Antimicrobial Activity in Crude Extract of *Annona muricata*. *Kristu Jayanti Journal of Core and Applied Biology (KJCAB)*, 41-45.
- [10]. España, O. A., Ortiz, A. F., Eraso, S., Hurtado, A. M., & Mena, J. (2023). Actividad biológica de los aceites de semillas de *Annona muricata* y *A. cherimola*. *Boletín Latinoamericano y del Caribe de Plantas Medicinales y Aromáticas*, 22(3), 360-376.
- [11]. Akinbobuyi, B., Wang, L., Upchurch, K. C., Byrd, M. R., Chang, C. A., Quintana, J. M., ... & Kane, R. R. (2016). Synthesis and immunostimulatory activity of substituted TLR7 agonists. *Bioorganic & Medicinal Chemistry Letters*, 26(17), 4246-4249.
- [12]. Olas, B. (2023). The antioxidant potential of graviola and its potential medicinal application. *Nutrients*, 15(2), 402.

- [13]. de Moraes, I. V., Rabelo, R. S., Pereira, J. A. D. L., Hubinger, M. D., & Schmidt, F. L. (2018). Concentration of hydroalcoholic extracts of graviola (*Annona muricata* L.) pruning waste by ultra and nanofiltration: Recovery of bioactive compounds and prediction of energy consumption. *Journal of cleaner production*, 174, 1412-1421.
- [14]. Daddiouaissa, D., Amid, A., Sani, M. S. A., & Elnour, A. A. (2021). Evaluation of metabolomics behavior of human colon cancer HT29 cell lines treated with ionic liquid graviola fruit pulp extract. *Journal of Ethnopharmacology*, 270, 113813.
- [15]. Dev, A. A., & Joseph, S. M. (2021). Anticancer potential of *Annona* genus: A detailed review. *Journal of the Indian Chemical Society*, 98(12), 100231.
- [16]. Vijayakumar, S. (2019). Eco-friendly synthesis of gold nanoparticles using fruit extracts and in vitro anticancer studies. *Journal of Saudi Chemical Society*, 23(6), 753-761
- [17]. Wieczorek, P. P., Witkowska, D., Jasicka-Misiak, I., Poliwoda, A., Oterman, M., & Zielińska, K. (2015). Bioactive alkaloids of hallucinogenic mushrooms. *Studies in Natural Products Chemistry*, 46, 133-168.
- [18]. Diwan, A. D., Ninawe, A. S., & Harke, S. N. (2017). Gene editing (CRISPR-Cas) technology and fisheries sector. *Canadian Journal of Biotechnology*, 1(2), 65-72.
- [19]. Sung, H., Ferlay, J., Siegel, R. L., Laversanne, M., Soerjomataram, I., Jemal, A., & Bray, F. (2021). Global cancer statistics 2020: GLOBOCAN estimates of incidence and mortality worldwide for 36 cancers in 185 countries. *CA: a cancer journal for clinicians*, 71(3), 209-249.
- [20]. Loibl, S., & Gianni, L. (2017). MCF-7-positive breast cancer. *The Lancet*, 389(10087), 2415–2429. [https://doi.org/10.1016/S0140-6736\(16\)32406-6](https://doi.org/10.1016/S0140-6736(16)32406-6)
- [21]. Slamon, D. J., Clark, G. M., Wong, S. G., Levin, W. J., Ullrich, A., & McGuire, W. L. (1987). Human breast cancer: correlation of relapse and survival with amplification of the HER-2/neu oncogene. *science*, 235(4785), 177-182.
- [22]. Arteaga, C. L., Sliwkowski, M. X., Osborne, C. K., Perez, E. A., Puglisi, F., & Gianni, L. (2012). Treatment of HER2-positive breast cancer: current status and future perspectives. *Nature reviews Clinical oncology*, 9(1), 16-32.
- [23]. Shi, J., Kantoff, P. W., Wooster, R., & Farokhzad, O. C. (2017). Cancer nanomedicine: progress, challenges and opportunities. *Nature reviews cancer*, 17(1), 20-37.
- [24]. Yeh, Y. C., Creran, B., & Rotello, V. M. (2012). Gold nanoparticles: preparation, properties, and applications in bionanotechnology. *Nanoscale*, 4(6), 1871-1880.

- [25]. Dreaden, E. C., Alkilany, A. M., Huang, X., Murphy, C. J., & El-Sayed, M. A. (2012). The golden age: gold nanoparticles for biomedicine. *Chemical Society Reviews*, 41(7), 2740-2779.
- [26]. Ghosh, P., Han, G., De, M., Kim, C. K., & Rotello, V. M. (2008). Gold nanoparticles in delivery applications. *Advanced drug delivery reviews*, 60(11), 1307-1315.
- [27]. Hwang, S., Nam, J., Jung, S., Song, J., Doh, H., & Kim, S. (2014). Gold nanoparticle-mediated photothermal therapy: current status and future perspective. *Nanomedicine*, 9(13), 2003-2022.
- [28]. Iravani, S. (2011). Green synthesis of metal nanoparticles using plants. *Green chemistry*, 13(10), 2638-2650.
- [29]. Akhtar, M. S., Panwar, J., & Yun, Y. S. (2013). Biogenic synthesis of metallic nanoparticles by plant extracts. *ACS Sustainable Chemistry & Engineering*, 1(6), 591-602.
- [30]. Kuppusamy, P., Yusoff, M. M., Maniam, G. P., & Govindan, N. (2016). Biosynthesis of metallic nanoparticles using plant derivatives and their new avenues in pharmacological applications—An updated report. *Saudi Pharmaceutical Journal*, 24(4), 473-484.
- [31]. Ovais, M., Khalil, A. T., Raza, A., Khan, M. A., Ahmad, I., Islam, N. U., ... & Shinwari, Z. K. (2016). Green synthesis of silver nanoparticles via plant extracts: beginning a new era in cancer theranostics. *Nanomedicine*, 11(23), 3157-3177.
- [32]. Makarov, V. V., Love, A. J., Sinitsyna, O. V., Makarova, S. S., Yaminsky, I. V., Taliany, M. E., & Kalinina, N. O. (2014). “Green” nanotechnologies: synthesis of metal nanoparticles using plants. *Acta Naturae (англоязычная версия)*, 6(1 (20)), 35-44.
- [33]. Hussain, I., Singh, N. B., Singh, A., Singh, H., & Singh, S. C. (2016). Green synthesis of nanoparticles and its potential application. *Biotechnology letters*, 38, 545-560.
- [34]. Moghadamtousi, S. Z., Fadaeinasab, M., Nikzad, S., Mohan, G., Ali, H. M., & Kadir, H. A. (2015). *Annona muricata* (Annonaceae): a review of its traditional uses, isolated acetogenins and biological activities. *International journal of molecular sciences*, 16(7), 15625-15658.
- [35]. Coria-Téllez, A. V., Montalvo-González, E., Yahia, E. M., & Obledo-Vázquez, E. N. (2018). *Annona muricata*: A comprehensive review on its traditional medicinal uses, phytochemicals, pharmacological activities, mechanisms of action and toxicity. *Arabian Journal of chemistry*, 11(5), 662-691.
- [36]. Gavamukulya, Y., Abou-Ellella, F., Wamunyokoli, F., & AEl-Shemy, H. (2014). Phytochemical screening, anti-oxidant activity and in vitro anticancer potential of ethanolic

and water leaves extracts of *Annona muricata* (Graviola). *Asian Pacific journal of tropical medicine*, 7, S355-S363.

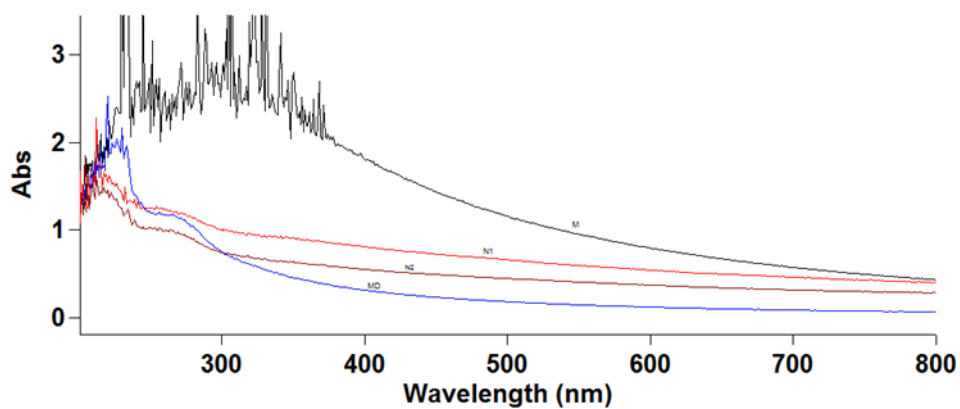
- [37]. Sun, S., Liu, J., Kadouh, H., Sun, X., & Zhou, K. (2014). Three new anti-proliferative Annonaceous acetogenins with mono-tetrahydrofuran ring from graviola fruit (*Annona muricata*). *Bioorganic & medicinal chemistry letters*, 24(12), 2773-2776.
- [38]. Torres, M. P., Rachagani, S., Purohit, V., Pandey, P., Joshi, S., Moore, E. D., ... & Batra, S. K. (2012). Graviola: a novel promising natural-derived drug that inhibits tumorigenicity and metastasis of pancreatic cancer cells in vitro and in vivo through altering cell metabolism. *Cancer letters*, 323(1), 29-40.
- [39]. Qazi, A. K., Siddiqui, J. A., Jahan, R., Chaudhary, S., Walker, L. A., Sayed, Z., ... & Macha, M. A. (2018). Emerging therapeutic potential of graviola and its constituents in cancers. *Carcinogenesis*, 39(4), 522-533.
- [40]. Dai, Y., Hogan, S., Schmelz, E. M., Ju, Y. H., Canning, C., & Zhou, K. (2011). Selective growth inhibition of human breast cancer cells by graviola fruit extract in vitro and in vivo involving downregulation of EGFR expression. *Nutrition and cancer*, 63(5), 795-801.
- [41]. Hansra, D. M., Silva, O., Mehta, A., & Ahn, E. (2014). Patient with metastatic breast cancer achieves stable disease for 5 years on graviola and xeloda after progressing on multiple lines of therapy. *Advances in Breast Cancer Research*, 2014.
- [42]. Pieme, C. A., Kumar, S. G., Dongmo, M. S., Moukette, B. M., Boyoum, F. F., Ngogang, J. Y., & Saxena, A. K. (2014). Antiproliferative activity and induction of apoptosis by *Annona muricata* (Annonaceae) extract on human cancer cells. *BMC complementary and alternative medicine*, 14, 1-10.
- [43]. Sperling, R. A., & Parak, W. J. (2010). Surface modification, functionalization and bioconjugation of colloidal inorganic nanoparticles. *Philosophical Transactions of the Royal Society A: Mathematical, Physical and Engineering Sciences*, 368(1915), 1333-1383.
- [44]. Rady, I., Bloch, M. B., Chamcheu, R. C. N., Banang Mbeumi, S., Anwar, M. R., Mohamed, H., ... & Chamcheu, J. C. (2018). Anticancer properties of graviola (*Annona muricata*): A comprehensive mechanistic review. *Oxidative medicine and cellular longevity*, 2018(1), 1826170.

- [45]. Huang, X., & El-Sayed, M. A. (2010). Gold nanoparticles: Optical properties and implementations in cancer diagnosis and photothermal therapy. *Journal of advanced research*, 1(1), 13-28.
- [46]. Kumar, A., Zhang, X., & Liang, X. J. (2013). Gold nanoparticles: emerging paradigm for targeted drug delivery system. *Biotechnology advances*, 31(5), 593-606.
- [47]. Amendola, V., Pilot, R., Frascioni, M., Maragò, O. M., & Iatì, M. A. (2017). Surface plasmon resonance in gold nanoparticles: a review. *Journal of physics: Condensed matter*, 29(20), 203002.
- [48]. Khlebtsov, N., & Dykman, L. (2011). Biodistribution and toxicity of engineered gold nanoparticles: a review of in vitro and in vivo studies. *Chemical Society Reviews*, 40(3), 1647-1671.
- [49]. Boisselier, E., & Astruc, D. (2009). Gold nanoparticles in nanomedicine: preparations, imaging, diagnostics, therapies and toxicity. *Chemical society reviews*, 38(6), 1759-1782.
- [50]. Mosmann, T. (1983). Rapid colorimetric assay for cellular growth and survival: application to proliferation and cytotoxicity assays. *Journal of immunological methods*, 65(1-2), 55-63.
- [51]. Brand-Williams, W., Cuvelier, M. E., & Berset, C. L. W. T. (1995). Use of a free radical method to evaluate antioxidant activity. *LWT-Food science and Technology*, 28(1), 25-30.
- [52]. Riccardi, C., & Nicoletti, I. (2006). Analysis of apoptosis by propidium iodide staining and flow cytometry. *Nature protocols*, 1(3), 1458-1461.
- [53]. Vermes, I., Haanen, C., Steffens-Nakken, H., & Reutellingsperger, C. (1995). A novel assay for apoptosis flow cytometric detection of phosphatidylserine expression on early apoptotic cells using fluorescein labelled annexin V. *Journal of immunological methods*, 184(1), 39-51.
- [54]. Rao, P. V., Nallappan, D., Madhavi, K., Rahman, S., & Selvaraj, S. (2016). Phytosynthesis of silver nanoparticles using *Helicteres isora* root extract and their antimicrobial and catalytic activities. *Journal of the Taiwan Institute of Chemical Engineers*, 66, 336–344. <https://doi.org/10.1016/j.jtice.2016.06.020>
- [55]. Thakkar, K. N., Mhatre, S. S., & Parikh, R. Y. (2010). Biological synthesis of metallic nanoparticles. *Nanomedicine: nanotechnology, biology and medicine*, 6(2), 257-262.
- [56]. Yeo, C. I., Ooi, K. K., Akim, A. M., Ahmad, H., Awang, N., & Fun, H. K. (2020). The role of metal complexes in medicine and the modulation of their toxicity. *Molecules*, 25(7), 1564.

- [57]. Ovais, M., Khalil, A. T., Ayaz, M., Ahmad, I., Nethi, S. K., & Mukherjee, S. (2018). Biosynthesis of metal nanoparticles via microbial enzymes: a mechanistic approach. *International journal of molecular sciences*, 19(12), 4100.
- [58]. Barabadi, H., Ovais, M., Shinwari, Z. K., & Saravanan, M. (2017). Anti-cancer green bionanomaterials: present status and future prospects. *Green Chemistry Letters and Reviews*, 10(4), 285-314.
- [59]. Elia, P., Zach, R., Hazan, S., Kolusheva, S., Porat, Z. E., & Zeiri, Y. (2014). Green synthesis of gold nanoparticles using plant extracts as reducing agents. *International journal of nanomedicine*, 4007-4021.
- [60]. Kharissova, O. V., Dias, H. R., Kharisov, B. I., Pérez, B. O., & Pérez, V. M. J. (2013). The greener synthesis of nanoparticles. *Trends in biotechnology*, 31(4), 240-248.
- [61]. Lynch, I., & Dawson, K. A. (2020). Protein–nanoparticle interactions. *Nano-enabled medical applications*, 231-250.
- [62]. Monopoli, M. P., Aberg, C., Salvati, A., & Dawson, K. A. (2020). Biomolecular coronas provide the biological identity of nanosized materials. *Nano-enabled medical applications*, 205-229.
- [63]. Wehbe, N., Mesmar, J. E., El Kurdi, R., Al-Sawalmih, A., Badran, A., Patra, D., & Baydoun, E. (2025). Halodule uninervis extract facilitates the green synthesis of gold nanoparticles with anticancer activity. *Scientific Reports*, 15(1), 4286.
- [64]. Folorunso, A., Akintelu, S., Oyebamiji, A. K., Ajayi, S., Abiola, B., Abdusalam, I., & Morakinyo, A. (2019). Biosynthesis, characterization and antimicrobial activity of gold nanoparticles from leaf extracts of *Annona muricata*. *Journal of Nanostructure in Chemistry*, 9, 111-117.
- [65]. Barasinski, M., Jasper, V., Görke, M., & Garnweitner, G. (2025). In Situ Tracking of Nanoparticles During Electrophoresis in Hydrogels Using a Fiber-Based UV-Vis System. *Powders*, 4(1), 3.
- [66]. Redjili, S., Ghodbane, H., Bourzami, R., Mayouf, F., Chebli, D., Boudechicha, A., & Djelloul, C. (2025). Green synthesis of silver oxide nanoparticles: Eco-friendly approach for sustainable solutions. *Industrial Crops and Products*, 223, 120168.
- [67]. Grobelny, J., DelRio, F. W., Pradeep, N., Kim, D. I., Hackley, V. A., & Cook, R. F. (2011). Size measurement of nanoparticles using atomic force microscopy. *Characterization of nanoparticles intended for drug delivery*, 71-82.

- [68]. Faber, T., McConville, J. T., & Lamprecht, A. (2024). Focused ion beam-scanning electron microscopy provides novel insights of drug delivery phenomena. *Journal of Controlled Release*, 366, 312-327.
- [69]. Clogston, J. D., & Vermilya, A. (2005). Measuring Zeta Potential of Nanoparticles: Version 1.2. National Cancer Institute's Nanotechnology Characterization Laboratory Assay Cascade Protocols [Internet].
- [70]. Yirankinyuki, F. F., Magaji, B., Danbature, W. L., & Abdullah, A. M. (2020). Identification of Active Compounds of *Annona muricata* (Soursop) Leaf Wax Extract Using GC-MS. *Arch. Curr. Res. Int*, 20(4), 17-21.
- [71]. Medhe, S., Bansal, P., & Srivastava, M. M. (2014). Enhanced antioxidant activity of gold nanoparticle embedded 3, 6-dihydroxyflavone: a combinational study. *Applied Nanoscience*, 4, 153-161.
- [72]. Figat, A. M., Bartosewicz, B., Liszewska, M., Budner, B., Norek, M., & Jankiewicz, B. J. (2023). α -Amino acids as reducing and capping agents in gold nanoparticles synthesis using the Turkevich method. *Langmuir*, 39(25), 8646-8657.
- [73]. Ezirim, A. U., Ezekwesili-Ofili, J. O., Igwilo, I. O., & Izunna, C. (2024). GC-MS analysis, pharmaceutical and industrial significance of phytochemicals present in *Annona muricata* from Eziobodo, Imo State, Nigeria. *GSC Biological and Pharmaceutical Sciences*, 27(1).
- [74]. Mary, S. J., Veeravarmal, V., Thankappan, P., Arumugam, P., Augustine, P. I., & Franklin, R. (2024). Anti-cancer effects of green synthesized gold nanoparticles using leaf extract of *Annona muricata* L against squamous cell carcinoma cell line 15 through apoptotic pathway. *Dental Research Journal*, 21(1), 14.

Appendices



Scan Analysis Report

Tue 25 Sep 04:52:33 AM 2012

C:\Users\dell\Desktop\عدال.د ماني مستخلص
5.0.0.999

Report Time :

Method

Batch:

Software version:

Operator:

Instrument Parameters

Cary 60

2.00

800.0

200.0

Nanometers

Abs

600.00

1.00

0.1000

Dual Beam

On

Baseline correction

C:\Users\dell\Desktop\عدال.د ماني مستخلص

Off

Instrument

Instrument Version

Start (nm)

Stop (nm)

X Mode

Y Mode

UV-Vis Scan Rate (nm/min)

UV-Vis Data Interval (nm)

UV-Vis Ave. Time (sec)

Beam Mode

Baseline Correction

Baseline Type

Baseline File Name

Baseline Std Ref File Name

Cycle Mode

Comments

مائي مستخلص

9/25/2012 4:52:41 AM

Sample Name:

Collection Time

Peaks

0.0100

800.0nm to 200.0nm

Abs

0.451

1.753

1.805

1.869

1.991

2.065

2.067

2.104

2.432

2.698

2.491

2.347

2.367

2.522

2.343

2.802

2.706

2.521

3.253

2.550

10.000

10.000

2.923

10.000

3.379

2.647

2.501

2.996

2.797

10.000

10.000

3.294

2.902

2.674

2.919

2.917

3.298

3.585

2.579

2.689

2.691

2.914

2.519

2.548

2.494

2.588

2.731

Peak Table

Peak Style

Peak Threshold

Range

Wavelength
(nm)

785.0

409.0

402.0

397.0

381.0

378.0

376.0

374.0

371.0

368.0

364.0

361.0

358.0

356.0

354.0

350.0

346.0

344.0

341.0

335.0

331.0

328.0

325.0

323.0

319.0

317.0

315.0

312.0

309.0

307.0

305.0

303.0

301.0

298.0

296.0

293.0

288.0

283.0

281.0

277.0

275.0

271.0

267.0

265.0

263.0

260.0

256.0

2.725	254.0
3.161	251.0
2.732	249.0
3.499	245.0
2.700	242.0
2.703	240.0
2.515	237.0
10.000	234.0
10.000	230.0
2.403	226.0
2.246	221.0
2.128	219.0
1.950	217.0
2.096	215.0
1.976	213.0
1.793	209.0
1.765	207.0
1.814	205.0
1.463	202.0

X-Y Pairs Table

Abs	Wavelength (nm)	Abs	Wavelength (nm)	Abs	Wavelength (nm)
1.840	398.0	0.796	599.0	0.429	800.0
1.869	397.0	0.795	598.0	0.429	799.0
1.864	396.0	0.796	597.0	0.438	798.0
1.849	395.0	0.804	596.0	0.431	797.0
1.865	394.0	0.807	595.0	0.433	796.0
1.869	393.0	0.804	594.0	0.435	795.0
1.870	392.0	0.812	593.0	0.439	794.0
1.902	391.0	0.812	592.0	0.441	793.0
1.909	390.0	0.815	591.0	0.438	792.0
1.917	389.0	0.823	590.0	0.440	791.0
1.910	388.0	0.825	589.0	0.442	790.0
1.930	387.0	0.823	588.0	0.440	789.0
1.930	386.0	0.830	587.0	0.449	788.0
1.949	385.0	0.831	586.0	0.444	787.0
1.967	384.0	0.836	585.0	0.450	786.0
1.967	383.0	0.836	584.0	0.451	785.0
1.964	382.0	0.839	583.0	0.441	784.0
1.991	381.0	0.846	582.0	0.448	783.0
1.968	380.0	0.843	581.0	0.451	782.0
1.964	379.0	0.851	580.0	0.455	781.0
2.065	378.0	0.853	579.0	0.456	780.0
2.033	377.0	0.856	578.0	0.453	779.0
2.067	376.0	0.856	577.0	0.460	778.0
2.036	375.0	0.861	576.0	0.462	777.0
2.104	374.0	0.866	575.0	0.459	776.0
2.048	373.0	0.867	574.0	0.457	775.0
2.075	372.0	0.871	573.0	0.459	774.0
2.432	371.0	0.875	572.0	0.464	773.0
2.031	370.0	0.878	571.0	0.465	772.0
2.075	369.0	0.880	570.0	0.461	771.0
2.698	368.0	0.886	569.0	0.469	770.0
2.177	367.0	0.887	568.0	0.471	769.0
2.074	366.0	0.893	567.0	0.471	768.0
2.110	365.0	0.898	566.0	0.469	767.0

2.491	364.0	0.897	565.0	0.468	766.0
2.159	363.0	0.902	564.0	0.471	765.0
2.106	362.0	0.900	563.0	0.475	764.0
2.347	361.0	0.909	562.0	0.473	763.0
2.185	360.0	0.915	561.0	0.478	762.0
2.188	359.0	0.920	560.0	0.475	761.0
2.367	358.0	0.920	559.0	0.483	760.0
2.125	357.0	0.919	558.0	0.479	759.0
2.522	356.0	0.923	557.0	0.483	758.0
2.201	355.0	0.930	556.0	0.479	757.0
2.343	354.0	0.933	555.0	0.484	756.0
2.279	353.0	0.934	554.0	0.485	755.0
2.344	352.0	0.940	553.0	0.495	754.0
2.638	351.0	0.945	552.0	0.487	753.0
2.802	350.0	0.944	551.0	0.491	752.0
2.670	349.0	0.948	550.0	0.495	751.0
2.042	348.0	0.954	549.0	0.494	750.0
2.452	347.0	0.956	548.0	0.496	749.0
2.706	346.0	0.958	547.0	0.496	748.0
2.480	345.0	0.962	546.0	0.493	747.0
2.521	344.0	0.967	545.0	0.500	746.0
2.410	343.0	0.972	544.0	0.500	745.0
2.561	342.0	0.977	543.0	0.501	744.0
3.253	341.0	0.980	542.0	0.507	743.0
2.695	340.0	0.981	541.0	0.508	742.0
2.314	339.0	0.986	540.0	0.507	741.0
2.335	338.0	0.990	539.0	0.507	740.0
2.345	337.0	0.995	538.0	0.510	739.0
2.429	336.0	0.997	537.0	0.507	738.0
2.550	335.0	1.004	536.0	0.514	737.0
2.423	334.0	1.003	535.0	0.512	736.0
2.392	333.0	1.010	534.0	0.515	735.0
2.633	332.0	1.012	533.0	0.516	734.0
10.000	331.0	1.017	532.0	0.514	733.0
2.354	330.0	1.020	531.0	0.521	732.0
2.853	329.0	1.027	530.0	0.520	731.0
10.000	328.0	1.027	529.0	0.525	730.0
2.654	327.0	1.031	528.0	0.524	729.0
2.565	326.0	1.036	527.0	0.525	728.0
2.923	325.0	1.038	526.0	0.528	727.0
2.911	324.0	1.046	525.0	0.530	726.0
10.000	323.0	1.049	524.0	0.529	725.0
10.000	322.0	1.051	523.0	0.531	724.0
3.283	321.0	1.055	522.0	0.533	723.0
2.873	320.0	1.060	521.0	0.534	722.0
3.379	319.0	1.066	520.0	0.536	721.0
2.422	318.0	1.066	519.0	0.541	720.0
2.647	317.0	1.076	518.0	0.544	719.0
2.484	316.0	1.076	517.0	0.541	718.0
2.501	315.0	1.085	516.0	0.543	717.0
2.439	314.0	1.085	515.0	0.544	716.0
2.497	313.0	1.093	514.0	0.545	715.0
2.996	312.0	1.097	513.0	0.546	714.0
2.417	311.0	1.097	512.0	0.551	713.0
2.284	310.0	1.111	511.0	0.551	712.0
2.797	309.0	1.107	510.0	0.552	711.0

2.500	308.0	1.108	509.0	0.553	710.0
10.000	307.0	1.119	508.0	0.556	709.0
2.421	306.0	1.122	507.0	0.556	708.0
10.000	305.0	1.127	506.0	0.561	707.0
2.605	304.0	1.131	505.0	0.561	706.0
3.294	303.0	1.130	504.0	0.559	705.0
2.706	302.0	1.142	503.0	0.562	704.0
2.902	301.0	1.141	502.0	0.564	703.0
2.860	300.0	1.154	501.0	0.567	702.0
2.520	299.0	1.155	500.0	0.570	701.0
2.674	298.0	1.158	499.0	0.568	700.0
2.660	297.0	1.161	498.0	0.574	699.0
2.919	296.0	1.171	497.0	0.571	698.0
2.731	295.0	1.173	496.0	0.574	697.0
2.538	294.0	1.183	495.0	0.575	696.0
2.917	293.0	1.185	494.0	0.579	695.0
2.759	292.0	1.193	493.0	0.587	694.0
2.659	291.0	1.195	492.0	0.584	693.0
2.674	290.0	1.193	491.0	0.589	692.0
3.120	289.0	1.205	490.0	0.587	691.0
3.298	288.0	1.213	489.0	0.587	690.0
2.785	287.0	1.215	488.0	0.590	689.0
2.396	286.0	1.220	487.0	0.594	688.0
2.330	285.0	1.224	486.0	0.597	687.0
2.827	284.0	1.233	485.0	0.597	686.0
3.585	283.0	1.237	484.0	0.596	685.0
2.537	282.0	1.242	483.0	0.604	684.0
2.579	281.0	1.244	482.0	0.601	683.0
2.513	280.0	1.249	481.0	0.603	682.0
2.406	279.0	1.255	480.0	0.604	681.0
2.377	278.0	1.264	479.0	0.606	680.0
2.689	277.0	1.266	478.0	0.608	679.0
2.430	276.0	1.265	477.0	0.613	678.0
2.691	275.0	1.275	476.0	0.614	677.0
2.537	274.0	1.282	475.0	0.614	676.0
2.261	273.0	1.285	474.0	0.617	675.0
2.777	272.0	1.294	473.0	0.615	674.0
2.914	271.0	1.304	472.0	0.619	673.0
2.657	270.0	1.304	471.0	0.622	672.0
2.642	269.0	1.312	470.0	0.631	671.0
2.306	268.0	1.325	469.0	0.628	670.0
2.519	267.0	1.327	468.0	0.627	669.0
2.351	266.0	1.333	467.0	0.632	668.0
2.548	265.0	1.340	466.0	0.636	667.0
2.144	264.0	1.341	465.0	0.637	666.0
2.494	263.0	1.341	464.0	0.639	665.0
2.351	262.0	1.359	463.0	0.640	664.0
2.243	261.0	1.366	462.0	0.641	663.0
2.588	260.0	1.368	461.0	0.644	662.0
2.509	259.0	1.373	460.0	0.642	661.0
2.415	258.0	1.375	459.0	0.647	660.0
2.014	257.0	1.384	458.0	0.648	659.0
2.731	256.0	1.391	457.0	0.654	658.0
2.400	255.0	1.396	456.0	0.655	657.0
2.725	254.0	1.403	455.0	0.656	656.0
2.592	253.0	1.410	454.0	0.663	655.0

2.195	252.0	1.414	453.0	0.660	654.0
3.161	251.0	1.416	452.0	0.666	653.0
2.114	250.0	1.426	451.0	0.664	652.0
2.732	249.0	1.434	450.0	0.666	651.0
2.538	248.0	1.440	449.0	0.673	650.0
2.451	247.0	1.444	448.0	0.671	649.0
2.362	246.0	1.449	447.0	0.674	648.0
3.499	245.0	1.464	446.0	0.670	647.0
2.381	244.0	1.461	445.0	0.676	646.0
2.345	243.0	1.477	444.0	0.681	645.0
2.700	242.0	1.481	443.0	0.685	644.0
2.624	241.0	1.484	442.0	0.684	643.0
2.703	240.0	1.496	441.0	0.684	642.0
2.584	239.0	1.505	440.0	0.687	641.0
2.199	238.0	1.507	439.0	0.685	640.0
2.515	237.0	1.516	438.0	0.699	639.0
2.066	236.0	1.529	437.0	0.693	638.0
2.493	235.0	1.531	436.0	0.699	637.0
10.000	234.0	1.544	435.0	0.703	636.0
10.000	233.0	1.544	434.0	0.707	635.0
10.000	232.0	1.555	433.0	0.707	634.0
2.636	231.0	1.565	432.0	0.706	633.0
10.000	230.0	1.569	431.0	0.703	632.0
2.335	229.0	1.573	430.0	0.716	631.0
2.339	228.0	1.588	429.0	0.714	630.0
2.381	227.0	1.584	428.0	0.718	629.0
2.403	226.0	1.594	427.0	0.719	628.0
2.384	225.0	1.605	426.0	0.721	627.0
2.236	224.0	1.610	425.0	0.729	626.0
2.053	223.0	1.622	424.0	0.728	625.0
2.045	222.0	1.635	423.0	0.725	624.0
2.246	221.0	1.638	422.0	0.734	623.0
1.823	220.0	1.646	421.0	0.735	622.0
2.128	219.0	1.658	420.0	0.741	621.0
1.676	218.0	1.659	419.0	0.742	620.0
1.950	217.0	1.678	418.0	0.739	619.0
1.699	216.0	1.673	417.0	0.742	618.0
2.096	215.0	1.675	416.0	0.748	617.0
1.788	214.0	1.688	415.0	0.752	616.0
1.976	213.0	1.694	414.0	0.751	615.0
1.772	212.0	1.690	413.0	0.755	614.0
1.693	211.0	1.715	412.0	0.758	613.0
1.555	210.0	1.714	411.0	0.761	612.0
1.793	209.0	1.721	410.0	0.764	611.0
1.722	208.0	1.753	409.0	0.763	610.0
1.765	207.0	1.750	408.0	0.766	609.0
1.576	206.0	1.742	407.0	0.771	608.0
1.814	205.0	1.782	406.0	0.770	607.0
1.396	204.0	1.774	405.0	0.772	606.0
1.172	203.0	1.791	404.0	0.776	605.0
1.463	202.0	1.791	403.0	0.781	604.0
1.282	201.0	1.805	402.0	0.782	603.0
1.090	200.0	1.791	401.0	0.781	602.0
		1.806	400.0	0.789	601.0
		1.818	399.0	0.792	600.0

Scan Analysis Report

Tue 25 Sep 04:54:49 AM 2012

C:\Users\del\\Desktop\تخفيف المائي مستخلص.DSW
5.0.0.999

Report Time :

Method

Batch:

Software version:

Operator:

Instrument Parameters

Cary 60

2.00

800.0

200.0

Nanometers

Abs

600.00

1.00

0.1000

Dual Beam

On

Baseline correction

C:\Users\del\\Desktop\تخفيف المائي مستخلص عادل.د مائي مستخلص

Off

Instrument

Instrument Version

Start (nm)

Stop (nm)

X Mode

Y Mode

UV-Vis Scan Rate (nm/min)

UV-Vis Data Interval (nm)

UV-Vis Ave. Time (sec)

Beam Mode

Baseline Correction

Baseline Type

Baseline File Name

Baseline Std Ref File Name

Cycle Mode

Comments

تخفيف المائي مستخلص

9/25/2012 4:54:52 AM

Sample Name:

Collection Time

Peaks

0.0100

800.0nm to 200.0nm

Abs

1.175

1.207

1.322

1.963

2.168

2.044

1.998

2.527

1.732

1.967

1.768

1.887

1.702

1.499

Peak Table

Peak Style

Peak

Threshold

Range

Wavelength
(nm)

264.0

256.0

243.0

233.0

230.0

226.0

223.0

220.0

217.0

215.0

213.0

211.0

208.0

204.0

X-Y Pairs Table

Abs	Wavelength (nm)	Abs	Wavelength (nm)	Abs	Wavelength (nm)
0.314	398.0	0.118	599.0	0.062	800.0
0.316	397.0	0.119	598.0	0.061	799.0
0.318	396.0	0.121	597.0	0.063	798.0
0.322	395.0	0.120	596.0	0.061	797.0
0.324	394.0	0.121	595.0	0.062	796.0
0.325	393.0	0.120	594.0	0.062	795.0
0.328	392.0	0.121	593.0	0.065	794.0
0.329	391.0	0.122	592.0	0.065	793.0
0.332	390.0	0.122	591.0	0.061	792.0
0.335	389.0	0.122	590.0	0.063	791.0
0.337	388.0	0.124	589.0	0.060	790.0
0.340	387.0	0.123	588.0	0.065	789.0
0.342	386.0	0.126	587.0	0.066	788.0
0.346	385.0	0.124	586.0	0.066	787.0
0.348	384.0	0.125	585.0	0.064	786.0
0.350	383.0	0.125	584.0	0.066	785.0
0.351	382.0	0.126	583.0	0.062	784.0
0.356	381.0	0.126	582.0	0.062	783.0
0.357	380.0	0.127	581.0	0.066	782.0
0.362	379.0	0.128	580.0	0.066	781.0
0.362	378.0	0.127	579.0	0.066	780.0
0.366	377.0	0.128	578.0	0.063	779.0
0.368	376.0	0.129	577.0	0.062	778.0
0.374	375.0	0.130	576.0	0.066	777.0
0.375	374.0	0.131	575.0	0.069	776.0
0.379	373.0	0.130	574.0	0.063	775.0
0.379	372.0	0.131	573.0	0.069	774.0
0.385	371.0	0.131	572.0	0.068	773.0
0.388	370.0	0.132	571.0	0.067	772.0
0.393	369.0	0.132	570.0	0.066	771.0
0.396	368.0	0.133	569.0	0.067	770.0
0.395	367.0	0.133	568.0	0.068	769.0
0.402	366.0	0.134	567.0	0.070	768.0
0.400	365.0	0.135	566.0	0.067	767.0
0.402	364.0	0.135	565.0	0.066	766.0
0.413	363.0	0.136	564.0	0.066	765.0
0.411	362.0	0.135	563.0	0.067	764.0
0.413	361.0	0.136	562.0	0.067	763.0
0.420	360.0	0.138	561.0	0.069	762.0
0.422	359.0	0.139	560.0	0.069	761.0
0.425	358.0	0.139	559.0	0.070	760.0
0.426	357.0	0.140	558.0	0.070	759.0
0.435	356.0	0.139	557.0	0.071	758.0
0.439	355.0	0.141	556.0	0.069	757.0
0.437	354.0	0.141	555.0	0.068	756.0
0.447	353.0	0.142	554.0	0.070	755.0
0.450	352.0	0.141	553.0	0.073	754.0
0.449	351.0	0.143	552.0	0.072	753.0
0.453	350.0	0.142	551.0	0.073	752.0
0.460	349.0	0.144	550.0	0.071	751.0
0.462	348.0	0.144	549.0	0.071	750.0
0.460	347.0	0.145	548.0	0.073	749.0
0.475	346.0	0.145	547.0	0.072	748.0
0.475	345.0	0.146	546.0	0.072	747.0
0.477	344.0	0.147	545.0	0.072	746.0

0.485	343.0	0.147	544.0	0.072	745.0
0.490	342.0	0.149	543.0	0.073	744.0
0.498	341.0	0.148	542.0	0.074	743.0
0.494	340.0	0.149	541.0	0.073	742.0
0.500	339.0	0.151	540.0	0.073	741.0
0.513	338.0	0.151	539.0	0.074	740.0
0.513	337.0	0.152	538.0	0.073	739.0
0.506	336.0	0.152	537.0	0.072	738.0
0.522	335.0	0.152	536.0	0.075	737.0
0.523	334.0	0.153	535.0	0.075	736.0
0.532	333.0	0.154	534.0	0.074	735.0
0.534	332.0	0.155	533.0	0.075	734.0
0.540	331.0	0.155	532.0	0.074	733.0
0.544	330.0	0.156	531.0	0.076	732.0
0.549	329.0	0.157	530.0	0.074	731.0
0.558	328.0	0.157	529.0	0.077	730.0
0.562	327.0	0.158	528.0	0.076	729.0
0.567	326.0	0.158	527.0	0.077	728.0
0.571	325.0	0.159	526.0	0.076	727.0
0.582	324.0	0.160	525.0	0.077	726.0
0.590	323.0	0.161	524.0	0.079	725.0
0.588	322.0	0.161	523.0	0.077	724.0
0.592	321.0	0.162	522.0	0.078	723.0
0.602	320.0	0.162	521.0	0.077	722.0
0.608	319.0	0.164	520.0	0.077	721.0
0.615	318.0	0.164	519.0	0.079	720.0
0.618	317.0	0.165	518.0	0.079	719.0
0.625	316.0	0.166	517.0	0.080	718.0
0.630	315.0	0.167	516.0	0.079	717.0
0.632	314.0	0.166	515.0	0.078	716.0
0.643	313.0	0.168	514.0	0.080	715.0
0.650	312.0	0.168	513.0	0.079	714.0
0.659	311.0	0.169	512.0	0.078	713.0
0.670	310.0	0.171	511.0	0.080	712.0
0.665	309.0	0.170	510.0	0.081	711.0
0.679	308.0	0.172	509.0	0.081	710.0
0.692	307.0	0.173	508.0	0.080	709.0
0.688	306.0	0.173	507.0	0.080	708.0
0.698	305.0	0.174	506.0	0.081	707.0
0.711	304.0	0.175	505.0	0.082	706.0
0.718	303.0	0.176	504.0	0.080	705.0
0.723	302.0	0.177	503.0	0.082	704.0
0.733	301.0	0.177	502.0	0.083	703.0
0.739	300.0	0.178	501.0	0.082	702.0
0.759	299.0	0.179	500.0	0.083	701.0
0.765	298.0	0.180	499.0	0.083	700.0
0.782	297.0	0.180	498.0	0.084	699.0
0.788	296.0	0.182	497.0	0.083	698.0
0.802	295.0	0.183	496.0	0.084	697.0
0.815	294.0	0.183	495.0	0.084	696.0
0.828	293.0	0.183	494.0	0.084	695.0
0.841	292.0	0.185	493.0	0.085	694.0
0.856	291.0	0.185	492.0	0.085	693.0
0.866	290.0	0.187	491.0	0.085	692.0
0.882	289.0	0.188	490.0	0.086	691.0
0.896	288.0	0.189	489.0	0.086	690.0
0.917	287.0	0.189	488.0	0.086	689.0

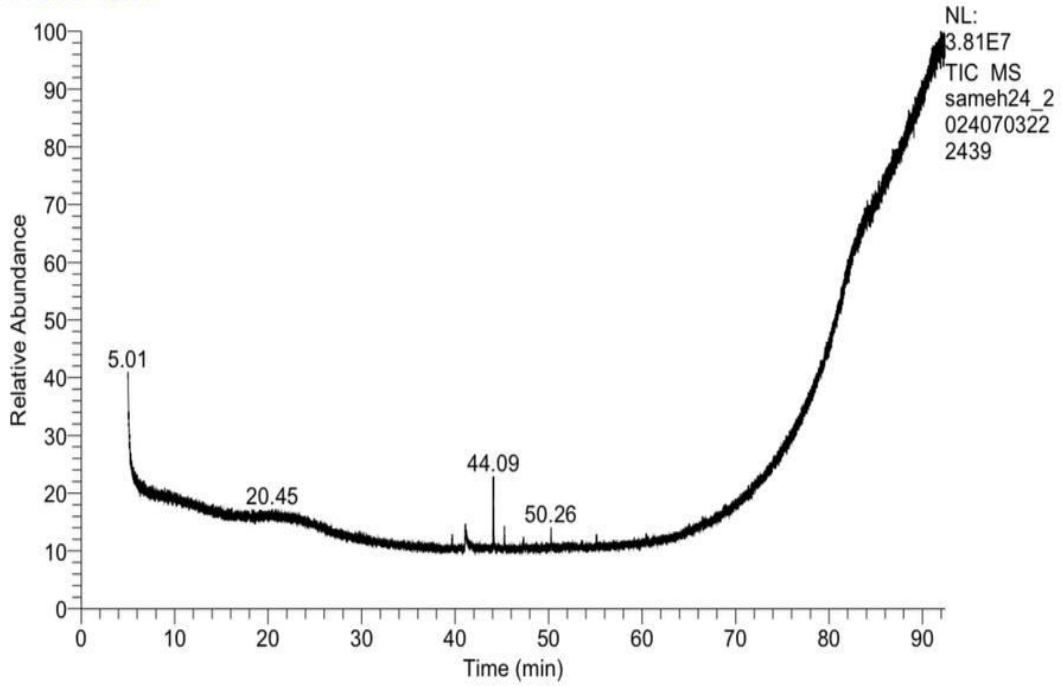
0.937	286.0	0.190	487.0	0.087	688.0
0.955	285.0	0.192	486.0	0.085	687.0
0.977	284.0	0.193	485.0	0.088	686.0
0.987	283.0	0.193	484.0	0.088	685.0
1.004	282.0	0.194	483.0	0.088	684.0
1.013	281.0	0.195	482.0	0.089	683.0
1.036	280.0	0.196	481.0	0.088	682.0
1.045	279.0	0.197	480.0	0.088	681.0
1.041	278.0	0.198	479.0	0.089	680.0
1.075	277.0	0.199	478.0	0.090	679.0
1.068	276.0	0.200	477.0	0.088	678.0
1.088	275.0	0.202	476.0	0.089	677.0
1.110	274.0	0.202	475.0	0.092	676.0
1.117	273.0	0.203	474.0	0.092	675.0
1.128	272.0	0.204	473.0	0.090	674.0
1.136	271.0	0.205	472.0	0.091	673.0
1.131	270.0	0.206	471.0	0.091	672.0
1.143	269.0	0.206	470.0	0.092	671.0
1.149	268.0	0.207	469.0	0.092	670.0
1.159	267.0	0.210	468.0	0.093	669.0
1.168	266.0	0.210	467.0	0.095	668.0
1.166	265.0	0.212	466.0	0.092	667.0
1.175	264.0	0.213	465.0	0.094	666.0
1.175	263.0	0.213	464.0	0.094	665.0
1.165	262.0	0.215	463.0	0.094	664.0
1.175	261.0	0.216	462.0	0.095	663.0
1.169	260.0	0.217	461.0	0.095	662.0
1.166	259.0	0.218	460.0	0.095	661.0
1.183	258.0	0.219	459.0	0.095	660.0
1.183	257.0	0.220	458.0	0.095	659.0
1.207	256.0	0.220	457.0	0.094	658.0
1.186	255.0	0.222	456.0	0.096	657.0
1.179	254.0	0.223	455.0	0.096	656.0
1.171	253.0	0.225	454.0	0.098	655.0
1.197	252.0	0.225	453.0	0.096	654.0
1.198	251.0	0.227	452.0	0.098	653.0
1.189	250.0	0.229	451.0	0.097	652.0
1.212	249.0	0.229	450.0	0.098	651.0
1.210	248.0	0.231	449.0	0.097	650.0
1.219	247.0	0.232	448.0	0.099	649.0
1.253	246.0	0.233	447.0	0.099	648.0
1.254	245.0	0.234	446.0	0.100	647.0
1.280	244.0	0.235	445.0	0.099	646.0
1.322	243.0	0.237	444.0	0.101	645.0
1.273	242.0	0.238	443.0	0.100	644.0
1.363	241.0	0.239	442.0	0.101	643.0
1.389	240.0	0.242	441.0	0.101	642.0
1.400	239.0	0.242	440.0	0.101	641.0
1.422	238.0	0.244	439.0	0.102	640.0
1.460	237.0	0.245	438.0	0.102	639.0
1.569	236.0	0.247	437.0	0.103	638.0
1.655	235.0	0.248	436.0	0.102	637.0
1.886	234.0	0.250	435.0	0.104	636.0
1.963	233.0	0.251	434.0	0.104	635.0
1.889	232.0	0.252	433.0	0.104	634.0
1.821	231.0	0.254	432.0	0.103	633.0
2.168	230.0	0.255	431.0	0.104	632.0

1.886	229.0	0.257	430.0	0.106	631.0
1.955	228.0	0.258	429.0	0.106	630.0
1.984	227.0	0.259	428.0	0.106	629.0
2.044	226.0	0.262	427.0	0.105	628.0
1.944	225.0	0.263	426.0	0.107	627.0
1.952	224.0	0.265	425.0	0.107	626.0
1.998	223.0	0.266	424.0	0.107	625.0
1.874	222.0	0.267	423.0	0.107	624.0
1.868	221.0	0.270	422.0	0.107	623.0
2.527	220.0	0.271	421.0	0.108	622.0
2.191	219.0	0.273	420.0	0.110	621.0
1.700	218.0	0.275	419.0	0.109	620.0
1.732	217.0	0.276	418.0	0.110	619.0
1.698	216.0	0.277	417.0	0.110	618.0
1.967	215.0	0.280	416.0	0.111	617.0
1.600	214.0	0.280	415.0	0.110	616.0
1.768	213.0	0.284	414.0	0.111	615.0
1.630	212.0	0.285	413.0	0.113	614.0
1.887	211.0	0.287	412.0	0.112	613.0
1.501	210.0	0.289	411.0	0.113	612.0
1.483	209.0	0.291	410.0	0.113	611.0
1.702	208.0	0.293	409.0	0.113	610.0
1.398	207.0	0.294	408.0	0.114	609.0
1.356	206.0	0.297	407.0	0.115	608.0
1.332	205.0	0.299	406.0	0.116	607.0
1.499	204.0	0.301	405.0	0.115	606.0
1.329	203.0	0.303	404.0	0.116	605.0
1.306	202.0	0.304	403.0	0.117	604.0
1.254	201.0	0.307	402.0	0.117	603.0
1.264	200.0	0.308	401.0	0.117	602.0
		0.310	400.0	0.118	601.0
		0.312	399.0	0.118	600.0

Sample Header

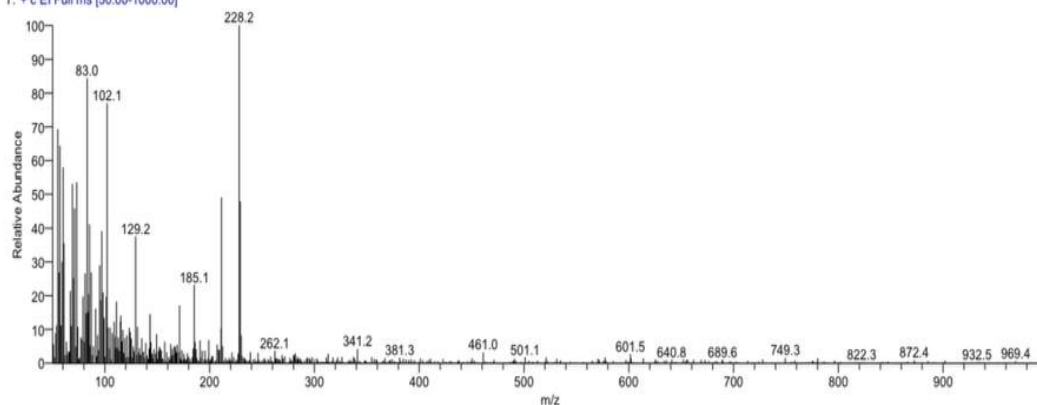
Sample ID:	sameh24	Original Data Path:	D:\work\DR.SYED\27-6-2024
Sample Volume(µl):	0.00	Original Processing Method:	D:\work\DR.SYED\DR.SYED PROC
Instrument Software Version:	4.0.0.29	Instrument Name:	ISQ Series
Acquisition Date:	07/03/24 10:35:32 PM	Injection Volume(µl):	1.00
Instrument Method:	D:\work\DR.SYED\Dr sayed 45.meth	Instrument Model:	ISQ 7000
Sample Name:		Run Time(min):	87.44

RT: 0.00 - 92.44



There is no signature data to report.

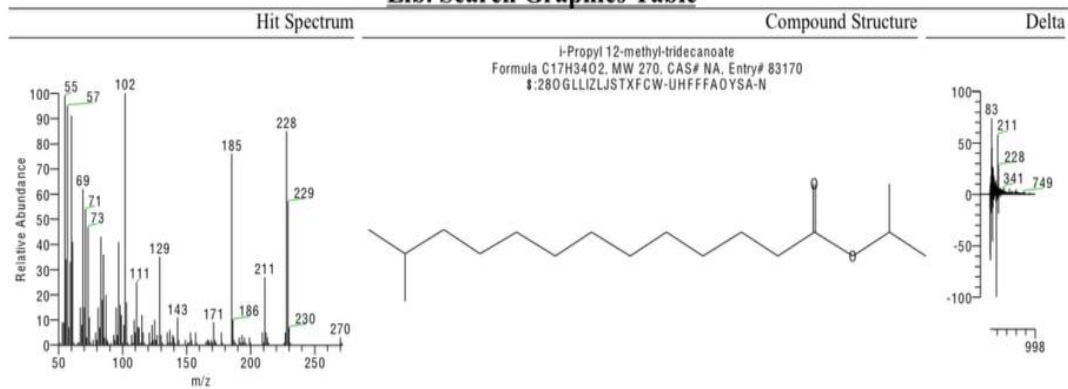
sameh24_20240703222439 #11493 RT: 44.09 AV: 1 NL: 4.18E5
T: + c EI Full ms [50.00-1000.00]



Library Search Results Table

RT	Compound Name	Molecular Formula	Molecular Weight	Cas #	Probability	Area	Area %	Library	S	MF
44.09	ISOPROPYL TETRADECANOATE	C17H34O2	270	110-27-0	25.29	181	100.00	WileyR	6	831
	791						cgistry	4		
	21.36					8e	8			
44.09	ISOPROPYL TETRADECANOATE	C17H34O2	270	110-27-0	25.29	181	100.00	WileyR	6	814
	791						egistry	4		
	21.36					8e	3			
44.09	ISOPROPYL TETRADECANOATE	C17H34O2	270	110-27-0	25.29	181	100.00	WileyR	6	788
	791						egistry	4		
	21.36					8e	3			
44.09	Isopropyl myristate	C17H34O2	270	110-27-0	25.29	181	100.00	replib	6	814
	791							4		
	21.36							3		
44.09	i-Propyl 12-methyl-tridecanoate	C17H34O2	270	NA	27.42	181	100.00	mainlib	6	826
	791							5		
	21.36							0		

Lib. Search Graphics Table



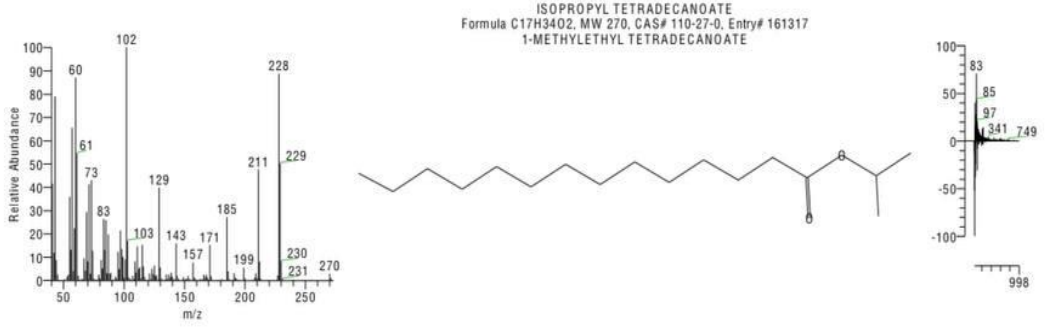
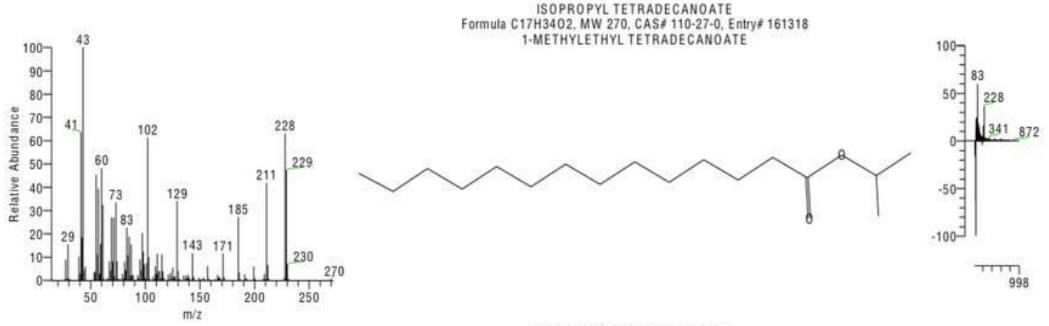
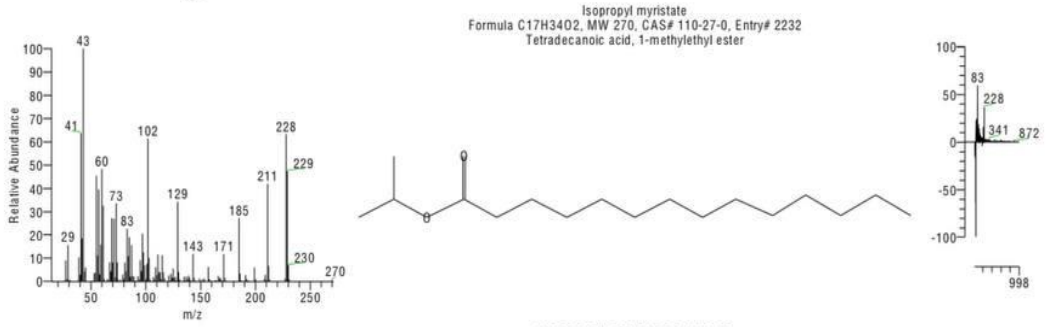
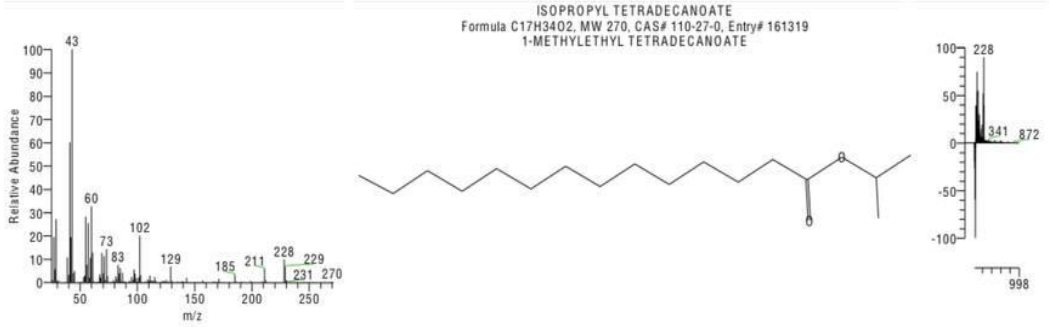
There is no signature data to report.

Library Search Report

Hit Spectrum

Compound Structure

Delta



There is no signature data to report.

الملخص

تم في هذه الدراسة تخليق حيوي لجسيمات الذهب النانوية (AuNPs) باستخدام مستخلص بذور نبات ثمرة القشطة (*Annona muricata*) وتقييم إمكاناتها المضادة للسرطان ضد خلايا سرطان الثدي الإيجابية لـ MCF-7. تم توصيف جسيمات الذهب النانوية المصنعة باستخدام تقنيات مختلفة من بينها التحليل الطيفي للأشعة فوق البنفسجية المرئية، حيود الأشعة السينية (XRD)، المجهر الإلكتروني النافذ (TEM)، المجهر القوة الذرية (AFM)، التشتت الضوئي الديناميكي (DLS)، وتحليل الجهد زيتا. تم تحليل الملف الكيميائي النباتي لمستخلص بذور ثمرة القشطة باستخدام كروماتوغرافيا الغاز-مطياف الكتلة (GC-MS). أظهرت جسيمات الذهب النانوية المصنعة حيويًا شكلًا كرويًا إلى شبه كروي بأحجام تتراوح من 20 إلى 90 نانومتر (TEM/AFM) وقطر هيدروديناميكي يبلغ حوالي 75 نانومتر (DLS). يشير الجهد زيتا السالب (-36 مللي فولت) إلى استقرار غرواني ممتاز. وقد حدد تحليل كروماتوغرافيا الغاز-مطياف الكتلة رباعي ديكانوات الأيزوبروبيل كمكون رئيسي في مستخلص البذور، مما قد يساهم في تخليق وتثبيت جزيئات الذهب النانوية. وتم تقييم النشاط المضاد للسرطان لجسيمات الذهب النانوية باستخدام اختبار MTT ضد خلايا سرطان الثدي الإيجابية لـ MCF-7، مع قيمة IC50 تبلغ 0.33 ± 22.44 ميكروجرام/مل. وكشف تحليل قياس التدفق الخلوي أن جزيئات الذهب النانوية تسبب توقف دورة الخلية في مرحلة G1/S وموت الخلايا بشكل ملحوظ. وأظهر اختبار DPPH نشاطًا مضادًا للأكسدة قويًا لجسيمات الذهب النانوية، مع إزالة الجذور الحرة المعتمدة على التركيز. وتوضح هذه الدراسة إمكانات التخليق الحيوي لجسيمات الذهب النانوية بوساطة *A. muricata* كنهج واعد لتطوير علاجات نانوية جديدة ضد سرطان الثدي الإيجابي لـ MCF-7، من خلال الجمع بين خصائص مكافحة السرطان لكل من مستخلص النبات والجسيمات النانوية.

الكلمات المفتاحية: التخليق الحيوي؛ جسيمات الذهب النانوية؛ بذور ثمرة القشطة؛ سرطان الثدي MCF-7 إيجابي. النشاط المضاد للسرطان. الخصائص المضادة للأكسدة. موت الخلايا المبرمج. إيقاف دورة الخلية. المواد الكيميائية النباتية. تكنولوجيا النانو.



الجامعة الإسلامية
كلية العلوم
قسم الكيمياء

التخليق الحيوي لجسيمات الذهب النانوية لمستخلص بذور ثمرة القشطة (*Annona muricata*) كعامل محفز لموت الخلايا في سرطان الثدي

إعداد الطالبة: أمينة مفتاح علي الفلوس

تحت إشراف: أ.د. عادل محمد مليطان

أستاذ كيمياء حيوية جامعة مصراتة

مشرف مشارك: د. مختار المبروك أبورزيزة

أستاذ مشارك كيمياء عضوية بالجامعة الإسلامية

قدمت الرسالة استكمالاً لمتطلبات الإجازة العلمية (ماجستير) في علوم الكيمياء

العام الجامعي (2025)